BOUND STATES NEAR THE INTERFACE OF A DISTORTED GRAPHENE SHEET AND A SUPERCONDUCTOR

By

Hendrik Jacobus Rust van Zyl

Thesis presented in partial fulfilment of the requirements for the degree of MASTER OF SCIENCE at the University of Stellenbosch.

Supervisor : Doctor Izak Snyman

Co-supervisor : Professor Frederik G Scholtz

December 2011

Stellenbosch University http://scholar.sun.ac.za

DECLARATION

By submitting this thesis electronically, I declare that the entirety of the work contained therein is my own, original work, that I am the sole author thereof (save to the extent explicitly otherwise stated), that reproduction and publication thereof by Stellenbosch University will not infringe any third party rights and that I have not previously in its entirety or in part submitted it for obtaining any qualification.

Copyright © 2011 University of Stellenbosch

All rights reserved

Stellenbosch University http://scholar.sun.ac.za

ABSTRACT

The goal of this thesis is to investigate the effects of distorting a graphene lattice and connecting this distorted graphene sheet to a superconductor. At low energies the possible excitation states in graphene are restricted to two distinct regions in momentum space called valleys. Many electronic applications are possible if one can design a graphene system where excitations can be forced to occupy a single valley in a controllable way. Investigating the spectrum of the distorted graphene sheet reveals that, if the chemical potential is chosen to coincide with a bulk Landau level, the normal-superconductor interface always supports propagating modes in both directions. Excitations from opposite valleys travel in opposite directions along the interface. The spectrum of a distorted graphene sheet terminated by an armchair edge, in contrast, is dispersionless. We verify this insulating nature of the armchair edge for finite samples by numerical means. Furthermore, we verify previous analytical results pertaining to a graphene sheet with NS interface and an applied perpendicular real magnetic field numerically. In the process, it is shown that considering graphene sheets of perfect width is not necessary, as long as the width a few magnetic lengths away from the interface is well-defined. By then considering a finite graphene sheet, terminated by armchair edges, that is distorted and connected to a superconductor, we find bound states near the NS interface that can be changed by distorting the graphene lattice further.

Stellenbosch University http://scholar.sun.ac.za

OPSOMMING

Die doel van hierdie tesis is om die uitwerking van die vervorming van 'n grafeenrooster te ondersoek wanneer die met 'n supergeleier verbind word. By lae energieë word die moontlike opwekkings in grafeen beperk tot twee aparte gebiede van momentumruimte — die sogenaamde valleie. Verskeie elektroniese toepassings is moontlik indien 'n grafeenstelsel ontwerp kan word waar opwekkings slegs 'n enkele vallei beset en die besetting beheer kan word. Deur die spektrum van die vervormde grafeenrooster te ondersoek word daar gevind dat, indien die chemiese potensiaal gekies word om saam te val met 'n Landauvlak, die NS-tussenvlak geleiding in beide rigtings ondersteun. Opwekkings van verskillende valleie beweeg in teenoorgestelde rigtings langs die tussenvlak. Daarteenoor is die spektrum van 'n vervormde grafeenroster met 'n leunstoelrand dispersieloos. Ons bevestig hierdie insulerende gedrag van 'n leunstoelrand vir eindige grafeenroosters deur middel van 'n numeriese berekening. Verder word vorige analitiese resultate wat verband hou met 'n grafeenrooster met normaal-supergeleiertussenvlakstelsel en loodregte magneetveld op die vlak bevestig deur middel van numeriese berekeninge. In die proses word dit ook aangedui dat die grafeenrooster nie 'n perfekte wydte hoef te hê nie, solank die wydte goed gedefinieer is vir 'n paar magnetiese lengtes in die omgewing van die tussenvlak. Deur dan die eindige grafeenrooster met leunstoelrande te koppel aan 'n supergeleier word gebonde toestande naby aan die NS tussenvalk gevind. Hierdie toestande kan gemanipuleer word deur die grafeenrooster verder te vervorm.

Stellenbosch University http://scholar.sun.ac.za

CONTENTS

ABSTRACT iii

1. Introduction 1

2. A Discussion of the Basics 4
   - 2.1 The structure of graphene 4
   - 2.2 The graphene tight binding Hamiltonian 5
   - 2.3 Plane wave expansion 7
   - 2.4 Dispersion relation for an infinite graphene sheet 9
   - 2.5 The Dirac Equation 11
   - 2.6 Terminated lattice boundary conditions 13
     - 2.6.1 The armchair edge 14
     - 2.6.2 The zig-zag edge 15
     - 2.6.3 Final Remarks 16
   - 2.7 Adding electromagnetic fields and the Quantum Hall Effect 16

3. Different Dynamics for the Valleys 21
   - 3.1 Lattice Distortions and the Pseudo Magnetic Field 21
   - 3.2 Superconductivity 23
   - 3.3 A Superconductor as a Boundary Condition 26
   - 3.4 Specular Andreev reflection vs Retro Andreev reflection in graphene 28

4. Green's function formalism for calculating conductance 30
   - 4.1 Green's function conductance relation 30
   - 4.2 The tight binding Hamiltonian 32
   - 4.3 Self-energy calculation 36
     - 4.3.1 The calculation of the surface Green's functions of the leads 38
     - 4.3.2 The graphene geometry in the algorithm 41
   - 4.4 Extending the algorithm to include an NS interface 43
   - 4.5 Hole excitations in the Hamiltonian 44
   - 4.6 Andreev vs. normal reflection 44

Stellenbosch University http://scholar.sun.ac.za

5. The effect of lattice distortions of graphene near an NS interface 46
5.1 Mathematical formulation of the problem (for a semi-infinite graphene sheet) . . 46
5.2 Transformations between excitations 48
5.3 Constant pseudo magnetic field 50
5.3.1 Dependence on the superconducting gap potential 53
5.3.2 Dependence on the chemical potential 55
5.3.3 Comparison with a real magnetic field — spectrum and kinematics 56
5.4 Armchair edge and Normal-Superconductor equivalence 58
5.5 A semi-infinite graphene sheet with armchair edge 61
6. Conductance in the real magnetic field problem 65
6.1 Connecting with analytical results 65
6.1.1 Quantum Hall effect 66
6.1.2 Conductance in an NS interface armchair edged system with real magnetic field 68
6.2 Conductance in non-perfect armchair edge system 71
7. The finite distorted graphene with an NS interface problem 75
7.1 The non-propagation of armchair edge states in finite graphene 76
7.2 Bound states near the NS interface 77
7.2.1 Size of the system and width of the peaks 78
7.2.2 The number of peaks 78
7.3 A numerical confirmation of resonances associated with the NS interface 78
7.3.1 System size 79
7.3.2 Dependence on the length, L_A 79
7.3.3 Dependence on the width of the system 81
7.4 Summary 83
8. Conclusion 85
BIBLIOGRAPHY 88

Stellenbosch University http://scholar.sun.ac.za

CHAPTER 1
Introduction

In 1946, P.R. Wallace wrote the first paper [1] on the properties of a two-dimensional carbon allotrope with its atoms arranged in hexagons so that this allotrope resembled the structure of a honeycomb. This carbon allotrope was later called graphene [2]. The investigation of graphene's properties was a starting point to study the electronic properties of graphite, an important material in nuclear reactions at that time and a material that can be seen as layers of graphene stacked on top of each other. These studies revealed that the dispersion relation of graphene, at low energies, is linear at the corners of the Brillouin zone, leading to a zero effective mass for electrons and holes. The implication of this is that the particles and holes show relativistic properties — this without accelerating the particles to relativistic speeds. The particles are thus massless Dirac fermions and thus endow graphene with many exotic properties.

However, since graphene is a two-dimensional crystal, the stability of such a configuration was questioned [3, 4] and intensive studies on the material's properties did not ensue. Instead, other materials which can be built up from graphene sheets such as graphite (once it is stacked into layers) or carbon nanotubes (when rolled up) which were known to be stable were the main focus of theoretical studies. The Slonczewski-Weiss-McClure band structure of graphite [5, 6] is a famous result giving great detail of graphite's electronic properties. The fact that graphene can be seen as a building block of graphite (among others) was the major source of interest in it for many years and the largescale theoretical interest in this material by itself is a recent phenomenon.

In 2004, a single sheet of graphene was isolated [7] from graphite and placed on a weakly interacting SiO_2 wafer. This isolated the graphene layer while generating only weak wafer-graphene interactions, leading to nearly charge-neutral graphene sheets. Subsequent experiments verified the Dirac fermion behavior of the graphene quasiparticles [8], which sparked immense theoretical interest in this material. These feats, along with other groundbreaking experiments on graphene, contributed to Konstantin Novoselov and Andre Geim being awarded the Nobel Prize in Physics in 2010.

Graphene can, in the presence of a superconductor, acquire superconducting properties by means of the proximity effect [9]. This, along with the relativistic behavior of the graphene

Stellenbosch University http://scholar.sun.ac.za

quasi-particles, prompted investigations into graphene systems with a normal-superconductor interface [10]. The prospect of incorporating some aspects of relativity and superconductivity in a real material is something that was not possible before the discovery of graphene [9].

Along with the linear dispersion relation in the low-energy regime, the excitations of graphene can only exist in two distinct regions of momentum space at low energies - the so-called valleys. Physical applications like valley-valves and valley filters, electronic devices that would filter out and utilise valley polarisation, were postulated [11]. However, the construction of such a device relies on a way that particles can be forced, in a reliable way, to occupy only a single valley [11]. The proposed way to do this in [11] was shown in [12] to run into difficulties. Suprisingly, even smooth potentials can be sources of intervalley scattering and the conductance of the device depends on the exact boundary details of a given graphene sheet, specifically the number of hexagons across the sample. This is something that is very difficult to manipulate in a precise way in a real graphene sample.

In the light of the above we would like to investigate ways in which different dynamics can be given to the different valleys. Distorting a graphene sheet gives rise to what is called a pseudo magnetic field [13]. This is a momentum augmenting term, similar to that of a magnetic field, that has an opposite sign in the two valleys. Consequently, edge transport should be in opposite directions for the two valleys. The study of a graphene sheet subject to a pseudo magnetic field will thus be our point of departure.

This study will aim to investigate the effect of lattice distortions and see specifically whether or not stable valley-specific excitation states can be created in a graphene lattice subject to a pseudo magnetic field. A superconductor, which is sensitive to the valley index of excitations, will be added to the system and the effects of this in conjunction with the pseudo magnetic field investigated. In the process we will be required to formulate numerical means to calculate conductance. Edge transport in a system consisting of a graphene sheet, subject to a magnetic field, connected to a superconductor has been investigated before [10] and we will supplement this study with a numerical analysis. We will then finally turn our attention to the edge transport problem of a distorted graphene sheet connected to a superconductor.

At all times we will be wary of the fact that graphene is a difficult material to manufacture and the way the sheets are manipulated will be considered carefully as well as the non-perfect

Stellenbosch University http://scholar.sun.ac.za

nature of boundaries and graphene samples. This will ensure that the study stays as close as possible to what is physically realisable.

Stellenbosch University http://scholar.sun.ac.za

CHAPTER 2
A Discussion of the Basics

In this chapter we will be studying some of the basic properties of graphene, much of which is available in the literature (especially [9] and [13] are good reviews). Though this information is present in the literature, it is stated here for the sake of establishing the notation of the text and to identify those aspects of graphene that will be relevent to later sections.

2.1 The structure of graphene

The carbon atoms in graphene are arranged in a two dimensional honeycomb lattice. A honeycomb lattice is a bipartite lattice and consists of two triangular sublattices, denoted as A and B. These are arranged such that each A (B) site is located at the centroid of the triangle formed by its three nearest neighbours which are all from the B (A) sublattice. For a picture of this lattice see Fig. (2.1). The unit cell of graphene is also indicated in Fig. (2.1) and a close-up

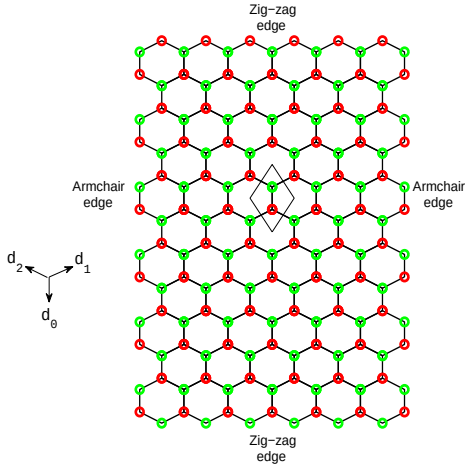

Figure 2.1: A graphene flake with two zig-zag and two armchair edges. Atoms from the A (B) sublattice are coloured green (red). A diamond-shaped unit cell is also indicated along with the vectors $\vec{d_0}$, $\vec{d_1}$ and $\vec{d_2}$, that connect an atom on the A sublattice to its nearest neighbours on the B sublattice.

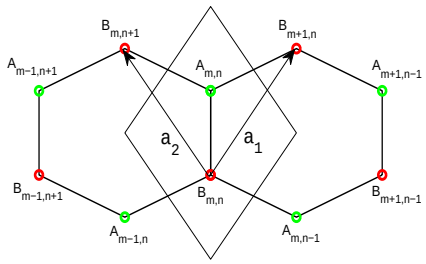

Figure 2.2: Two hexagons centered around the unit cell at position $\vec{r}_{mn}$ in the graphene lattice which shows the labelling scheme for atoms in the lattice after making use of the lattice vectors $\vec{a_1}$ and $\vec{a_2}$.

Stellenbosch University http://scholar.sun.ac.za

picture in Fig. (2.2). The position of a given unit cell is given by $\vec{r}_{mn} = m\vec{a}_1 + n\vec{a}_2$, where m and n are integers and the lattice vectors $\vec{a}_1$ and $\vec{a}_2$ are equal in length (defined as a) and make an angle of $\frac{\pi}{3}$. The unit cell contains two atoms, one from the A sublattice and one from the B sublattice. Thus the atoms in the graphene lattice are uniquely labelled by the two integers pertaining to the position of the unit cell and a binary index indicating the type of sublattice (m, n, X).

2.2 The graphene tight binding Hamiltonian

Graphene, or any lattice that one may consider, is actually a non-tractable many-body problem since each atom has several electrons which can occupy many different energy levels of the individual atoms. Furthermore these electrons interact with the electrons of all the other atoms in the lattice. We need to consider reasonable approximations that will provide us with a model that is analytically tractable and that is still physically sensible.

This is possible since graphene, as mentioned before, is a carbon lattice. A neutral carbon atom has six electrons of which four are valence electrons. Three of these, which one can check by referring to Fig. (2.1), are necessary to form bonds with other carbon atoms in the graphene lattice. The approximation we will be employing, known as the tight binding approximation [14], is that the electrons involved in the interatomic bonds are bound tightly and are not free to move around the lattice. The same holds for the two non-valence electrons and they are approximated to be bound tightly in the inner shell.

This approximation thus only allows one of the electrons of each carbon atom to move around the lattice. The system needs to be simplified a bit further, though, since this free electron can still occupy any one of infinitely many energy levels on a given carbon atom. A second approximation is made, namely that these free electrons are only allowed to occupy the lowest available valence energy level of each carbon atom.

This approximation should be valid at sufficiently low temperatures and is still a very accurate approximation of the full many-body problem.

The free electrons are clearly still allowed to move from one atom to another. Qualitatively, considering that these electrons are forced to occupy the lowest available valence energy level on the carbon atoms, one can think of the overlap of the orbitals as an indication of how likely it is

Stellenbosch University http://scholar.sun.ac.za

for an electron to move from one atom to the next. The idea is shown schematically in Fig. (2.3).

Clearly it is far more likely for electrons to hop to nearest neighbours than to any other atoms

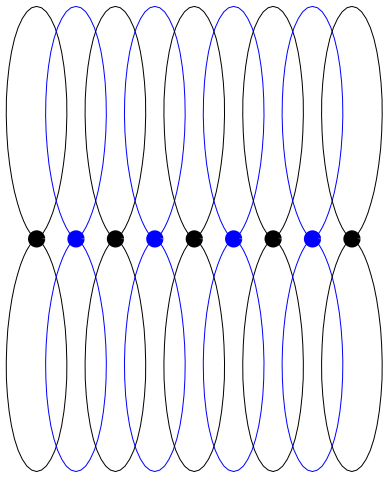

Figure 2.3: An illustration of the tight binding idea in one dimension. The p-orbitals of atoms are coloured by blue and black alternately. The area of the regions where these overlap is an indication of how probable it is for an electron to move to the orbital of a nearest neighbour atom.

that are further away. Indeed, for the purposes of this investigation we will only be considering nearest neighbour hopping, motivated by studies [13] that have shown that the amplitude for next nearest neighbour hopping is smaller than nearest neighbour hopping by a factor between 5 and 50.

The explicit form of the nearest neighbour tight binding Hamiltonian, in the absence of an external potential or magnetic field, is then

$$\begin{aligned} H &= \Sigma_{mn}\, E_0 \left(|m,n,A\rangle \langle m,n,A| + |m,n,B\rangle \langle m,n,B|\right) \\ &\quad + \Sigma_{mn}\, t \left(|m,n,B\rangle + |m+1,n,B\rangle + |m,n+1,B\rangle\right) \langle m,n,A| + h.c. \end{aligned} \tag{2.1}$$

where $|m,n,X\rangle$ is the single electron ket of the X sublattice in the unit cell at position $\vec{r}_{mn}$, t is the hopping matrix amplitude (assumed to be constant in all directions for now) and $h.c.$ refers to the hermitian conjugate of the previous terms. Restrictions may be placed on the allowed values of m and n in order to incorporate the boundaries of the graphene lattice. One can verify the above form of the Hamiltonian by noting, in Fig. (2.2), that an electron can move to an

Stellenbosch University http://scholar.sun.ac.za

atom on the A sublattice from a nearest neighbour B sublattice either in the same unit cell or the unit cells that are $\vec{a}_1$ and $\vec{a}_2$ away.

Since the on-site term has the same energy at each site (the energy of the lowest available valence level), one can simply use as convention that all energies are measured relative to E_0 and effectively set this term to zero.

$$H = \Sigma_{mn}\, t\left(|m,n,B\rangle + |m+1,n,B\rangle + |m,n+1,B\rangle\right)\langle m,n,A| + h.c. \tag{2.2}$$

The Hamiltonian (2.2) will be the starting point of all subsequent analysis.

2.3 Plane wave expansion

Since the Hamiltonian (2.2) is translationlly invariant, it is convenient to make a plane wave expansion. We define

$$\left|\vec{k},X\right\rangle = \frac{1}{N}\Sigma_{uv}e^{i\vec{k}\cdot\vec{r}_{uv}}\left|u,v,X\right\rangle \tag{2.3}$$

where N is a normalisation constant that ensures that $\left\langle \vec{k},X\right|\left.\vec{k},X\right\rangle = 1$. Since the complex exponential is a periodic function this labelling scheme does not label states uniquely and we need to restrict ourselves to the region in momentum space where it does. This is the so-called Brillouin zone.

The reciprocal lattice vectors $\vec{b}_1$ and $\vec{b}_2$ are defined through

$$\vec{a}_i \cdot \vec{b}_j = 2\pi\delta_{ij} \tag{2.4}$$

Points in momentum space that differ by a reciprocal lattice vector (more generally any integer combination of reciprocal lattice vectors) label the same state in momentum space.

At this point it is convenient to fix the orientation of the coordinate system. We choose the y-axis to run along the line connecting the A and B sites in the unit cell, pointing from the B site to the A site, see Fig. (2.4). It is important to realise that in all subsequent calculations these axes will refer to this specific orientation of the graphene lattice. This choice of axes then yields

$$\vec{a}_1 \;=\; a\left(\frac{1}{2}\widehat{x} + \frac{\sqrt{3}}{2}\widehat{y}\right) \tag{2.5}$$

Stellenbosch University http://scholar.sun.ac.za

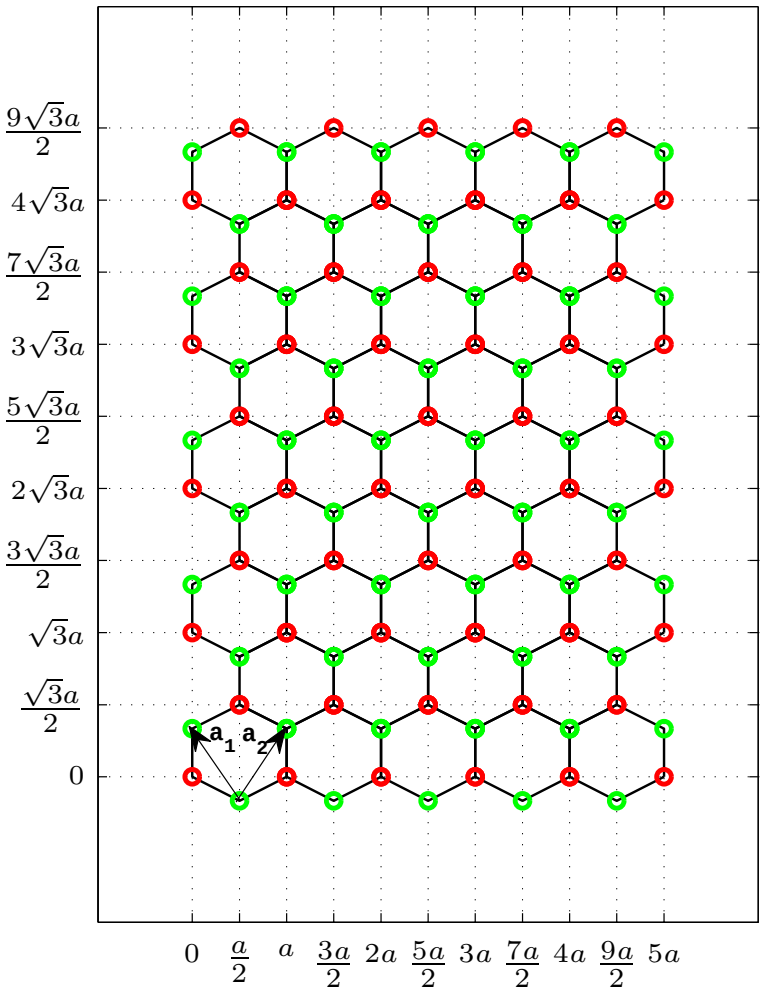

Figure 2.4: Our choice of axes from this point onwards. The length of the lattice vectors, $\vec{a}_1$ and $\vec{a}_2$ as indicated, is defined as a and consequently the interatomic spacing $d = \frac{a}{\sqrt{3}}$.

$$\vec{a}_2 = a\left(-\frac{1}{2}\hat{x} + \frac{\sqrt{3}}{2}\hat{y}\right) \tag{2.6}$$

where a is the lattice spacing, the length of the lattice vectors. Furthermore one also yields from (2.4) that

$$\vec{b}_1 = \frac{2\pi}{a}\left(\hat{x} + \frac{1}{\sqrt{3}}\hat{y}\right) \tag{2.7}$$

Stellenbosch University http://scholar.sun.ac.za

$$\vec{b}_2 = \frac{2\pi}{a}\left(-\widehat{x} + \frac{1}{\sqrt{3}}\widehat{y}\right) \tag{2.8}$$

Fig. (2.5) shows the Brillouin zone for graphene. Points on opposite edges of the Brillouin zone are seperatede by a reciprocal lattice vector and therefore refer to the same state in k-space. From any Brillouin zone corner, two other corners can be reached by reciprocal lattice vectors. Thus the set of six corners are partitioned into two sets off three (indicated by different colors in Fig. (2.5)). The three members of each set refer to the same state in k-space. There are therefore only two independent states in k-space associated with the six corners. We use the convention of labeling one of these states with the k-vector $\vec{K} = -\frac{4\pi}{3a}\hat{x}$ (the vector from the origin to the left-most corner of the Brillouin zone) and the other with $\vec{K}' = \frac{4\pi}{3a}\hat{x}$ (the vector from the origin to the right-most corner).

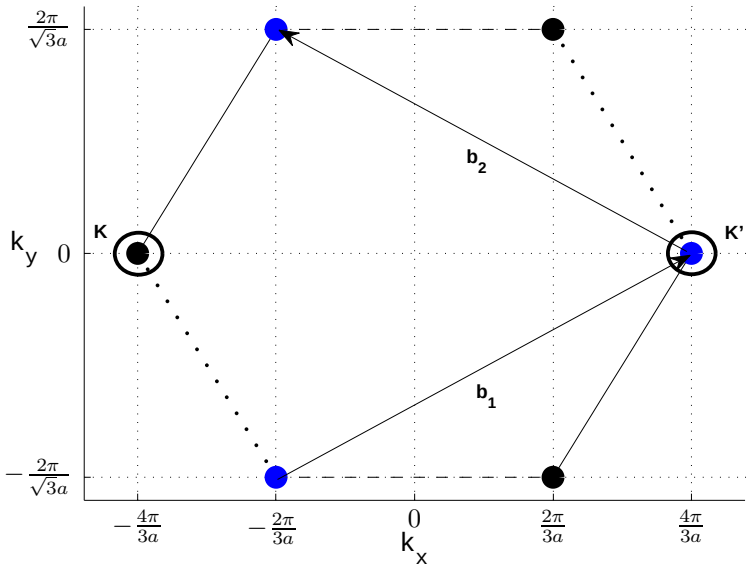

Figure 2.5: The Brillouin zone of graphene with the reciprocal lattice vectors, $\vec{b}_1$ and $\vec{b}_2$ indicated. Equivalent sides of the Brillouin zone are drawn the same way (line, dotted line or dots) and equivalent corners are made the same colour. The two non-equivalent corners chosen for this text, $\vec{K}$ and $\vec{K}'$, are circled.

2.4 Dispersion relation for an infinite graphene sheet

The plane wave expansion allows us to diagonalise the graphene tight binding Hamiltonian for the case of an infinite graphene sheet because of translational invariance. This becomes explicitly clear when the Hamiltonian is cast into the plane wave basis. The associated basis

Stellenbosch University http://scholar.sun.ac.za

transformation can be implemented since the states labelled by plane waves form a basis so that

$$\sum_{\vec{k}} \sum_{X} \left|\vec{k}, X\right\rangle \left\langle \vec{k}, X\right| = I \tag{2.9}$$

where the summation must be carried out over the Brillouin zone for $\vec{k}$ and A and B for the X summation. Making the associated basis transformation of the Hamiltonian then yields

$$\begin{aligned} H &= H \sum_{\vec{k}} \sum_{X} \left|\vec{k}, X\right\rangle \left\langle \vec{k}, X\right| \\ &= \frac{t}{N} \sum_{\vec{k}} \sum_{mn} e^{i\vec{k}\cdot\vec{r}_{mn}} \left(|m,n,B\rangle + |m+1,n,B\rangle + |m,n+1,B\rangle\right) \left\langle \vec{k}, A\right| + h.c. \\ &= t \sum_{\vec{k}} \left(1 + e^{-i\vec{k}\cdot\vec{r}_{10}} + e^{-i\vec{k}\cdot\vec{r}_{01}}\right) \left|\vec{k}, B\right\rangle \left\langle \vec{k}, A\right| + h.c. \end{aligned} \tag{2.10}$$

The translational invariance of the infinite graphene sheet is explicitly used when the summation index is changed from step two to three. This is not possible in a finite graphene sheet where boundaries are present and each unit cell is unique with regard to its position relative to the boundaries. The summation index cannot be changed in such a case. The Hamiltonian (2.10) is very close to diagonal form and only a diaganolisation in the sublattice degree of freedom is still necessary. An eigenket of the Hamiltonian can at most be a linear combination of eigenkets of both sublattices. Thus we make the ansatz that

$$|\Psi\rangle = \alpha \left|\vec{k}, A\right\rangle + \beta \left|\vec{k}, B\right\rangle \tag{2.11}$$

is an eigenfunction of the Hamiltonian. By working further with the ansatz one finds from eq. (2.10)

$$\begin{aligned} H|\Psi\rangle &= \alpha t \left(1 + e^{-i\vec{k}\cdot\vec{a}_1} + e^{-i\vec{k}\cdot\vec{a}_2}\right) \left|\vec{k}, B\right\rangle + \beta t \left(1 + e^{i\vec{k}\cdot\vec{a}_1} + e^{i\vec{k}\cdot\vec{a}_2}\right) \left|\vec{k}, A\right\rangle \\ \Rightarrow E\beta &= t \left(1 + e^{-i\vec{k}\cdot\vec{a}_1} + e^{-i\vec{k}\cdot\vec{a}_2}\right) \alpha \qquad (2.12) \\ E\alpha &= t \left(1 + e^{i\vec{k}\cdot\vec{a}_1} + e^{i\vec{k}\cdot\vec{a}_2}\right) \beta \qquad (2.13) \end{aligned}$$

which implies that

$$E^2 = t^2 \left(1 + e^{-i\vec{k}\cdot\vec{a}_1} + e^{-i\vec{k}\cdot\vec{a}_2}\right) \left(1 + e^{i\vec{k}\cdot\vec{a}_1} + e^{i\vec{k}\cdot\vec{a}_2}\right) \tag{2.14}$$

Stellenbosch University http://scholar.sun.ac.za

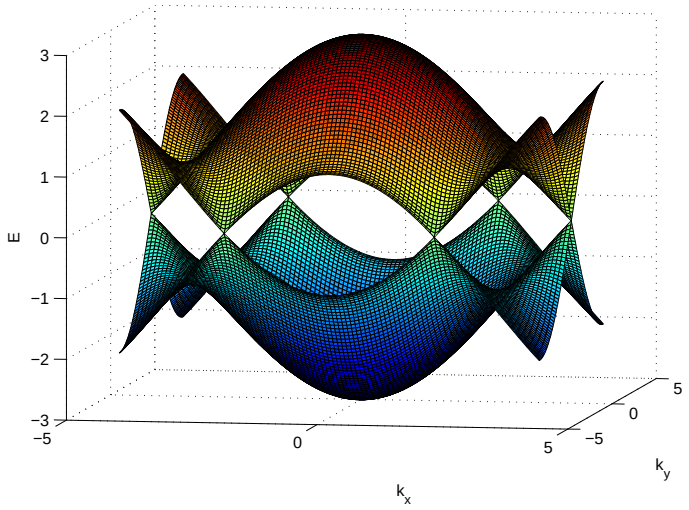

Figure 2.6: The bulk (far away from the edges) spectrum of graphene plotted over an area of k-space that contains one Brillouin zone

The dispersion relation, eq. (2.14), is plotted in Fig. (2.6). The dispersion relation is symmetric around $E = 0$. Our derivation for the spectrum is only strictly valid for an infinite graphene sheet, but we may approximate the bulk spectrum (i.e. far way from the boundaries) by the spectrum of the infinite graphene sheet.

2.5 The Dirac Equation

From Fig. (2.6) it is clear that all states with energies $|E| \ll t$ have wave-vectors $\vec{k}$ that are close to one of the corners of the Brillouin zone. The two unique corners here are labelled $\vec{K}$ and $\vec{K}'$. We refer to these two corners as the valleys. Due to degeneracy our full wave function may be a linear combination of states with both these wave-vectors (or from both valleys), i.e.

$$\Psi_X(\vec{r}_{mn}) = e^{i\vec{K}\cdot\vec{r}_{mn}}\psi_X^+(\vec{r}_{mn}) + e^{-i\vec{K}\cdot\vec{r}_{mn}}\psi_X^-(\vec{r}_{mn}) \tag{2.15}$$

where $\psi_X^{\pm}(\vec{r}_{mn})$ are the amplitudes associated with each valley and X is the index referring to sublattice (either A or B). Note that we allow for these amplitudes to differ from unit cell to unit cell, which is the most general case.

We will now represent the Hamiltonian in the position basis. For this purpose we postulate smooth wave functions $\psi_X^{\pm}(\vec{r})$ that interpolate between discrete amplitudes on the lattice, i.e. $\psi_X^{\pm}(\vec{r} = \vec{r}_{mn}) = \psi_X^{\pm}(\vec{r}_{mn})$. We will solve for each valley independently. By taking the Hamiltonian (2.2) and representing it in the position basis one finds two equations - one for each of the

Stellenbosch University http://scholar.sun.ac.za

sublattices. The equation for the A sublattice reads

$$\begin{aligned}
\langle \vec{r}_{mn} | H | m,n,A \rangle &= e^{\pm i\vec{K}\cdot\vec{r}_{mn}} E\psi_A^{\pm}(\vec{r}_{mn}) \\
&= te^{\pm i\vec{K}\cdot\vec{r}_{mn}}\psi_B^{\pm}(\vec{r}_{mn}) + te^{\pm i\vec{K}\cdot\vec{r}_{m+1,n}}\psi_B^{\pm}(\vec{r}_{m+1,n}) + te^{\pm i\vec{K}\cdot\vec{r}_{m,n+1}}\psi_B^{\pm}(\vec{r}_{m,n+1}) \\
\Rightarrow E\psi_A^{\pm}(\vec{r}_{mn}) &= t\psi_B^{\pm}(\vec{r}_{mn}) + te^{\pm i\frac{2\pi}{3}}\psi_B^{\pm}(\vec{r}_{m+1,n}) + te^{\mp i\frac{2\pi}{3}}\psi_B^{\pm}(\vec{r}_{m,n+1}) \qquad (2.16)
\end{aligned}$$

and also

$$E\psi_B^{\pm}(\vec{r}_{mn}) = t\psi_A^{\pm}(\vec{r}_{mn}) + te^{\mp i\frac{2\pi}{3}}\psi_A^{\pm}(\vec{r}_{m-1,n}) + te^{\pm i\frac{2\pi}{3}}\psi_A^{\pm}(\vec{r}_{m,n-1}) \qquad (2.17)$$

By now making a Taylor expansion around the point $\vec{r}_{mn}$ of eqs. (2.16), (2.17) and keeping everything up to the first order term one finds

$$\begin{aligned}
E\psi_A^{\pm}(\vec{r}_{mn}) &= t\left(e^{\pm i\frac{2\pi}{3}}\vec{a}_1\cdot\partial_{\vec{r}} + e^{\mp i\frac{2\pi}{3}}\vec{a}_2\cdot\partial_{\vec{r}}\right)\psi_B^{\pm}(\vec{r})\Big|_{\vec{r}=\vec{r}_{mn}} \\
&= \frac{\sqrt{3}at}{2\hbar}\left(\pm p_x - ip_y\right)\psi_B^{\pm}(\vec{r})\Big|_{\vec{r}=\vec{r}_{mn}} \qquad (2.18)
\end{aligned}$$

and

$$\begin{aligned}
E\psi_B^{\pm}(\vec{r}_{mn}) &= t\left(-e^{\mp i\frac{2\pi}{3}}\vec{a}_1\cdot\partial_{\vec{r}} - e^{\pm i\frac{2\pi}{3}}\vec{a}_2\cdot\partial_{\vec{r}}\right)\psi_A^{\pm}(\vec{r})\Big|_{\vec{r}=\vec{r}_{mn}} \\
&= \frac{\sqrt{3}at}{2\hbar}\left(\pm p_x + ip_y\right)\psi_A^{\pm}(\vec{r})\Big|_{\vec{r}=\vec{r}_{mn}} \qquad (2.19)
\end{aligned}$$

Where $p_x = -i\hbar\frac{\partial}{\partial x}$ and $p_y = -i\hbar\frac{\partial}{\partial x}$ are the x and y components of the momentum operator. By making use of the Pauli spin matrices

$$\sigma_x = \begin{pmatrix} 0 & 1 \\ 1 & 0 \end{pmatrix} \quad \sigma_y = \begin{pmatrix} 0 & -i \\ i & 0 \end{pmatrix} \quad \sigma_z = \begin{pmatrix} 1 & 0 \\ 0 & 1 \end{pmatrix} \quad \sigma_0 = \begin{pmatrix} 1 & 0 \\ 0 & 1 \end{pmatrix} \qquad (2.20)$$

one obtains the so-called valley isotropic Dirac equation

$$H\Phi = E\Phi = v\begin{pmatrix} \vec{\sigma}\cdot\vec{p} & 0 \\ 0 & \vec{\sigma}\cdot\vec{p} \end{pmatrix}\Phi = v\ \tau_0\otimes\vec{\sigma}\cdot\vec{p}\,\Phi \qquad \Phi = \begin{pmatrix} \psi_A^+ \\ \psi_B^+ \\ -\psi_B^- \\ \psi_A^- \end{pmatrix} \qquad (2.21)$$

Stellenbosch University http://scholar.sun.ac.za

where $v = \frac{\sqrt{3}at}{2\hbar}$. This will be the standard way the Hamiltonians present in the text will be expressed.

Eq. (2.21) is the Dirac equation for relativistic particles except that the speed of light, c, is replaced by the constant v, which is much smaller. This is one of the qualitative reasons why graphene, at low excitation energies, is such an interesting material to investigate, since the particles have properties of relativistic particles, though at a much reduced speed. However, it must be emphasised that this Hamiltonian acts on spinors that have a completely different meaning to the spinors in relativistic quantum mechanics.

2.6 Terminated lattice boundary conditions

Though we now have a differential equation that can describe the wave functions of electrons in graphene, the statement in eq. (2.21) is not complete. The reason for this is that we have not specified a boundary condition for the equation. The type that will be introduced here, and used most often in the literature (see [10], [9], [13]) is that of the terminated lattice or insulating edge i.e. where the wave function is restricted to exist on the graphene lattice - this is something which must be enforced on a finite graphene lattice. We will begin by writing down the general form of the boundary conditions from general considerations and then look at specific cases, namely the armchair and zig-zag edge. This is not a derivation, but an explanation of why the boundary condition takes its specific form. In all of the discussion that is to follow, boundary conditions are introduced in the following way [15]

$$\Phi|_b = M\ \Phi|_b \tag{2.22}$$

where b refers to the boundary of the graphene lattice. M at this point is still a general 4×4 matrix. Following the example of [10] and [9], by focusing on physical restrictions, one can deduce the sensible insulating edge boundary matrices in the following way. Firstly, the states we will be working with by solving (2.21) will be of the form $\Phi^T = \left(\psi_A^+, \psi_B^+, -\psi_B^-, \psi_A^-\right)$. The time reverse of a state $\psi_X^+ e^{i\vec{K}\cdot\vec{r}} + \psi_X^- e^{-i\vec{K}\cdot r}$ is reached by taking the complex congugate and is $(\psi_X^+)^* e^{-i\vec{K}\cdot\vec{r}} + (\psi_X^-)^* e^{i\vec{K}\cdot r}$. Consequently, in the framework of the four-vectors Φ, the time reverse

Stellenbosch University http://scholar.sun.ac.za

operator should be

$$T\begin{pmatrix}\psi_A^+\\ \psi_B^+\\ -\psi_B^-\\ \psi_A^-\end{pmatrix}=\begin{pmatrix}(\psi_A^-)^*\\ (\psi_B^-)^*\\ -(\psi_B^+)^*\\ (\psi_A^+)^*\end{pmatrix}\quad\Rightarrow\quad T=\begin{pmatrix}0&0&0&1\\0&0&-1&0\\0&-1&0&0\\1&0&0&0\end{pmatrix}C=-(\tau_y\otimes\sigma_y)C \tag{2.23}$$

where C is the operator affecting complex conjugation and the τ's are a second set of Pauli spin matrices. Unless there is a local magnetisation at the edge, one would expect the boundary condition to obey time reversal symmetry, so that M should commute with T i.e. $MT = TM$. Secondly, the matrix M should be hermitian and unitary. Lastly, no current may escape through the edges so that the matrix M must anti-commute with the particle current operator $\vec{J} = v\tau_0\otimes\vec{\sigma}$ (see [10]) projected onto the vector pointing outward from the boundary

$$M(\vec{n}\cdot\vec{J})+(\vec{n}\cdot\vec{J})M=0 \tag{2.24}$$

where $\vec{n}$ is perpendicular to the boundary, pointing outward and $\vec{n_\perp}$.

The most general matrix M that satisfies all these conditions is given by [10]

$$M=(\vec{\nu}\cdot\tau)\otimes(\vec{n}_\perp\cdot\sigma) \tag{2.25}$$

where $\vec{\nu}$ and $\vec{n}_\perp$ are general 3-component, real unit vectors. $\vec{\nu}$ has no restrictions, but $\vec{n}_\perp$ must be normal to $\hat{n}$, the vector pointing perpendicularly outward from the boundary. It must be noted here that the Pauli spin matrices denoted by τ act on the valley degree of freedom while those denoted σ act on the sublattice degree of freedom.

Though this casts some light on how to interpret the boundary condition matrix M one does not become any wiser with regards to how to ultimately choose the boundary condition for a given physical situation. Two situations, both of which arise from terminating the graphene lattice, will now be looked at explicitly.

2.6.1 The armchair edge

When both atoms from the A and B sublattice are present at the boundary, forming a sort of armchair-like shape that repeats along the edge, this is referred to as an armchair edge, see Fig. (2.1). What one will require is for the wave function on both sublattices to vanish at the

Stellenbosch University http://scholar.sun.ac.za

boundary, since a row of atoms containing both the A and B sublattice is missing at the edge.

$$\psi_X^+ e^{i\vec{K}\cdot\vec{r}} + \psi_X^- e^{-i\vec{K}\cdot\vec{r}} = 0 \qquad X = A \text{ and } B \tag{2.26}$$

where the point $\vec{r}$ lies on the boundary of the sample. This implies

$$\psi_X^+ = -\psi_X^- e^{-2i\vec{K}\cdot\vec{r}} \tag{2.27}$$

The implication of this is that the matrix M may only have off-diagonal elements in all four blocks. This will imply that both $\vec{\nu}$ and $\vec{n}_\perp$ may not have a z-component. The vector $\vec{n}_\perp$ can be easily parametrised by

$$\vec{n} = \cos(\alpha)\hat{x} + \sin(\alpha)\hat{y} \quad \Rightarrow \quad \vec{n}_\perp = \cos(\alpha + \frac{\pi}{2})\hat{x} + \sin(\alpha + \frac{\pi}{2})\hat{y} \tag{2.28}$$

where the vector $\vec{n}$ is orthogonal to the graphene lattice pointing outward. The vector $\vec{\nu}$ must be parametrised in general

$$\vec{\nu} = \cos(\theta)\hat{x} + \sin(\theta)\hat{y} \quad \text{i.e.} \quad \vec{\nu}\cdot\vec{\hat{z}} = 0. \tag{2.29}$$

This then leads to the boundary matrix M being

$$M = \begin{pmatrix} 0 & 0 & 0 & -e^{-i(\theta+\alpha-\frac{\pi}{2})} \\ 0 & 0 & e^{-i(\theta-\alpha-\frac{\pi}{2})} & 0 \\ 0 & e^{i(\theta-\alpha-\frac{\pi}{2})} & 0 & 0 \\ -e^{i(\theta+\alpha-\frac{\pi}{2})} & 0 & 0 & 0 \end{pmatrix} \tag{2.30}$$

which is consistent with the general considerations discussed above.

2.6.2 The zig-zag edge

The zig-zag edge arises when atoms from just one of the sublattices are missing at the edge (a row of atoms are either missing all A sublattice atoms or all B sublattice atoms). This time one requires the wave function of the missing sublattice to disappear at the boundary, in both valleys

$$\psi_X^+ = \psi_X^- = 0, \quad X = A \text{ or } B \tag{2.31}$$

Stellenbosch University http://scholar.sun.ac.za

where X will be A or B depending on which type of atom is missing from the edge. This we can rewrite as

$$\psi_X^{\pm} = -\psi_X^{\pm} \tag{2.32}$$

The way this information can be put into our boundary condition matrix is

$$M = \begin{pmatrix} 1 & 0 & 0 & 0 \\ 0 & -1 & 0 & 0 \\ 0 & 0 & -1 & 0 \\ 0 & 0 & 0 & 1 \end{pmatrix} \quad \text{or} \quad M = \begin{pmatrix} -1 & 0 & 0 & 0 \\ 0 & 1 & 0 & 0 \\ 0 & 0 & 1 & 0 \\ 0 & 0 & 0 & -1 \end{pmatrix} \tag{2.33}$$

for the missing atom type being B (in the first parametrisation) or A (in the second parametrisation). One can rewrite the above condition by parametrising as

$$\vec{\nu} = \pm\hat{z} \qquad \vec{n}_{\perp} = \hat{z} \tag{2.34}$$

where the plus is used when atoms from the A sublattice are missing and the minus is used when atoms from the B sublattice are missing.

2.6.3 Final Remarks

Though we have derived the above expressions for certain boundary conditions and consequently found relations for the different valley wave functions, it is necessary to remember that the boundary condition follow from the restrictions on the full wave function

$$\Psi_X = \psi_X^{+} e^{i\vec{K}\cdot\vec{r}} + \psi_X^{-} e^{-i\vec{K}\cdot\vec{r}} \tag{2.35}$$

and not from restrictions of the individual valleys ψ_X^{+} and ψ_X^{-}. If we may write the boundary condition in a form that places restrictions on the individual valleys, this will be a special case of the boundary condition.

2.7 Adding electromagnetic fields and the Quantum Hall Effect

Electromagnetic fields (see [9]) are added to the Hamiltonian in the usual way

$$H\Phi = E\Phi = v \begin{pmatrix} \vec{\sigma}\cdot(\vec{p} + e\vec{A}(\vec{r})) + I_2 U(\vec{r}) & 0 \\ 0 & \vec{\sigma}\cdot(\vec{p} + e\vec{A}(\vec{r})) + I_2 U(\vec{r}) \end{pmatrix} \Phi \tag{2.36}$$

Stellenbosch University http://scholar.sun.ac.za

where $\vec{A}(\vec{r})$ is a vector potential of some magnetic field, $U(\vec{r})$ is a scalar potential and I_2 is the 2×2 unit matrix. The electrostatic potential can be derived by adding a position dependence to E_0 in eq. (2.1) in the derivation of the Dirac equation. The vector potential, $\vec{A}$, can be derived by giving the hopping amplitudes an additional phase gain, i.e. $t \to te^{-i\frac{e}{\hbar}\int_r d\vec{r}.\vec{A}}$, where the integral goes over the path between atoms with the direction of the hop taken into account by the vector $\vec{r}$. The addition of both an electrostatic potential and magnetic field are just extentions of our previous derivation of the Dirac equation and are not done explicitly in this text.

Adding a strong magnetic field at low temperature to any two-dimensional sample is known to give rise to the quantum Hall effect. This is the effect that the Hall conductance takes on quantised values. In the integer quantum Hall effect [16], which is what we will be considering, the Hall conductivity is quantised in integer multiples of $\frac{e^2}{\hbar}$. We will now examine the specifics of the graphene quantum Hall effect as this will play a big part in later analysis.

We now discuss the spectrum and wave functions of a graphene sheet in the presence of a constant magnetic field perpendicular to the sheet. The gauge is chosen as $\vec{A} = By\hat{x}$. We consider the regime $l_m = \sqrt{\frac{\hbar}{eB}} \gg a$ where the Dirac equation is expected to be valid. First we consider an infinite sheet. The equation to solve is

$$E\Phi = v \begin{pmatrix} \vec{\sigma} \cdot (\vec{p} + eBy\hat{x}) & 0 \\ 0 & \vec{\sigma} \cdot (\vec{p} + eBy\hat{x}) \end{pmatrix} \Phi. \tag{2.37}$$

This calculation is a special case of a later calculation in Chapter 5 and only the results are given here. After rescaling energies to $E \to \frac{E}{\sqrt{eB\hbar v^2}}$ and distances to $\vec{r} \to \frac{\vec{r}}{l_m}$ one finds two possible solution functions of (2.37). Each one of the four components of Φ must then be a yet undetermined linear combination of the following two functions

$$\begin{aligned} f_1 &= e^{iqx} e^{-\frac{1}{2}(y-q)^2} H_{\frac{E^2}{2}}(y-q) \\ f_2 &= e^{iqx} P(-\frac{2+E^2}{2}, i\sqrt{2}(y-q)) \end{aligned}$$

where $H(y)$ is the Hermite function and P the parabolic cylinder function. The position and energy arguments of the functions may vary depending on the valley.

The function f_2 is divergent for large positive or negative y, so that these are not allowed solutions in the case of the infinite graphene sheet. The function f_1 is convergent for large positve y

Stellenbosch University http://scholar.sun.ac.za

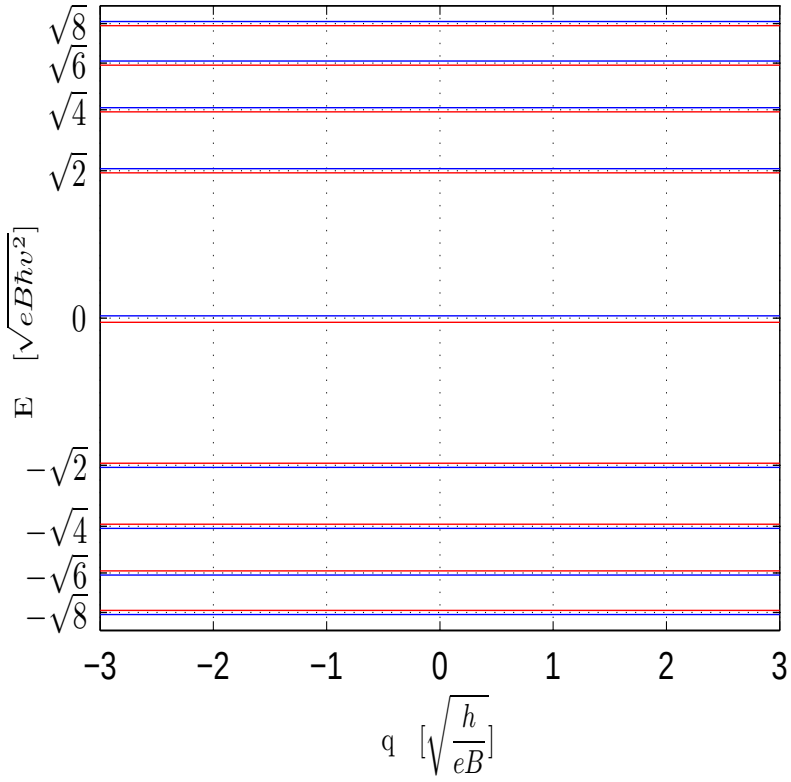

Figure 2.7: The Landau levels in an infinite graphene sheet are quantised like $E = \pm\sqrt{2n}$ for all values of the wave number in the free direction. All levels are valley degenerate where different valleys are coloured blue and red.

for all values of q and E, but it is convergent at large negative y only if $E = \pm\sqrt{2n}$ where n is an integer. It does then converge for all values of q. Thus, for the infinite graphene sheet, the spectrum is shown in Fig. (2.7)

We now consider a graphene sheet that is finite in the y-direction, though still infinite in the x-direction. Specifically the graphene sheet is restricted to $y \in [-\frac{L}{l_m}, \frac{L}{l_m}]$ in rescaled units. Here we do not give a quantitative argument, but rather a qualitative one to guide ones thinking about the problem.

Since we do not run into convergence problems, both f_1 and f_2 are allowed and their linear combination, that satisfies both boundary conditions, simply needs to be chosen appropriately for each value of q. For a given q one will still, however, only find a finite number of solutions. We do not do this calculation explicitly, as we are only interested in the qualitative behavior.

Stellenbosch University http://scholar.sun.ac.za

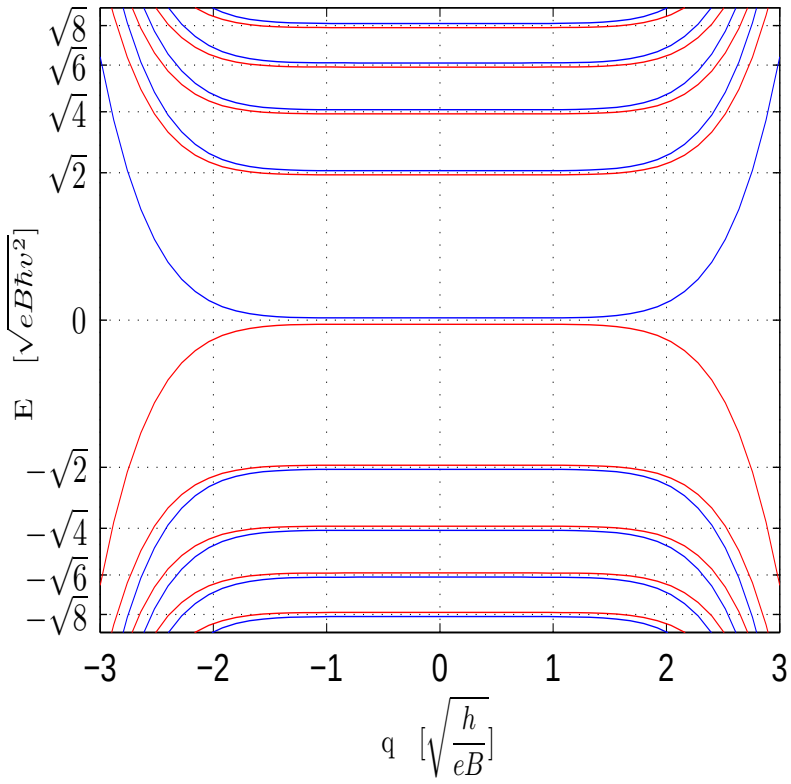

Figure 2.8: The spectrum for a finite graphene sheet deviates from the bulk Landau levels for large values of the wave number in the free direction. All levels except the $n = 0$ level are still valley degenerate and different valleys are coloured blue and red.

Certain edge conditions (like the armchair edge described above) may, in the most general case, split the spectrum for the two valleys slightly. The result is plotted (schematically) in Fig. (2.8).

Since the wave functions are exponentially suppressed (via the $e^{-\frac{1}{2}(y-q)^2}$ term), one may loosely refer to the "position" where or rather "region" wherin certain excitations exist. This is because all modes for a given wave number q, except where $q \approx y$, are exponentially suppressed. Thus certain modes are the dominant excitations in certain regions of the graphene sheet. Clearly, the states with small q are still very similar to those of Fig. (2.7), so that in the bulk (far away from the edge) the bulk Landau levels should be retained, as indicated in Fig. (2.8).

The group velocity of excitations can be extracted from figures like Fig. (2.7) and (2.8) by

Stellenbosch University http://scholar.sun.ac.za

taking the derivative of the excitation energy with regards to wave number i.e.

$$v_{\text{group}} = \frac{1}{\hbar}\frac{dE}{dq} \tag{2.38}$$

Except for a small window around the bulk Landau levels, it is the edge states that are responsible for transport.

Stellenbosch University http://scholar.sun.ac.za

CHAPTER 3
Different Dynamics for the Valleys

In the previous chapter we introduced our labelling scheme of atoms in the graphene lattice which led to a discrete representation where the wave kets are defined for each atom. We used this to derive the spectrum for an infinite graphene sheet. The long wave length limit allowed a continuous spinor representation where wave functions could be defined over the entire two dimensional plane, rather than at discrete lattice points. This is possible in the low energy regime (where the excitation energy is much lower than the hopping amplitude). It was also shown how boundary conditions are applied in the continuous representation (for terminated lattices) and how classic electromagnetic potentials can be added in the continuous picture.

At low energies, states in the bulk are restricted to two small regions of the Brillouin zone, the so-called valleys. Manipulations that we have considered so far, namely adding electrostatic potentials or magnetic fields, affect both valleys equally. In this chapter we will look at additional manipulations, again from existing literature, that can be imposed upon the graphene lattice that will not affect the valleys in identical ways and can bring about different dynamics for the two valleys. We will show how connecting the lattice to a superconductor can expose this experimentally. A short discussion of how to deal with the presence of the superconductor and some of the kinematics it induces is also discussed.

We begin by discussing the effect of lattice distortions, as described, for instance, in [13].

3.1 Lattice Distortions and the Pseudo Magnetic Field

By distorting the graphene lattice geometrically (this can be done by stretching or bending the lattice), the interatomic spacing may be varied from atom to atom, as indicated in Fig. (3.1). The result of this is that the overlap between neighbouring electron orbitals may vary over the extent of the grapene lattice and thus the hopping amplitudes may vary (unlike eq. (2.2)). The resulting Hamiltonian (which can be found by augmenting (2.2) appropriately) is then

$$H = \Sigma_{mn} \ \left(t_0^{mn} \left|m,n,B\right\rangle + t_1^{mn} \left|m+1,n,B\right\rangle + t_2^{mn} \left|m,n+1,B\right\rangle\right) \left\langle m,n,A\right| + h.c. \tag{3.1}$$

where the hopping amplitude's dependance on unit cell, and thus position, must be noted. We use t_i to indicate the hopping amplitude in the direction of the vector $\vec{d_i}$ from Fig. (2.1). We

Stellenbosch University http://scholar.sun.ac.za

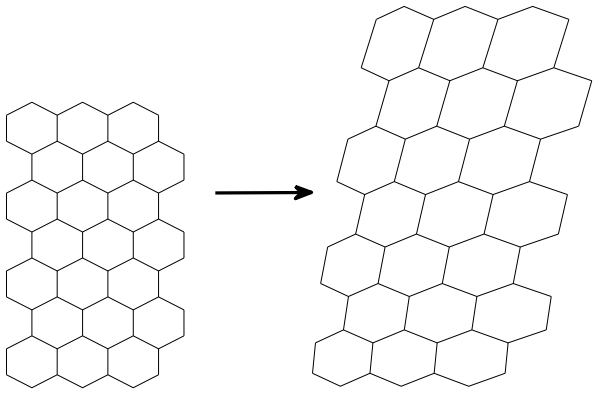

Figure 3.1: A graphene strip that is distorted. In this particular example the graphene strip is stretched in both the x and y directions

assume these lattice distortions to be small so that we may still restrict our analysis to the $\vec{K}$ and $-\vec{K}$ valleys for low energy excitations. This is achieved concretely by writing

$$t_j^{mn} = t(1 + \lambda_j(\vec{r}_{mn})) \tag{3.2}$$

and assuming the λ_j's to be small. Such a perturbation (under the assumption that we can still restrict our analysis to the valleys) does not change the derivation of (2.16) and one can quickly recover

$$\begin{aligned} E\psi_A^{\pm}(\vec{r}_{mn}) &= t_0(\vec{r}_{mn})\psi_B^{\pm} + t_1(\vec{r}_{m+1,n})e^{\pm i\frac{2\pi}{3}}\psi_B^{\pm}(\vec{r}_{m+1,n}) + t_2(\vec{r}_{m,n+1})e^{i\mp\frac{2\pi}{3}}\psi_B^{\pm}(\vec{r}_{m,n+1}) \\ E\psi_B^{\pm}(\vec{r}_{mn}) &= t_0(\vec{r}_{mn})\psi_A^{\pm} + t_1(\vec{r}_{m-1,n})e^{\mp i\frac{2\pi}{3}}\psi_A^{\pm}(\vec{r}_{m-1,n}) + t_2(\vec{r}_{m,n-1})e^{i\pm\frac{2\pi}{3}}\psi_A^{\pm}(\vec{r}_{m,n+1}) \end{aligned}$$

By now making another Taylor expansion in $\vec{r}_{mn}$ and dropping all terms of the form $a\lambda(\vec{\nabla}\psi)$, $a(\vec{\nabla}\lambda)\psi$, $a^2(\vec{\nabla}\psi)^2$ and higher order terms, one arrives (for the valley isotropic form) at

$$H\Phi = E\Phi = v\begin{pmatrix} \vec{\sigma}\cdot(\vec{p}+\vec{\alpha}) & 0 \\ 0 & \vec{\sigma}\cdot(\vec{p}-\vec{\alpha}) \end{pmatrix}\Phi \qquad \Phi = \begin{pmatrix} \psi_A^+ \\ \psi_B^+ \\ -\psi_B^- \\ \psi_A^- \end{pmatrix} \tag{3.3}$$

where

$$\vec{\alpha} = \frac{t}{v}\left[(\lambda_0 - \frac{1}{2}\lambda_1 - \frac{1}{2}\lambda_2)\hat{x} + \frac{\sqrt{3}}{2}(\lambda_1 - \lambda_2)\hat{y}\right]. \tag{3.4}$$

Stellenbosch University http://scholar.sun.ac.za

Basically the effect of lattice distortions of the graphene lattice is very similar to adding a magnetic field to the system (since both augment the momentum operator) with the only difference that the effect is opposite in the two valleys. The resulting system is said to possess a pseudo magnetic field. One can view the effect of the pseudo magnetic field as that of a real magnetic field being applied, but with the different valleys possessing an artificial opposite charge.

It is worthwhile to note that the fact that the valleys are altered differently would imply we cannot choose the pseudo vector potential $\vec{\alpha}$ as freely as would be the case for a real magnetic field. This does make sense since a specific pseudo magnetic field is directly linked to a specific distortion of the graphene lattice. While valleys are uncoupled, it is possible to still perform different transformations in the two valleys and not affect the physical results. Specifically, one would like to perform a transformation in the $\vec{K}$ valley that adds (so that $\vec{\alpha} \to \vec{\alpha} + \vec{\nabla} f$) while subtracting (so that, again, $\vec{\alpha} \to \vec{\alpha} + \vec{\nabla} f$) the desired term in the $\vec{K}'$ valley. However, once the valleys are coupled, for instance via a boundary condition, or if valley dependent perturbations are added to the system, such transformations can start to affect the physical results.

Since the dynamics of excitations from the different valleys are different, richer dynamics may result for the system if we couple the valleys. One way is to introduce an armchair edge to a graphene sheet whilst another is to couple the sheet to a superconductor.

3.2 Superconductivity

If we are to couple the graphene sheet to a superconductor we will make hole excitations (the absence of particle excitations) physically relevant. This is because electrons enter into the superconductor in pairs, so that a hole excitation is left behind in the graphene sheet. This is useful since the coupled particle and hole excitations are from opposite valleys, so that the superconductor is sensitive to valley polarisation.

Inside a superconductor charge is conducted in the form of Cooper pairs (pairs of coupled electrons of opposite spin) [17]. Inside the attached sample charge is conducted by either particle or hole excitations. Consider a graphene sheet with a superconducting electrode on top of it. Superconductivity is induced in the graphene sheet by means of the proximity effect [9] under the electrode, forming two different regions — a superconducting region and a normal region. We will focus on the interfacial region between the normal and superconducting regions in the graphene sheet. In order for a particle that is incident (in the conduction band) on the interface

Stellenbosch University http://scholar.sun.ac.za

to continue into the superconductor (Fig. (3.2) and (3.3)), it needs to couple to an electron from the Fermi sea and continue into the superconductor as a Cooper pair. A hole excitation results in the normal region.

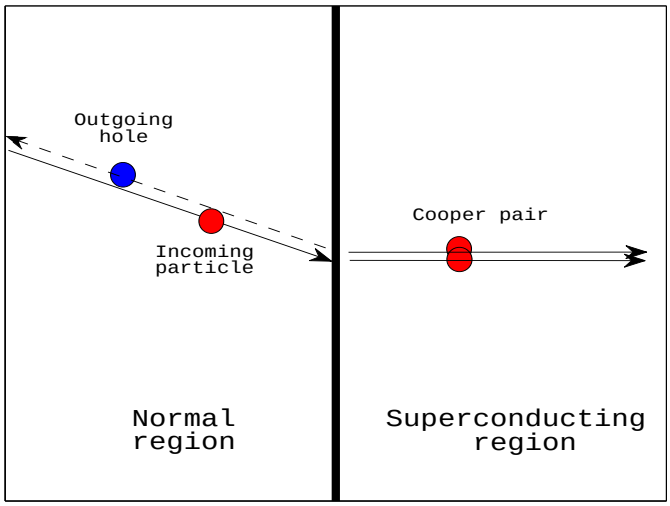

Figure 3.2: An illustration of retro Andreev reflection in which the reflected hole travels in the opposite direction as the incoming particle. The latter enters the superconductor as a Cooper pair

A short mathematical summary of how one deals with such a graphene sheet - superconductor (normal-superconductor or NS) interface is in order. The easiest way to derive the equation that governs the dynamics inside a superconductor (or near a superconductor) is by means of the self-consistent field method, which is explained in [17].

Consider an interacting Hamiltonian of the BCS type

$$\begin{aligned} H &= \sum_{\alpha} \int d^3r \Psi^{\dagger}(\vec{r},\alpha) H_e \Psi(\vec{r},\alpha) \\ &\quad -\frac{1}{2} V \sum_{\alpha\beta} \int_S d^3r \Psi^{\dagger}(\vec{r},\alpha)\Psi^{\dagger}(\vec{r},\beta)\Psi(\vec{r},\alpha)\Psi(\vec{r},\beta) \end{aligned} \tag{3.5}$$

where the indices α, β refer to spin, H_e is the single particle Hamiltonian and the BCS interaction is the quartic interaction term with constant coupling, V. The domain of integration for the second integral is only inside the superconducting region of the system, denoted by S. In order

Stellenbosch University http://scholar.sun.ac.za

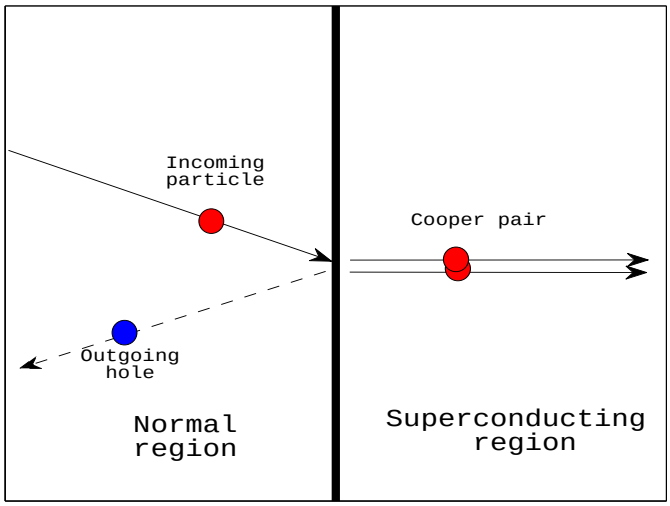

Figure 3.3: An illustration of specular Andreev reflection. Here the angle of the incoming particle is the same as the angle of the outgoing hole

to deal with this object, one approximates the quartic interaction term with an average potential acting only on one particle at a time. The approach is very similar to the Hartree-Fock method, where one makes use of Wick's theorem, defining

$$-V\left\langle \Psi^{\dagger}(\vec{r},\alpha)\Psi(\vec{r},\beta)\right\rangle \equiv \delta_{\alpha\beta}U(\vec{r}) \tag{3.6}$$

and also

$$-V\left\langle \Psi(\vec{r},\downarrow)\Psi(\vec{r},\uparrow)\right\rangle \equiv \Delta(\vec{r}) \tag{3.7}$$

which is non-zero only inside the superconducting region. Given these, one then arrives at the approximate Hamiltonian

$$\begin{aligned} H_{eff} &= \sum_{\alpha}\int d^3r\Psi^{\dagger}(\vec{r},\alpha)H_e\Psi(\vec{r},\alpha) - U(\vec{r})\Psi^{\dagger}(\vec{r},\alpha)\Psi(\vec{r},\alpha) \\ &\quad + \int_S d^3r\Delta(\vec{r})\Psi^{\dagger}(\vec{r},\uparrow)\Psi^{\dagger}(\vec{r},\downarrow) + \Delta^*(\vec{r})\Psi(\vec{r},\downarrow)\Psi(\vec{r},\uparrow). \end{aligned} \tag{3.8}$$

What one notices is that the effective Hamiltonian is slightly problematic in the sense that the wave functions of it will no longer be eigenfunctions of the number operator, though they were for the initial Hamiltonian. This is because of the double creation and double annihilation operator terms. However, the error here then scales like $\frac{1}{\sqrt{N}}$ so that the approximation becomes exact in

Stellenbosch University http://scholar.sun.ac.za

the thermodynamic limit. We must reinterpret the role of these operators. This can be done by finding a set of operators $\gamma_{n\alpha}$ that have

$$\Psi(\vec{r},\uparrow) = \sum_n \left(\gamma_{n\uparrow}u_n(\vec{r}) - \gamma^\dagger_{n\downarrow}v^*_n(\vec{r})\right) \tag{3.9}$$

$$\Psi(\vec{r},\downarrow) = \sum_n \left(\gamma_{n\downarrow}u_n(\vec{r}) + \gamma^\dagger_{n\uparrow}v^*_n(\vec{r})\right) \tag{3.10}$$

and that still obey the fermionic operator anticommutation relations

$$\left\{\gamma^\dagger_{n,\alpha}, \gamma_{n',\alpha'}\right\} = \delta_{n,n'}\delta_{\alpha,\alpha'} \tag{3.11}$$

so that

$$H_{eff} = E_0 + \sum_{n,\alpha} \epsilon_n \gamma^\dagger_{n\alpha}\gamma_{n\alpha} \tag{3.12}$$

This transformation is known as the Bogoliubov transformation. For the effective Hamiltonian one thus has to redefine the creation and annihilation operators i.e. $\gamma^\dagger$ is the new creation and γ the new annihilation operator of excitations. By enforcing eq. (3.12) one then finds

$$\begin{pmatrix} H_e + U(\vec{r}) - \mu(\vec{r}) & \Delta(\vec{r}) \\ \Delta^*(\vec{r}) & -H_e - U(\vec{r}) + \mu(\vec{r}) \end{pmatrix} \begin{pmatrix} u(\vec{r}) \\ v(\vec{r}) \end{pmatrix} = \epsilon \begin{pmatrix} u(\vec{r}) \\ v(\vec{r}) \end{pmatrix} \tag{3.13}$$

the Bogoliubov-de Gennes equation. This needs to be interpreted as $u(\vec{r})$ refering to particle excitations (since it accompanies the original annihilation operator in (3.10)) and $v(\vec{r})$ refering to hole exciations (since it accompanies the original creation operator in (3.10)). μ is the chemical potential of the sample while Δ is called the superconducting gap energy or just the superconductor gap for short.

In the normal region, where Δ is zero, one recovers that the particle and hole excitations remain uncoupled, but in the region of the superconductor these excitations are necessarily coupled.

3.3 A Superconductor as a Boundary Condition

What one would do in an NS interface system is to solve for the wave function in the normal region, solve for the wave function in the superconducting region seperately and then ensure that the wave function is continuous across the NS interface.

In [19] it was shown that, with graphene and specific choices for the superconducting gap (zero

Stellenbosch University http://scholar.sun.ac.za

in the normal region and constant in the superconducting region), it is possible to recast the problem as a boundary condition, in a very similar fashion to the boundary conditions we used for the insulating edge (eq. (2.22)). This has the implication that one only has to solve the differential equation in the normal region and apply the boundary condition as opposed to solving the differential equation in both regions. This followed from a calculation done in [18]. Explicitly, the appropriate boundary condition is

$$\left.\begin{pmatrix}\Phi_e\\ \Phi_h\end{pmatrix}\right|_b = \begin{pmatrix}0 & M_{NS}\\ M_{NS}^\dagger & 0\end{pmatrix}\left.\begin{pmatrix}\Phi_e\\ \Phi_h\end{pmatrix}\right|_b \qquad M_{NS} = \tau_0 \otimes e^{i\phi + i\beta\vec{n}\cdot\sigma} \tag{3.14}$$

where

$$e^{i\beta\vec{n}\cdot\vec{\sigma}} = \begin{pmatrix}\cos(\beta) & ie^{-i\alpha'}\sin(\beta)\\ ie^{i\alpha'}\sin(\beta) & \cos(\beta)\end{pmatrix} \tag{3.15}$$

where the parameter $\beta = \cos^{-1}\left(\frac{\epsilon}{\Delta}\right)$ and the vector $\vec{n} = \cos(\alpha')\hat{x} + \sin(\alpha')\hat{y}$ is perpendicular to the NS interface, pointing from S to N. ϵ is the excitation energy relative to the chemical potential μ. ϕ is the superconducting phase which is not relevant unless more than one superconductors are present (in the case of Josephson junctions in [19]) and will thus be put to zero throughout this work.

A thorough derivation of eq. (3.14) can be found in [18], though it is only spelled out explicitly in [19]. For clarity, important assumptions and conditions under which it was derived is stated here. The system under consideration in that derivation is a regular graphene sheet attached to a superconductor, where the chemical potential μ is assumed constant and the superconductor gap assumes its bulk value of $\Delta(\vec{r}) = \Delta e^{i\phi}$ throughout the superconducting region. This has the Hamiltonian

$$H\begin{pmatrix}\Phi_e\\ \Phi_h\end{pmatrix} = \begin{pmatrix}\tau_0 \otimes (\vec{\sigma}\cdot\vec{p}) - V - \mu & \Delta e^{i\phi}\\ \Delta e^{-i\phi} & \mu + V - \tau_0 \otimes (\vec{\sigma}\cdot\vec{p})\end{pmatrix}\begin{pmatrix}\Phi_e\\ \Phi_h\end{pmatrix} = \epsilon\begin{pmatrix}\Phi_e\\ \Phi_h\end{pmatrix} \tag{3.16}$$

in the superconductor and

$$H\begin{pmatrix}\Phi_e\\ \Phi_h\end{pmatrix} = \begin{pmatrix}(\tau_0 \otimes (\vec{\sigma}\cdot\vec{p})) - \mu & 0\\ 0 & \mu - (\tau_0 \otimes (\vec{\sigma}\cdot\vec{p}))\end{pmatrix}\begin{pmatrix}\Phi_e\\ \Phi_h\end{pmatrix} = \epsilon\begin{pmatrix}\Phi_e\\ \Phi_h\end{pmatrix} \tag{3.17}$$

in the graphene, where the Φ's have the valley isotropic structure explained earlier. The set of equations (3.17) is then solved under the assumption of an "ideal" NS interface as explained in

Stellenbosch University http://scholar.sun.ac.za

[9, 18]. This essentially entails that the superconductor and graphene sheet meet perfectly so that there is no lattice mismatch at the NS interface, the interface is smooth and impurity free on the scale of the superconducting coherence length and the Fermi wave length in the superconductor is much smaller than the Fermi wave length in the normal region. Eq. (3.14) then follows after the continuity of the wave function between the two regions is ensured.

Furthermore it must be noted that the calculation in [18] is carried out under the circumstance of a potential step, V, between the superconductor and the graphene sheet. This is in order for the Fermi wave vector inside the superconductor ($\frac{\mu+V}{\hbar v}$) to be large compared to the Fermi wave vector inside the normal region ($\frac{\mu}{\hbar v}$). This assumes that the electrostatic potential in the normal and superconducting regions can be controlled independently by means of gate voltages or doping.

The crucial regime for the result to be valid is that $\epsilon < \Delta$.

3.4 Specular Andreev reflection vs Retro Andreev reflection in graphene

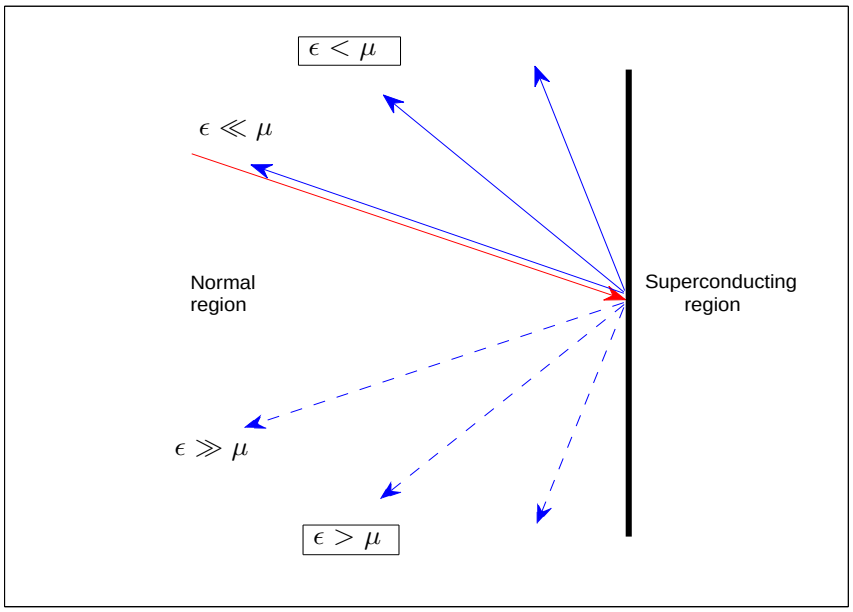

Figure 3.4: An illustration of Andreev reflected paths for holes for a fixed angle of incidence (red) [9]. Specular Andreev reflection dominates in the region $\epsilon > \mu$ (dashed blue) while retro Andreev reflection dominates in the region $\epsilon < \mu$ (solid blue).

The Beenakker paper [10] emphasises another difference of graphene when compared to other samples. This is related to the nature of Andreev reflection, the particle-hole conversion at the

Stellenbosch University http://scholar.sun.ac.za

NS interface and will be important later when later results are discussed. Usually retro-reflection takes place at an NS interface [9] as indicated in Fig. (3.2), where the hole travels in the opposite direction to that of the incoming particle.

In the case of graphene another kind of Andreev reflection namely specular Andreev reflection is also present [18]. This is indicated in Fig. (3.3). For $\epsilon < \Delta$, if $\epsilon > \mu$, specular Andreev reflection dominates while if $\epsilon < \mu$, retro Andreev reflection dominates. The reflection angle for a fixed angle of incidence is shown in Fig. (3.4).

In the case where $\epsilon \ll \mu$, the retro reflected hole excitation traces the reverse path of the incoming particle. As ϵ increases the retro reflected hole excitation follows a path that is more and more parallel to the NS interface. When the point $\epsilon = \mu$ is crossed, the path jumps through 180°. From this point onwards the Andreev reflection is specular. With increasing ϵ the path followed by the hole excitation makes an increasing angle with the NS interface. Finally, when $\epsilon \gg \mu$, the specularly reflected hole follows the path of the incoming particle with the component of velocity perpendicular to the interface reversed [9].

The implication of this to the kinematic of graphene will be discussed later in Chapter 5.

Stellenbosch University http://scholar.sun.ac.za

CHAPTER 4
Green's function formalism for calculating conductance

Later in this thesis we will study transport through several graphene devices. In particular we will calculate the conductance of devices. Analytical methods will be insufficient so that we require a suitable numerical method. The numerical approach chosen for the calculation is the Recursive Green's Function approach. This chapter will start by building up the algorithm for the purpose of calculating the transmission for any sample that does not exhibit an NS interface, using the methods of [20, 21, 22]. We will also extend the method to handle conductance problems where the system is in the presence of a superconductor.

4.1 Green's function conductance relation

The Green's function of a given Hamiltonian, H, is defined as the function that satisfies

$$\int d\vec{r}' \left[E - H(\vec{r_1}, \vec{r}')\right] G(\vec{r}', \vec{r_2}, E) = \delta(\vec{r_1} - \vec{r_2}) \tag{4.1}$$

or, if rewritten in operator form (so that $G(\vec{r_1}, \vec{r_2}, E) = \langle \vec{r_1} | \, G(E) \, | \vec{r_2}' \rangle$)

$$[E - H] \, G(E) = I \tag{4.2}$$

so that the Green's function is given by simple inversion of the operator, as long as the energy E is not an eigenvalue of the Hamiltonian. For this purpose an infinitesimal imaginary energy is added to or subtracted from the Hamiltonian and the advanced and retarded Green's functions (G^A and G^R) are defined

$$G^A = \lim_{\eta \to 0^+} [E + i\eta - H]^{-1} \qquad G^R = \lim_{\eta \to 0^+} [E - i\eta - H]^{-1} \tag{4.3}$$

which exist even for eigenvalues of the Hamiltonian. Since the advanced and retarded Green's functions are related by hermitian conjugation it is only necessary to consider one of the two. All formulas that ensue will be written in terms of the advanced Green's functions.

The Green's functions can be related to the conductance of a device by means of the Landauer-Büttiker formalism [24] and the Fischer-Lee relation which will be stated here for the sake of completeness.

Stellenbosch University http://scholar.sun.ac.za

The Landauer-Büttiker formalism gives the relations between the scattering matrix and conductance for devices. Setups that are investigated contain devices, specific lattices that wish to be investigated, and semi-infinite leads that transport excitations to and from the device. Even though the Landauer-Büttiker formalism holds for any number of leads, we will only be considering the simplified case where two leads are connected to the system.

The basic setup is given in Fig. (4.1) where a mesoscopic device is coupled to electron reservoirs via leads. Translational invariance is assumed in the leads in the direction of propogation. This assumption allows one to write the lead state eigenfunctions of the form $e^{ikz_1}\phi_n(z_2)$ where z_1 is the direction of translational invariance and z_2 the direction orthogonal to this. The quantum number n of these states are referred to as eigenchannels and k is the wave number.

The Landauer formula then states that the conductance, C, is given by

$$C(E) = g_0 T_{ij} \quad \text{where} \quad T_{ij} = \sum_n T_n(E) \tag{4.4}$$

where T_n are the eigenvalues of the transmission matrix between lead i and j and $g_0 = \frac{e^2}{h}$ is the conductance quantum.

In our numerical calculation we will be using the Fischer-Lee relation which provides the link between Green's functions and T_{ij} by stating that

$$T_{ij} = \mathrm{Tr}\left[\Gamma_i G_{ij} \Gamma_j G_{ij}^\dagger\right] = \frac{2e^2}{\hbar} C_{ij} \tag{4.5}$$

where the function Γ_k is linked to the self-energy of the lead Σ_k via

$$\Gamma_k = i\left(\Sigma_k - \Sigma_k^\dagger\right) \tag{4.6}$$

where the self-energy completely characterizes the effect of lead k on the device Green's function. The self-energy is a term that is introduced to represent the effect of the lead in the Hamiltonian so that, given a Hamiltonian for our device, H_D and one for the i'th lead, H_L^i and coupling between lead and device, V_{LD}^i and V_{DL}^i

$$H_D + H_L^i + V_{LD}^i + V_{DL}^i \to H_D + \Sigma_i \tag{4.7}$$

Stellenbosch University http://scholar.sun.ac.za

where Σ_i is defined over the device. The indices i and j can either indicate the left or right lead. G_{ij} is defined as the Green's function element associated with a particle entering the device through lead i and leaving through lead j. This is done by including the self-energies

$$G_{ij} = [E + i\eta - H_D - \Sigma_i - \Sigma_j]^{-1} \tag{4.8}$$

Our task now is to find effective numerical ways of calculating the self-energies and Green's functions, which is the topic of the next section.

4.2 The tight binding Hamiltonian

Since we are taking a numerical approach, we can return to the tight binding Hamiltonian of graphene, map the Hamiltonian onto an array or a finite set of arrays and do all the necessary manipulations to find the Green's functions and self-energies. How exactly the geometry of a graphene lattice (which is of course hexagonal) can be mapped onto an array will be discussed later. For now, in order to explain the method, we will be considering a general $M \times N$ device with nearest neighbour interactions as depicted in Fig. (4.1).

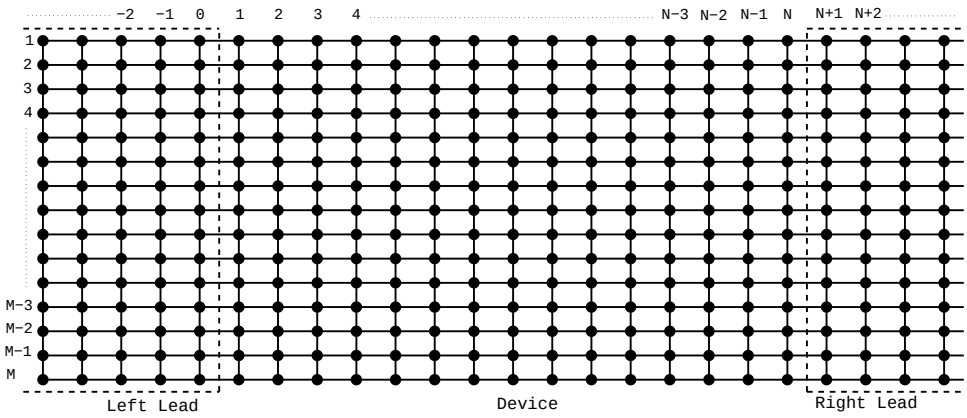

Figure 4.1: A picture of the device (the MxN section) coupled to a left and right lead (indicated by dashed lines)

We start with a general nearest neighbour tight binding Hamiltonian of a finite device where no sublattice distinction is made and atoms are labelled by row and column indices

$$H = \sum_{m=1}^{M}\sum_{n=1}^{N} U_{mn} |m,n\rangle \langle m,n| +$$

Stellenbosch University http://scholar.sun.ac.za

$$\sum_{m=1}^{M-1}\sum_{n=1}^{N} t^1_{mn}\left|m+1,n\right\rangle\left\langle m,n\right| + \sum_{m=1}^{M}\sum_{n=1}^{N-1} t^2_{mn}\left|m,n+1\right\rangle\left\langle m,n\right| + h.c. \tag{4.9}$$

where the t's indicate the hopping amplitudes and U is the site-specific potential energy. Casting this Hamiltonian into a full matrix form would entail taking into account the hopping between all atoms in the sample, so that one would have an $(M \times N) \times (M \times N)$ matrix. This is clearly not a feasible approach since it would be too taxing computationally. Fortunately, since we are only considering nearest neighbour interactions, we can make use of the fact that almost all matrix elements of this $(M \times N) \times (M \times N)$ matrix would be zero and apply the so-called Recursive Green's Function approach.

What we can do is think of sets of arrays that represent the Hamiltonian on a single column (in this case the k'th column) in the lattice

$$H^k_{ij} = \left\langle i,k\right| H \left|j,k\right\rangle = U_{i,k}\delta_{i,j} + (t^{(1)}_{jk})\delta_{i,j+1} + (t^{(1)}_{ik})^*\delta_{i,j-1} \tag{4.10}$$

where H^k_{ij} is the entry in row i, column j of the array H^k, the Hamiltonian of the k'th column. We also define another set of arrays that show how these different columns are coupled to each other. Here we make use of the fact that only adjacent columns are connected to each other and we again parametrize the connection of the columns with their neighbour columns

$$V^{k,k+1}_{ij} = \left\langle i,k+1\right| H \left|j,k\right\rangle = t^{(2)}_{ik}\delta_{i,j} \tag{4.11}$$

This representation of the Hamiltonian allows us to make use of the Dyson equation [20, 21, 22]. These elements will allow us to calculate the Green's function of the whole system by means of a recursive procedure. For this we now turn our attention to the Dyson equation (which will be derived for our special application later)

$$G = G^P + G^P V G = G^P + G V G^P \tag{4.12}$$

where G^P is the Green's function of some partial device with disjoint sections, V is the hopping matrices connecting these disjoint sections and G is the desired Green's function where these disjoint sections have been connected. For our purposes the partial device is always a group of n connected columns and a disjoint column $n+1$ so that G is then a group of $n+1$ connected columns.

Stellenbosch University http://scholar.sun.ac.za

Though the Dyson equation is true for any partial device we choose, it is easy to see why it is true for the case of a partial device consisting of n connected columns and a single, unconnected column.

The full Green's function of the connected $n+1$ columns can be calculated, for instance, by the following partition of the Hamiltonian

$$\begin{aligned} G &= \begin{pmatrix} E+i\eta-H^{1\to n} & -V^{n,n+1} \\ -V^{n+1,n} & E+i\eta-H^{n+1} \end{pmatrix}^{-1} \\ &= \left[\begin{pmatrix} E+i\eta-H^{1\to n} & 0 \\ 0 & E+i\eta-H^{n+1} \end{pmatrix} - \begin{pmatrix} 0 & -V^{n,n+1} \\ -V^{n+1,n} & 0 \end{pmatrix}\right]^{-1} \\ &= \left[(G^P)^{-1}-V\right]^{-1} \end{aligned}$$

where $H^{1\to n}$ are n $M\times M$ column Hamiltonians with connections calculated for columns 1 through n and H^{n+1} is the single column Hamiltonian of column $n+1$. Together these two form the partial device. This then leads to

$$\begin{aligned} \left[(G^P)^{-1}-V\right]G &= I \\ \Rightarrow \left[I-G^PV\right]G &= G^P \\ \Rightarrow G &= G^P+G^PVG. \end{aligned} \tag{4.13}$$

The second form of the Dyson equation follows similarly (by, for instance, multiplying with the inverse of G from the right). The two forms of the Dyson equation can both be used, though usually only one will yield a closed set of equations (an example of the Dyson equation not yielding a closed set of equations is done shortly). What the Dyson equation tells us is that we have the means to take the isolated column Green's functions (calculated via direct inversion since the column Hamiltonian is known) and attach them one by one until we have the Green's function of the full $M\times N$ device. This procedure will have to be done recursively since as each new column is added, the Green's function of the partial system changes and the Green's function we wish to calculate will be the new partial system and one additional column. We will denote the Green's functions associated with the already known partial system by a superscript P (i.e. G^P). Note that after each iteration (if the full system size has not yet been reached) the result of the Dyson equation (G) will form part of the partial system in the next iteration. V also changes since the unconnected columns of the partial device change.

Stellenbosch University http://scholar.sun.ac.za

It is important to note also that after each iteration the size of G increases (by M rows and M columns). This is since an $M \times M$ column Hamiltonian is connected to the device and this affects the Green's functions between all columns. Each $M \times M$ block represents a different Green's function between columns, the quantity we will be interested in. We define

$$\langle k| G |l\rangle = G_{kl} \tag{4.14}$$

as the Green's function between column k and column l for the device G. This is the k'th $M \times M$ block along the rows of G and the l'th $M \times M$ block along the columns of G. Note that this is still an $M \times M$ matrix.

Let's assume that we have already attached n columns to the partial device (so that the Green's functions G^P_{n1}, G^P_{1n}, G^P_{nn}, G^P_{11} are known. We know all the column Hamiltonians and thus column Green's functions, including $G^P_{n+1,n+1}$, now to be included for the partial device. The first form of the Dyson equation (4.12) for the next iteration then reads

$$\begin{aligned}
\langle n+1| G |1\rangle &= \langle n+1| G^P |1\rangle + \sum_{kl} \langle n+1| G^P |k\rangle \langle k| V |l\rangle \langle l| G^P |1\rangle \\
&= \langle n+1| G^P |n+1\rangle \langle n+1| V |n\rangle \langle n| G |1\rangle \\
&= G^P_{n+1,n+1} V^{n+1,n} G_{n,1}
\end{aligned}$$

where we have used that G^P is defined on the disconnected sections and that the only non-zero elements of the operator V are for $\langle n| V |n+1\rangle$ and $\langle n+1| V |n\rangle$. However, the above expression is not leading to a closed form, since we will now have to calculate $G_{n,1}$ and after that $G_{n-1,1}$ and so on, which is not useful in the recursive procedure. Using the second form of the Dyson equation (4.12) we find, however

$$\langle n+1| G |1\rangle = G_{n+1,n+1} V_{n+1,n} G^P_{n,1} \tag{4.15}$$

Clearly from the above equation we need $G_{n+1,n+1}$ so

$$\langle n+1| G |n+1\rangle = G^P_{n+1,n+1} + G^P_{n+1,n+1} V_{n+1,n} G_{n,n+1} \tag{4.16}$$

Stellenbosch University http://scholar.sun.ac.za

for which we require $G_{n,n+1}$

$$\begin{aligned} \langle n|\, G\, |n+1\rangle &= G^P_{n,n+1} + G^P_{n,n} V_{n,n+1} G_{n+1,n+1} \\ &= G^P_{n,n} V_{n,n+1} G_{n+1,n+1} \end{aligned} \tag{4.17}$$

which, after substitution into (4.16), reference to (4.15) yield

$$G_{n+1,n+1} = \left(I - G^P_{n+1,n+1} V^{n+1,n} G^P_{n,n} V^{n,n+1}\right)^{-1} G^P_{n+1,n+1} \tag{4.18}$$

$$G_{n+1,1} = G_{n+1,n+1} V^{n+1,n} G^P_{n,1} \tag{4.19}$$

$$G_{1,n+1} = G^P_{1,n} V^{n,n+1} G_{n+1,n+1} \tag{4.20}$$

$$G_{1,1} = G^P_{1,1} + G^P_{1,n} V^{n,n+1} G_{n+1,n+1} V^{n+1,n} G^P_{n,1} \tag{4.21}$$

As initial values all four Green's function types are assigned the Green's function of the first, single column, G^P_{11}, which will include the lead self-energy. The above procedure is carried out until a partial device of N columns is achieved. The four Green's functions $G_{1,1}, G_{N,1}, G_{1,N}$ and $G_{N,N}$ we associate with the different possibilities for particles to enter and leave the device, either leaving through the same lead they entered the device or through the other lead.

The last thing still necessary to construct our Green's functions is the self-energy, which will be covered in the following section.

4.3 Self-energy calculation

Since we are assuming that only nearest neighbour interactions are present in the system we have to restrict ourselves to leads that affect the first or last column in the above algorithm, in other words the leads can at most affect the column Hamiltonians of those columns. As was explained above, we will introduce the effect of the leads in the system by means of the self energy, i.e. for it to be a term that only augments the device Hamiltonian (H_D) such that

$$H_D + H^i_L + V^i_{LD} + V^i_{DL} \to H_D + \Sigma_i \tag{4.22}$$

Consider the setup as depicted in Fig. (4.1) where a perfect lead from the left conducts electrons to the device and a perfect lead then leads the electrons that transported through the sample away on the right.

If we only consider the effect of one of the two leads, labeled i, assuming the effect of mul-

Stellenbosch University http://scholar.sun.ac.za

tiple leads are additive in nature, we can split the Hamiltonian of the full system up into the following

$$H = H_D + H_L^i + V_{LD}^i + V_{DL}^i \tag{4.23}$$

where a subscript D indicates the device, a subscript L indicates the lead and DL/LD refers to coupling between the lead and device / device and lead. For the full Hamiltonian to be hermitian it is required that $V_{LD} = V_{DL}^\dagger$.

We partition the respective Green's function of the lead so that

$$\begin{pmatrix} (E+i\eta) - H_D & -V_{DL}^i \\ -V_{LD}^i & (E+i\eta) - H_L^i \end{pmatrix} \begin{pmatrix} G_D & G_{LD} \\ G_{DL} & G_L \end{pmatrix} = I \tag{4.24}$$

where we are now interested only in calculating G_D, the Green's function of the device given the lead Green's function and device-lead coupling.

The following two equations that are relevant result

$$\begin{aligned} (E+i\eta - H_D)G_D - V_{DL}^i G_{DL}^i &= 1 \\ (E+i\eta - H_L^i)G_{DL}^i - V_{LD}^i G_D &= 0 \end{aligned}$$

By now defining

$$g_L^i = (E+i\eta - H_L^i)^{-1} \tag{4.25}$$

we find the following expression for G_{DL}^i

$$G_{DL}^i = g_L^i V_{LD}^i G_D \tag{4.26}$$

and consequently the following expression for G_D

$$G_D = \left(E+i\eta - H_D - V_{DL}^i g_L^i V_{LD}^i\right)^{-1} \tag{4.27}$$

This expression in other words implies that we have the self-energy as $\Sigma^i = V_{DL}^i g_L^i V_{LD}^i = {V_{LD}^i}^\dagger g_L^i V_{LD}^i$ when comparing with (4.22). At first glance it would seem as if we have not made any progress, since the calculation of g_L^i still involves a semi-infinite lead. However, since we are considering nearest-neighbour hopping, only the hopping between the first column in the lead with the first column in the device $\langle 1^i | V_{LD}^i | 1 \rangle$ is non-zero. This implies as that we only need the matrix

Stellenbosch University http://scholar.sun.ac.za

element $\langle 1^i | \, g_L^i \, | 1^i \rangle$, the surface Green's function of the lead.

Two points are relevant regarding this observation. Firstly, our assumption of lead effects being additive is true in our case of two leads, since there is a non-zero spacing between the leads (the statement also holds even if this is not the case [20]). Secondly, g_L^i contains the full effect of the lead Hamiltonian (see eq. (4.25)). This will, similar to in the previous section, require a recursive method.

4.3.1 The calculation of the surface Green's functions of the leads

As will become clear as soon as the implementation of graphene's hexagonal lattice geometry is discussed, the recursive method for dealing with the calculation of the self-energy is very dependent on the geometry of the lead. The reason for this is that the geometry ultimately affects the way the column Hamiltonians look and how they are connected to each other. In the device, where we have a finite number of columns each column Hamiltonian may be different and this can be handled, but in the lead, which is infinite, our recursive procedure will have to depend on the fact that there is a pattern to the way the columns are attached to each other. The column Hamiltonians may change, but must do so cyclically. Since their are no other perturbances in the lead (like a change in magnetic field or electrostatic field), this will mean that we have to identify the geometric pattern and ensure that all different ways of attaching columns to each other are included. More will be said on this point in the next subsection.

For now, let's focus on the simplest possible pattern, namely a square lattice, in which all the columns are identical, as indicated in Fig. (4.1). Our goal here is to find the matrix element g_{11}^i of (4.25) so that the self-energy can be calculated from there. We will use the same representation of the Hamiltonian as we did for the recursive Green's function method in the device so that

$$(E + i\eta)I - H_L = \begin{pmatrix} d & -A & 0 & 0 & \cdots \\ -B & D & -A & 0 & \cdots \\ 0 & -B & D & -A & \cdots \\ 0 & 0 & -B & D & \ddots \\ \vdots & \vdots & \vdots & \ddots & \ddots \end{pmatrix} \tag{4.28}$$

where the matrices are constructed with the column representation of the Hamiltonian in mind

$$\langle i | \, d \, | j \rangle = \langle i | \, D \, | j \rangle \quad = \quad (E + i\eta)\delta_{i,j} - H_{ij}^1$$

Stellenbosch University http://scholar.sun.ac.za

$$\langle i|\, A\, |j\rangle \;=\; V_{jj}^{1,2}\delta_{i,j}$$

and $B = A^{\dagger}$. The column index $k = 1$ is irrelevant since we are assuming all the columns in the lead to be of the same structure and to be coupled in the same way (under our assumption of the square lead). Keep in mind here that the column representation now refers to the columns in the lead, so that the matrices are of the dimension $L \times L$ where L is the length of the column in the lead. Our Green's function can again be written as

$$\begin{pmatrix} d & -A & 0 & 0 & \cdots \\ -B & D & -A & 0 & \cdots \\ 0 & -B & D & -A & \cdots \\ 0 & 0 & -B & D & \ddots \\ \vdots & \vdots & \vdots & \ddots & \ddots \end{pmatrix} \begin{pmatrix} g_{11} & g_{12} & g_{13} & g_{14} & \cdots \\ g_{21} & g_{22} & g_{23} & g_{24} & \cdots \\ g_{31} & g_{32} & g_{33} & g_{34} & \cdots \\ g_{41} & g_{42} & g_{43} & g_{44} & \ddots \\ \vdots & \vdots & \vdots & \ddots & \ddots \end{pmatrix} = I \tag{4.29}$$

Now, the relevant equations in (4.29) can be written as follows

$$\begin{aligned} dg_{11} &= 1 + Ag_{21} \\ Dg_{2k,1} &= Bg_{2k-1,1} + Ag_{2k+1,1} \\ Dg_{2k+1,1} &= Bg_{2k,1} + Ag_{2k+2,1} \quad \forall k \geq 1 \end{aligned} \tag{4.30}$$

The equations are split into those for even-numbered columns and those for odd-numbered columns. The result is that we can express all odd-numbered columns as functions of odd-numbered columns, thus forming a closed set of equations

$$\begin{aligned} \left(d - AD^{-1}B\right) g_{11} &= 1 + AD^{-1}Ag_{31} \\ \left(D - BD^{-1}A - AD^{-1}B\right) g_{2k+1,1} &= BD^{-1}Bg_{2k-1,1} + AD^{-1}Ag_{2k+3,1} \end{aligned}$$

By now redefining our matrices and indices such that $d' = \left(d - AD^{-1}B\right)$, $A' = AD^{-1}A$, $B' = BD^{-1}Bg_{2k-1,1}$, $D' = \left(D - BD^{-1}Aj - AD^{-1}B\right)$ and $g_{2k-1,1} \to g_{l,1}$ we find the following set of equations

$$\begin{aligned} d'g_{11} &= 1 + A'g_{21} \\ D'g_{l+1,1} &= B'g_{l,1} + A'g_{l+2,1} \end{aligned} \tag{4.31}$$

Stellenbosch University http://scholar.sun.ac.za

which is precisely of the same form as (4.30) before being split up into even l and odd l. This means that the mapping we have just performed will be performed again, only with different matrices. This will then again lead to equations of the same form and we may perform the same mapping et cetera. This forms a recursive procedure. Concretely, in other words, the mapping between two steps in the recursive procedure looks as follows

$$d_{n+1} = d_n - A_n D_n^{-1} B_n \tag{4.32}$$

$$D_{n+1} = D_n - B_n D_n^{-1} A_n - A_n D_n^{-1} B_n \tag{4.33}$$

$$A_{n+1} = A_n D_n^{-1} A_n \tag{4.34}$$

$$B_{n+1} = B_n D_n^{-1} B_n \tag{4.35}$$

Of course, the above procedure would be rather useless if either we do not have a way to recover g_{11} or if the sequence does not ultimately converge. Fortunately, however, it does and there is a way to recover g_{11}. It is possible to understand the necessary extraction procedure if one understands the intuitive picture of the above procedure.

What we are essentially doing is taking the columns in the lead and grouping them together in clusters (see Fig.(4.2)), contracting all the information of those columns into the right-most column of the cluster. These clusters contain all the Hamiltonian information of the initial column as well as the information of it's nearest neighbours. A new set of equations is then derived for how these clusters are connected to its nearest neighbour clusters. These are then also grouped into bigger clusters (or rather clusters that incorporate the effects of more columns), which are then again grouped into bigger clusters et cetera. The size of these clusters grows exponentially, so that after enough steps the first cluster is huge and the first column of the cluster (the surface Green's function) is augmented to include enough information to approximate an infinite lead sufficiently.

Intuitively one would expect that columns (even combined columns) that are further and further apart (since their information is contracted into the rightmost column only) should interact more and more weakly, i.e $A_n \to 0$. This would imply that, if A_n is sufficiently close to the zero matrix (or if $d_n - d_{n-1}$ is sufficiently close to the zero matrix) we should have, according to (4.32)

$$g_{11} \approx d_n^{-1} \tag{4.36}$$

Stellenbosch University http://scholar.sun.ac.za

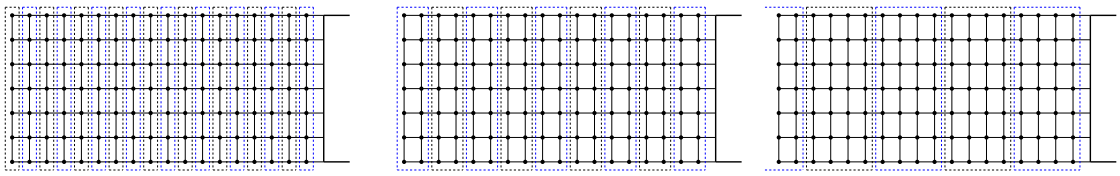

Figure 4.2: An illustration of how the self-energy of the lead is calculated. The columns are continuously grouped into bigger clusters and the equations are adjusted to relate these clusters.

The above derivation is only applicable to a lead with square structure, though the next subsection will show exactly how to incorporate the graphene geometry into both the device and the leads.

4.3.2 The graphene geometry in the algorithm

What we will be interested in during the subsequent simulations is a graphene lattice terminated by two armchair edges. The geometry of this can be mimicked by simply setting certain matrix elements, specifically some of the couplings between columns, to zero, see Fig. (4.3). A zig-zag edge can also be simulated by setting certain elements in the column Hamiltonian to zero, though these will not be applicable in the subsequent simulations.

One must take care with the coordinate posistions of the lattice points, which is now a more

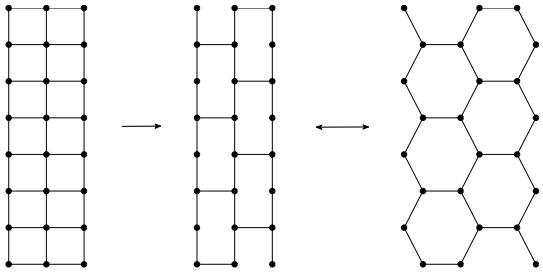

Figure 4.3: The hexagonal symmetry in the algorithm follows by setting certain elements connecting the columns to zero. Atoms in the same column no langer have the same y-dependence, see Fig. (2.4).

complicated function of the columns and rows than for a rectangular lattice, see Fig. (2.4) and compare with Fig. (4.3). Though atoms may lie in the same columns, their dependance on the x-coordinate and y-coordinate differ. Whenever a potential or vector potential that is dependent on position is added to the system this must be kept in mind.

Stellenbosch University http://scholar.sun.ac.za

The calculation for the self-energy is now also changed to incorporate the hexagonal lattice

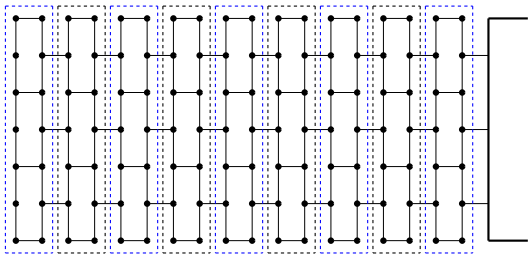

Figure 4.4: After the first step of the recursive procedure, the graphene geometry is incorporated into the clusters and the recursive procedure goes on from this step as if the geometry was that of a square lattice.

geometry. The difference here is now that the even and odd columns are coupled to their nearest neighbours differently and thus the construction of the Green's functions are augmented

$$\begin{pmatrix} d & -a & 0 & 0 & \cdots \\ -b & D & -A & 0 & \cdots \\ 0 & -B & D & -a & \cdots \\ 0 & 0 & -b & D & \ddots \\ \vdots & \vdots & \vdots & \ddots & \ddots \end{pmatrix} \begin{pmatrix} g_{11} & g_{12} & g_{13} & g_{14} & \cdots \\ g_{21} & g_{22} & g_{23} & g_{24} & \cdots \\ g_{31} & g_{32} & g_{33} & g_{34} & \cdots \\ g_{41} & g_{42} & g_{43} & g_{44} & \ddots \\ \vdots & \vdots & \vdots & \ddots & \ddots \end{pmatrix} = I. \tag{4.37}$$

The equations we generate from this are

$$\begin{aligned} dg_{11} &= 1 + ag_{21} \\ Dg_{2k,1} &= bg_{2k-1,1} + Ag_{2k+1,1} \\ Dg_{2k+1} &= Bg_{2k,1} + ag_{2k+2,1} \qquad \forall k \geq 2 \end{aligned}$$

By now making similar manipulations to that of the regtangular lattice calculation we find the mapping $d' = d - aD^{-1}b$, $D' = D - BD^{-1}A - aD^{1}b$, $B = BD^{-1}b$, $A' = aD^{-1}A$ and $g_{2l-1,1} \to g_{l,1}$ which then yields

$$\begin{aligned} d'g_{11} &= 1 + A'g_{2,1} \\ D'g_{l+1,1} &= B'g_{l,1} + A'g_{l+2,1} \end{aligned} \tag{4.38}$$

which is exactly of the same form as (4.31) so that the recursion process can proceed as previously. This again makes intuitive sense since if we contract the columns to include the nearest neighbours

Stellenbosch University http://scholar.sun.ac.za

in the clusters, all information about the hexagonal symmetry of the lattice is automatically taken care of in the first contraction (see Fig. (4.4)). All clusters are coupled to their nearest neighbour clusters in the same way, like the setup we had with square lattice leads. In other words, when calculating the self-energy, the above mapping is made as a first step and then the recursive procedure proceeds as before.

4.4 Extending the algorithm to include an NS interface

Though we already have a way to incorporate the hexagonal symmetry of graphene into the Recursive Green's Function approach, this is not the only aspect that we will have to be concerned with to simulate the system we are interested in. The algorithm we have put forward so far can only handle particle excitations. Since we are planning to couple our distorted graphene sheet to a superconductor we somehow need to populate our graphene sheet with hole excitations in addition to particle excitations.

This is not necessarily a straightforward problem, precisely because of the superconducting boundary. One of our analytical tools is the result of [18], that we can, within a certain energy regime, consider the NS-interface as a boundary condition. However, the Recursive Green's Function approach employ all boundary conditions in a geometric way. An armchair edge or zig-zag edge can be represented in terms of the hopping elements that we put to zero on the lattice. The boundary conditions follow automatically since the excitations are forced to only exist on the lattice. It is however not possible to do the same with the NS-interface boundary condition. Even if we were to populate our graphene sheet with two uncoupled types of excitations, namely particle and hole excitations, we would have no guarantee through the algorithm that this boundary condition would be appeased.

An equivalence has been shown previously between problems in a so-called p-n junction and problems with NS-interfaces, subject to certain restrictions [26]. This equivalence makes use of the M_{NS} boundary condition in a certain limit, so that, if our system was to be mapped onto an equivalent p-n junction, we would at least be guaranteed that we are respecting this condition.

However, this approach is not strictly necessary and the Green's function machinery is perfectly suited, given certain adjustments, to calculate the conductance of any NS-interface system. We will now show how this can be done.

Stellenbosch University http://scholar.sun.ac.za

4.5 Hole excitations in the Hamiltonian

In order to incorporate superconductivity, we modify the Hamiltonian to include hole excitations like we have before (see eq. (3.8))

$$H = \begin{pmatrix} H_e - \mu & \Delta \\ \Delta^* & \mu - H_e^* \end{pmatrix} \tag{4.39}$$

The Hamiltonian H_e is the particle Hamiltonain, which was precisely the topic of discussion in previous section. We can cast H_e and H_e^* into the form of column Hamiltonians and hopping matrices and as a consequence we can cast the full Hamiltonian, H, into the form of column Hamiltonians too. All changes that occur is that a sign swapping and complex conjugation takes place for the hole sector and that the sign of the chemical potential is different for the two sectors.

The coupling between holes and particles is something which we have not discussed yet in the context of the Recursive Green's Function method. Our model assumes the coupling between holes and particles to be onsite and spatially constant. In other words, our parametrisation should be

$$\Delta_{ij}^k = \langle i, k, e | \, \Delta \, | j, k, h \rangle = \Delta_{i,k}\delta_{i,j} \tag{4.40}$$

where the e and h indices indicate particle and hole excitations.

4.6 Andreev vs. normal reflection

The Recursive Green's Function approach allows us to calculate four different types of transmissions for excitations. These result from the fact that an excitation can either enter through the left or right lead and again leave through the left or right lead. Now that our system has been expanded to include hole excitations as well as particle excitations, each of these possibilities now has an additional 2 degrees of freedom, namely whether to enter and leave as a hole or particle excitation.

In a similar fashion to what was the case when we were discussing lead and device Hamiltonians and Green's functions, the resulting Green's function from eq. (4.39) can be partitioned as follows

$$G = \begin{pmatrix} G^{ee} & G^{eh} \\ G^{he} & G^{hh} \end{pmatrix} \tag{4.41}$$

Stellenbosch University http://scholar.sun.ac.za

where a superscript e refers to a particle excitation, h to a hole excitation. The first superscript refers to the type of excitation that enters the device while the second superscript refers to the type of excitation that leaves the device.

Later in this thesis we will be considering a system with a normal lead on the left and a superconducting lead on the right and wishing to calculate conductance at energies below the superconducting gap. Particle and hole excitations excitations can, in other words, not enter the superconductor, since their energies are below the superconductor gap.

However, there is another way that current can be transported. The particle can be absorbed as a Cooper pair inside the superconductor, carrying a charge of $2e$. The production of a Cooper pair inside the superconductor requires the production of a hole in the graphene sheet. This hole excitation can then leave through the normal lead. In other words, the matrix element we will be looking for is the G^{eh} element of the G_{11} Green's function.

As one may also suspect, the Fischer-Lee relation is now also adjusted since we are no longer looking at particle-particle transmissions. The transmission for particle-hole excitations (between the non-superconducting lead and the non-superconducting lead) is given by

$$T_{11}^{eh} = Tr\left[\Gamma_1^e G_{11}^{eh} \Gamma_1^h \, G_{11}^{eh\,\dagger}\right] \tag{4.42}$$

where the Γ's are still related to the self-energy as before, eq. (4.6). Γ_1^e and Γ_1^h are related to the self-energies of the (uncoupled) electron and hole sheets of the normal lead. The conductance is then given by $C = 4g_0 T_{11}^{eh}$ where the factor of four accounts for spin degeneracy and the fact that a charge of $2e$ is transferred to the superconductor in the conduction process. The spin degeneracy factor results since we no longer think of spin up and spin down excitations as two different channels.

Stellenbosch University http://scholar.sun.ac.za

CHAPTER 5
The effect of lattice distortions of graphene near an NS interface

The dispersion relation in the region of the valleys in the Brillouin zone is linear and leads to the Dirac equation. This ultimately implies that the electrons in graphene move around the lattice at a fixed speed, though one that is far less than the speed of light.

Applying a uniform magnetic field to a graphene sheet leads to the quantum hall effect in graphene - an infinite system consists of infinitely degenerate dispersionless Landau levels with energies $E_n = \text{sign}(n)\hbar\omega_c\sqrt{2|n|}, n \in Z$. A real magnetic field, however, affects the two valleys in an identical way so the dynamics of excitations are the same in the two valleys. By distorting the graphene lattice one is able to generate different Hamiltonians for the two valleys, since the resulting pseudo magnetic field affects the two valleys in opposite ways. One may view this as the particles in the one valley experiencing the magnetic field as if they had opposite charge.

Hole (or the absence of a particle) excitations are excitations of opposite charge to particles. This is due to the fact that holes are ejected where particles are absorbed and vice versa. One of the ways to make these excitation physicaly relevant to the setup is to attach the graphene sheet to a superconductor. What one should find, if a distorted lattice is attached to a superconductor, is that eight different species of excitations (valley, sublattice and particle/hole) are accessible and that superpositions of these can exist depending on various boundary effects.

It is within this rich structure that our investigation will begin.

5.1 Mathematical formulation of the problem (for a semi-infinite graphene sheet)

We start off with an infinite, distorted graphene sheet in two-dimensional space (R^2) and we define the region $y < 0$ as the graphene sheet while $y > 0$ is defined as the superconductor. The setup is drawn in Fig. (5.1). The differential equation that results from this is

$$H\Psi = \begin{pmatrix} H_+ - \mu & 0 & 0 & 0 \\ 0 & H_- - \mu & 0 & 0 \\ 0 & 0 & \mu - H_+ & 0 \\ 0 & 0 & 0 & \mu - H_- \end{pmatrix} \begin{pmatrix} \Psi_e \\ \Psi'_e \\ \Psi'_h \\ \Psi_h \end{pmatrix} = \epsilon \begin{pmatrix} \Psi_e \\ \Psi'_e \\ \Psi'_h \\ \Psi_h \end{pmatrix} \tag{5.1}$$

Stellenbosch University http://scholar.sun.ac.za

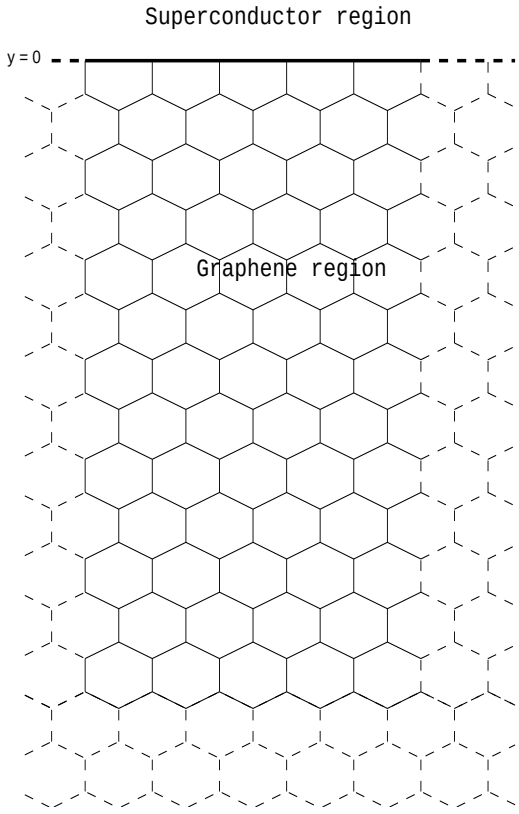

Figure 5.1: The setup that will be considered in this chapter. The graphene sheet is distorted, giving rise to a pseudo magnetic field.

where $H_\pm = \vec{\sigma} \cdot (\vec{p} \pm \vec{\alpha})$ and Ψ's are two-component spinors with components for the sublattice degrees of freedom. The valley isotropic convention is followed. Note that we have not yet thusfar chosen a specific distortion $\vec{\alpha}$. Inside the superconductor the differential equation looks the same

$$H\Psi = \begin{pmatrix} H_+ - \mu + V & 0 & \Delta & 0 \\ 0 & H_- - \mu + V & 0 & \Delta \\ \Delta^* & 0 & \mu - H_+ + V & 0 \\ 0 & \Delta^* & 0 & \mu - H_- + V \end{pmatrix} \begin{pmatrix} \Psi_e \\ \Psi'_e \\ \Psi'_h \\ \Psi_h \end{pmatrix} = \epsilon \begin{pmatrix} \Psi_e \\ \Psi'_e \\ \Psi'_h \\ \Psi_h \end{pmatrix} \tag{5.2}$$

with only the explicit particle-hole coupling (via the superconductor gap) and the step potential, V, (the result of placing the graphene sheet on a slab of metal) featuring explicitly. Now, during the calculation, one would ideally like to make use of the result of Beenakker [10] that one can write the presence of the superconductor as a boundary condition. For this purpose the NS interface is assumed to be "ideal" as explained earlier.

Stellenbosch University http://scholar.sun.ac.za

Consequently we may restrict ourselves to the differential equation (5.1) as long as we employ the following boundary condition

$$\begin{pmatrix} \Phi_e \\ \Phi_h \end{pmatrix} |_{y=0} = \begin{pmatrix} 0 & M_{NS} \\ M_{NS}^\dagger & 0 \end{pmatrix} \begin{pmatrix} \Phi_e \\ \Phi_h \end{pmatrix} |_{y=0} \qquad M_{NS} = \tau_0 \otimes e^{-i\beta\sigma_y} \tag{5.3}$$

where

$$e^{-i\beta\sigma_y} = \begin{pmatrix} \cos(\beta) & -\sin(\beta) \\ \sin(\beta) & \cos(\beta) \end{pmatrix} \tag{5.4}$$

from eq. (3.14) where $\alpha' = \frac{\pi}{2}$. The superconductor phase, ϕ is set to zero as discussed previously. We require that the wave function vanishes as $y \to -\infty$. Clearly this needs to hold for both valley wave functions independently in order to hold for the full wave function.

5.2 Transformations between excitations

In order to solve for the wave functions in the normal region it is useful and insightful to realise that certain properties of the Hamiltonian allows one to transform between the different excitation species easily. The Hamiltonian is block-diagonal (with 2×2 blocks) and thus we may diagonalise the blocks seperately. The different blocks, the 2×2 Hamiltonians of particle and hole excitations in both valleys, are related by certain symmetry operations. Furthermore, a transformation between the sublattice degree of freedom in each 2×2 block can also be found.

The differential equations associated with each block are coupled and of first order or decoupled and of second order and thus produce two independent solutions. We will assume that the boundary condition (that the wave functions much vanish as $y \to -\infty$) restricts the solution to up to a multiplicative constant. This implies that the solutions of all blocks must be unique up to a multiplicative constant and allows us to only having to explicitly solve a single differential equation. We can find the other wave functions by simply transforming from this one to the others.

First we consider the transformation between the particle-hole degree of freedom. For the particle spinors (i.e. Ψ_e and Ψ'_e) one has to solve something of the form $H_\pm\Psi = (\mu+\epsilon)\Psi$ while for the hole spinors (i.e. Ψ_h and Ψ'_h) one has to solve something of the form $H_\pm\Psi = (\mu-\epsilon)\Psi$. In other words, if one considers the eigenvalue expression of the more general $H_\pm\Psi = E\Psi$ one can solve for both simultaneously, keeping in mind that one can only resolve the eigenvectors up to a constant.

Stellenbosch University http://scholar.sun.ac.za

The second degree of freedom, the valley degree of freedom, can also be incorporated as a transformation. This takes the form in the Hamiltonian of eigenvectors of H_+ as opposed to H_-. For this derivation it must be noted that

$$\sigma_y\sigma_x\sigma_y = -\sigma_x \qquad \sigma_y\sigma_y\sigma_y = \sigma_y \tag{5.5}$$

which then implies that (see [9])

$$(i\sigma_y C)\vec{\sigma}\cdot(\vec{p}+e\vec{A})(-i\sigma_y C) = \vec{\sigma}\cdot(\vec{p}-e\vec{A}) \tag{5.6}$$

where C is the operator for complex congugation so that $C\sigma_y = -\sigma_y$, $C\vec{p} = -\vec{p}$ and $C^2 = I$. The consequence of this is that

$$v\vec{\sigma}\cdot\left(\vec{p}+e\vec{A}\right)\Psi = E\Psi \quad \Rightarrow \quad v\vec{\sigma}\cdot\left(\vec{p}-e\vec{A}\right)(i\sigma_y C)\Psi = E(i\sigma_y C)\Psi. \tag{5.7}$$

This is true since $(i\sigma_y C)(-i\sigma_y C) = I$. Thus we can also transform between eigenvectors of H_+ and H_- in a simple way, keeping in mind again that we can only resolve the eigenvectors up to a constant. Finally we turn our attention to a transformation between the sublattice degree of freedom. We will work with the arbitrary choice of H_+. For this block it means

$$H_+\Psi = v\vec{\sigma}\cdot\left(\vec{p}+e\vec{A}\right)\Psi = \begin{pmatrix} 0 & \hat{L} \\ \hat{L}^\dagger & 0 \end{pmatrix}\begin{pmatrix} \phi_1 \\ \phi_2 \end{pmatrix} = E\begin{pmatrix} \phi_1 \\ \phi_2 \end{pmatrix} \tag{5.8}$$

where $\hat{L} = v(p_x + eA_x - ip_y - ieA_y)$. The above set of differential equations can be decoupled by acting in with $v\vec{\sigma}\cdot\left(\vec{p}+e\vec{A}\right)$ from the left again to yield

$$\begin{pmatrix} \hat{L}\hat{L}^\dagger & 0 \\ 0 & \hat{L}^\dagger\hat{L} \end{pmatrix}\begin{pmatrix} \phi_1 \\ \phi_2 \end{pmatrix} = E^2\begin{pmatrix} \phi_1 \\ \phi_2 \end{pmatrix} \tag{5.9}$$

Now it follows that if

$$\hat{L}^\dagger\hat{L}\phi_2 = E^2\phi_2 \quad \Rightarrow \quad \hat{L}\hat{L}^\dagger(\hat{L}\phi_2) = \hat{L}(\hat{L}^\dagger\hat{L})\phi_2 = E^2\hat{L}\phi_2 \tag{5.10}$$

so that there exists also a transformation between the sublattice wave functions, again keeping in mind that we can only resolve the wave function up to a constant. This particular constant,

Stellenbosch University http://scholar.sun.ac.za

however, can be solved explicitly. The solution spinor for

$$H_+\Phi = E\Phi \quad \text{is} \quad \Phi = \begin{pmatrix} c\hat{L}\phi_2 \\ \phi_2 \end{pmatrix} \quad \text{where} \quad \hat{L}^\dagger\hat{L} = E^2\phi_2. \tag{5.11}$$

The constant c can be solved by referring back to the initial coupled differential equations in eq. (5.8) and thus requiring that

$$\hat{L}^\dagger(c\hat{L}\phi_2) = E\phi_2 = cE^2\phi_2 \quad \Rightarrow \quad c = \frac{1}{E}. \tag{5.12}$$

To sum up, this implies that for the eight-component spinor solution of our pseudo magnetic field graphene sheet we may write (up to a constant)

$$\begin{aligned}
\Psi_e &= c_e \begin{pmatrix} \frac{1}{\mu+\epsilon}\hat{L}\phi_2(\mu+\epsilon) \\ \phi_2(\mu+\epsilon) \end{pmatrix} \\
\Psi'_e &= c'_e \begin{pmatrix} C\phi_2(\mu+\epsilon) \\ -\frac{1}{\mu+\epsilon}C\hat{L}\phi_2(\mu+\epsilon) \end{pmatrix} \\
\Psi'_h &= c'_h \begin{pmatrix} \frac{1}{\mu-\epsilon}\hat{L}\phi_2(\mu-\epsilon) \\ \phi_2(\mu-\epsilon) \end{pmatrix} \\
\Psi_h &= c_h \begin{pmatrix} C\phi_2(\mu-\epsilon) \\ -\frac{1}{\mu-\epsilon}C\hat{L}\phi_2(\mu-\epsilon) \end{pmatrix}
\end{aligned} \tag{5.13}$$

so that we only have one differential equation to solve (keeping only the solutions that decay toward infinity fast enough), namely $\hat{L}^\dagger\hat{L} = E^2\phi_2$. With this result in hand, we can now turn our attention to a specific example.

5.3 Constant pseudo magnetic field

Let us consider an analytically tractable example, namely that of a distortion leading to a constant pseudo magnetic field. The specific distortion that will be presented here is the following

$$\hat{L} = \hat{l} = v\left(\hat{p}_x - Bey - i\hat{p}_y\right) \tag{5.14}$$

which correspondends to a vector potential of $\vec{\alpha} = By\hat{x}$. The operator $\hat{l}$ is used to emphasise the fact that we are working with the specific case of a constant pseudo magnetic field.

Stellenbosch University http://scholar.sun.ac.za

The first observation that one can make is that the excitations are free in the direction parallel to the NS interface (the x direction). Thus we may make use of the fact that the wave number along the NS interface is a good quantum number (like in [10]) and make the ansatz

$$\phi_2(x,y) = e^{iqx}\phi_2(y) \tag{5.15}$$

where $\phi_2(x,y)$ is an eigenfunction of $\hat{l}^\dagger\hat{l}$. The notation follows from the previous section. This then yields

$$\begin{aligned}
\hat{l}^\dagger\hat{l}\phi_2(x,y) &= E^2 e^{iqx}\phi_2(y) \\
&= v^2((\hbar q - eBy)^2 - \hbar eB + p_y^2)e^{iqx}\phi_2(y) \\
\Rightarrow \left(\frac{1}{\sqrt{eB\hbar v^2}}\hat{l}^\dagger\right)\left(\frac{1}{\sqrt{eB\hbar v^2}}\hat{l}\right)\phi_2(y) &= \frac{E^2}{eB\hbar v^2}\phi_2(y) \\
&= \left(-\frac{\hbar}{eB}\frac{d^2}{dy^2} + \left[\sqrt{\frac{\hbar}{eB}}q - \sqrt{\frac{eB}{\hbar}}y\right]^2 - 1\right)\phi_2(y)
\end{aligned}$$

where e^{iqx} was cancelled on both sides. To simplify notation, energy will be measured in units of $\hbar\omega_c = \sqrt{e\hbar Bv^2}$ and distance in units of $l_m = \sqrt{\frac{\hbar}{eB}}$. The implication of this is also that the operator $\hat{l}$ has been rescaled to $\hat{l} = -i\frac{d}{dx} - y - \frac{d}{dy}$. Defining $z = \frac{1}{l_m}y - l_m q$ this leads to

$$\left(-\frac{d^2}{dz^2} + z^2 - 1\right)\phi_2(z) = E^2\phi_2(z) \tag{5.16}$$

This differential equation can be solved by a substitution $\phi_2(z) = e^{-\frac{z^2}{2}}\phi(z)$ which implies

$$\frac{d^2\phi}{dz^2} - 2z\frac{d\phi}{dz} + E^2\phi = 0 \tag{5.17}$$

This is precisely the Hermite differential equation [23]

$$H_c''(z) - 2zH_c'(z) + 2cH_c(z) = 0 \tag{5.18}$$

where the decaying solutions are Hermite functions, H_c. In the case where $c \in \mathbb{N}_0$, the functions are Hermite polynomials. Taking this as well as the substitutions necessary to get here into account, the wave function follows as

$$\phi_2(x,y) = e^{iqx}e^{-\frac{1}{2}(y-q)^2}H_{\frac{E^2}{2}}(y-q) \tag{5.19}$$

Stellenbosch University http://scholar.sun.ac.za

With this function known, one can begin to write down all other seven components by applying the appropriate transformations discussed in the previous section. The one that requires the most calculation is the one involving the sublattice degree of freedom

$$\begin{aligned}\frac{1}{E}\hat{l}\phi_2(x,y) &= \frac{1}{E}\left(-i\frac{d}{dx}-y-\frac{d}{dy}\right)e^{iqy}e^{-\frac{1}{2}(y-q)^2}H_{\frac{E^2}{2}}(y-q)\\ &= \frac{1}{E}\left((q-y)H_{\frac{E^2}{2}}(y-q)-(q-y)H_{\frac{E^2}{2}}(y-q)-H'_{\frac{E^2}{2}}(y-q)\right)e^{iqx}e^{-\frac{1}{2}(y-q)^2}\\ &= -EH_{\frac{E^2}{2}-1}(y-q) \qquad (5.20)\end{aligned}$$

after making use of the identity $H'_c(z) = 2cH_{c-1}(z)$. Now, the wave functions that follow immediately from the above calculation are those for Ψ_e and Ψ'_h namely

$$\begin{aligned}\Psi_e &= c_e e^{iqx}e^{-\frac{1}{2}(y-q)^2}\begin{pmatrix}-(\mu+\epsilon)H_{\frac{(\mu+\epsilon)^2}{2}-1}(y-q)\\ H_{\frac{(\mu+\epsilon)^2}{2}}(y-q)\end{pmatrix}\\ \Psi'_h &= c'_h e^{iqx}e^{-\frac{1}{2}(y-q)^2}\begin{pmatrix}-(\mu-\epsilon)H_{\frac{(\mu-\epsilon)^2}{2}-1}(y-q)\\ H_{\frac{(\mu-\epsilon)^2}{2}}(y-q)\end{pmatrix}. \qquad (5.21)\end{aligned}$$

For this pair, the boundary condition (5.3) leads to two equations namely

$$\begin{aligned}(\mu+\epsilon)H_{\frac{(\mu+\epsilon)^2}{2}-1}(-q) &= \frac{c'_h}{c_e}\left(\cos(\beta)(\mu-\epsilon)H_{\frac{(\mu-\epsilon)^2}{2}-1}(-q)+\sin(\beta)H_{\frac{(\mu-\epsilon)^2}{2}}(-q)\right) \qquad (5.22)\\ H_{\frac{(\mu+\epsilon)^2}{2}}(-q) &= \frac{c'_h}{c_e}\left(-\sin(\beta)(\mu-\epsilon)H_{\frac{(\mu-\epsilon)^2}{2}-1}(-q)+\cos(\beta)H_{\frac{(\mu-\epsilon)^2}{2}}(-q)\right) \qquad (5.23)\end{aligned}$$

By taking the ratio of the above two equations in order to eliminate the constant $\frac{c'_h}{c_e}$ one arrives at the following

$$f_{\mu+\epsilon}(-q)-f_{\mu-\epsilon}(-q) = -\tan(\beta)(1+f_{\mu+\epsilon}(-q)f_{\mu-\epsilon}(-q)) \quad \text{where} \quad f_\alpha = \frac{H_{\frac{\alpha^2}{2}}}{\alpha H_{\frac{\alpha^2}{2}-1}} \qquad (5.24)$$

which is an implicit dispersion relation which determines ϵ as a function of q. Of course, eq. (5.24) is only one of the two pairs of wave function spinors for which the boundary condition must be applied. If we consider the other pair of wave function spinors (for which the valley transformation must be applied), we find

$$\Psi'_e = c'_e e^{-iqx}e^{-\frac{1}{2}(y-q)^2}\begin{pmatrix}H_{\frac{(\mu+\epsilon)^2}{2}}(y-q)\\ (\mu+\epsilon)H_{\frac{(\mu+\epsilon)^2}{2}-1}(y-q)\end{pmatrix} \qquad (5.25)$$

Stellenbosch University http://scholar.sun.ac.za

$$\Psi_h = c_h e^{-iqx} e^{-\frac{1}{2}(y-q)^2} \begin{pmatrix} H_{\frac{(\mu-\epsilon)^2}{2}}(y-q) \\ (\mu-\epsilon) H_{\frac{(\mu-\epsilon)^2}{2}-1}(y-q) \end{pmatrix} \tag{5.26}$$

We want to compare states with the same wave number, q, but Ψ'_e and Ψ_h are labelled by an opposite wave number to Ψ_e and Ψ'_h. Thus we map $q \rightarrow -q$ and continue the calculation. By applying the boundary condition (5.3) one then finds

$$f_{\mu+\epsilon}(q) - f_{\mu-\epsilon}(q) = -\tan(\beta)(1 + f_{\mu+\epsilon}(q) f_{\mu-\epsilon}(q)) \tag{5.27}$$

where the f's are as defined previously. The expressions (5.24) and (5.27) are solved numerically and the results are plotted for several choices of parameters in Figs. (5.2)-(5.9). We will discuss the effect of varying Δ and μ seperately, starting with Δ.

5.3.1 Dependence on the superconducting gap potential

Figs. (5.2) - (5.5) show some plots of ϵ vs q for different choices of Δ. In all four figures we have $\mu = 0$. It turns out that all of the observations in the $\mu = 0$ case can be applied, with only small adjustment, to the case where $\mu \neq 0$.

As we would expect, due to the restrictions placed on the NS boundary condition, ϵ is restricted to $-\Delta < \epsilon < \Delta$. In the region of allowed ϵ we find degenerate Landau levels in the bulk. In the case where the particle excitation is in the $\vec{K}'$ ($\vec{K}$) valley, the bulk is associated with $q \gg \frac{1}{l_m}$ ($q \ll -\frac{1}{l_m}$). Degenerate Landau levels, where $\epsilon_n = \hbar\omega_c \text{sign}(n)\sqrt{2|n|}$, result because these excitations exist far away from the NS-interface, and the superconductor has little effect on them. At values of q that correspond to positions closer to the NS interface, where the effect is much stronger, these excitations from Landau levels split. One of the split excitation states always lies above (below) the other and is thus referred to as the upper (lower) exciation. The only exception here is the state associated with the zero'th Landau level in the bulk.

For the one excitation, the upper excitation, $\frac{\partial\epsilon}{\partial q}$ always has the same sign so that this excitation will always propagate in the same direction along the NS interface. For the lower excitation there is a small window, $|q| \sim \frac{1}{l_m}$, in which the sign of $\frac{\partial\epsilon}{\partial q}$ changes. Except for this window, the lower excitation propagates in the same direction as the upper excitation, though this is in opposite directions for the two valleys.

Stellenbosch University http://scholar.sun.ac.za

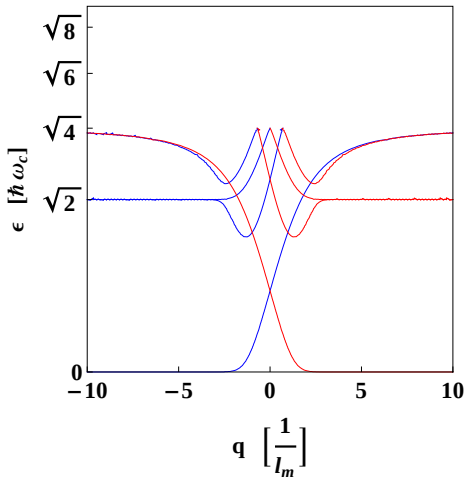

Figure 5.2: Excitation energy, ϵ, vs the wave number along the NS interface, q, for $\mu = 0$, $\Delta = 2$

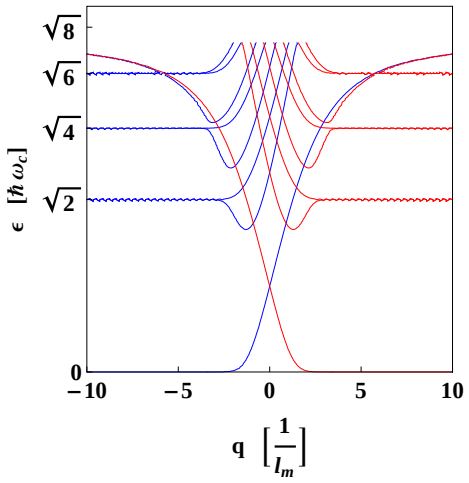

Figure 5.3: Excitation energy, ϵ, vs the wave number along the NS interface, q for $\mu = 0$, $\Delta = 2.7$

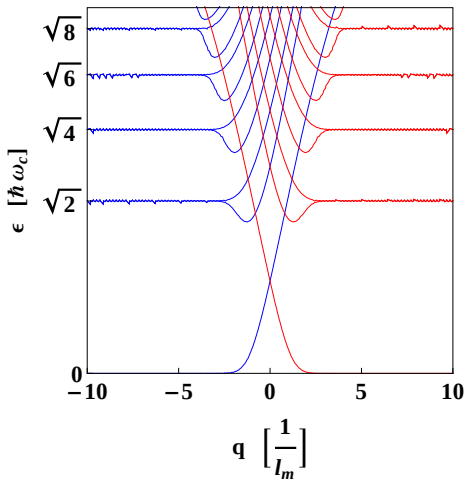

Figure 5.4: Excitation energy, ϵ, vs the wave number along the NS interface, q, for $\mu = 0$, $\Delta = 5$

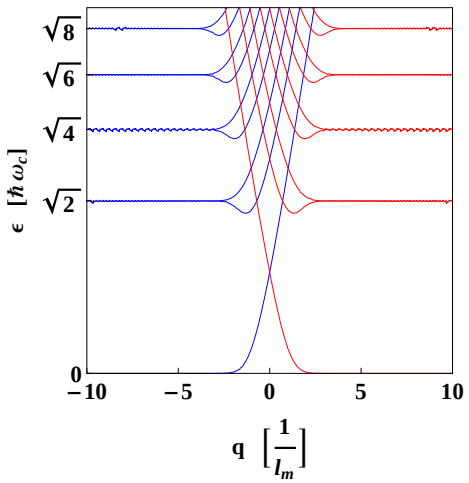

Figure 5.5: Excitation energy, ϵ, vs the wave number along the NS interface, q for $\mu = 0$, $\Delta \to \infty$

This propagation is allowed up to the point where $|\epsilon| < \Delta$. Beyond this point, as mentioned before, no excitation energies are allowed. All energies that lie inside these bounds are accessible, however, and the spectrum is thus entirely gapless (in the $\mu = 0$ case). An interesting feature to note is that for large $|q|$ the energies of states from the zero'th Landau levels converge to Δ. Also, an additional lower excitation appears that does not correspond to a bulk Landau level and also converges to Δ for large $|q|$.

Stellenbosch University http://scholar.sun.ac.za

5.3.2 Dependence on the chemical potential

We now consider cases where $\mu \neq 0$. Figs. (5.6) - (5.9) show the spectrum for some choices of the chemical potential as well as some that adjust the superconductor gap in addition to this.

The first observation one can make is that the energy of the excitations in the bulk have been

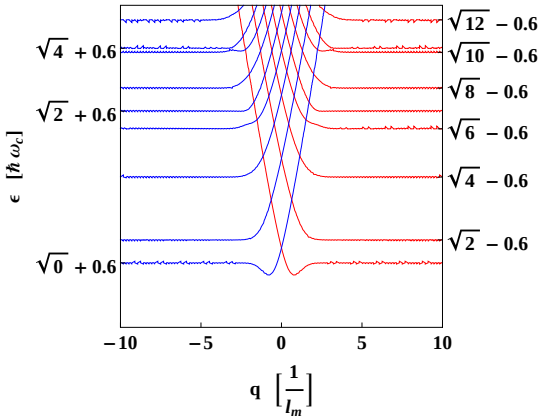

Figure 5.6: Excitation energy, ϵ, vs the wave number along the NS interface, q for $\mu = 0.6\hbar\omega_c$, $\Delta \to \infty$

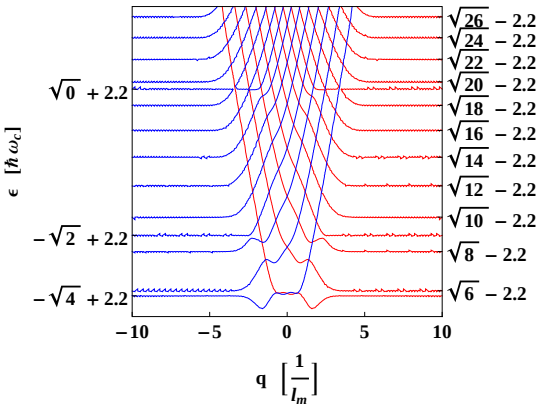

Figure 5.7: Excitation energy, ϵ, vs the wave number along the NS interface, q for $\mu = 2.2\hbar\omega_c$, $\Delta \to \infty$

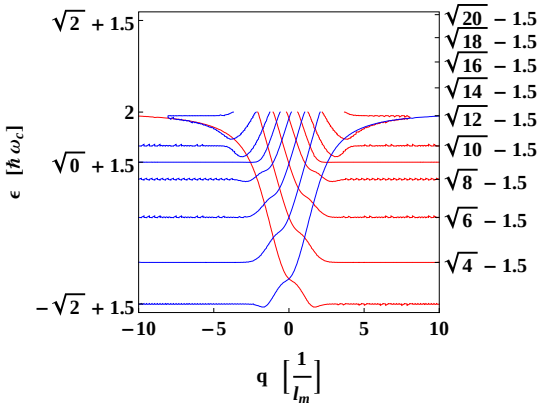

Figure 5.8: Excitation energy, ϵ, vs the wave number along the NS interface, q, for $\mu = 1.5\hbar\omega_c$, $\Delta = 2$

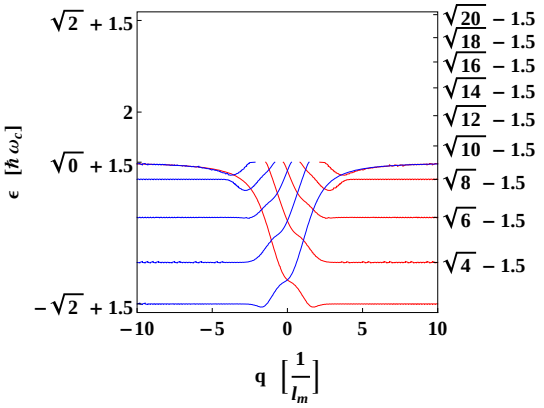

Figure 5.9: Excitation energy, ϵ, vs the wave number along the NS interface, q for $\mu = 1.5\hbar\omega_c$, $\Delta = 1.5$

shifted. Specifically the energies of all upper excitations (including the zero'th Landau level) have been shifted up by μ while the energies of all lower excitations have been shifted down by μ. In other words there are one set of Landau levels that converge to $\epsilon_n = \hbar\omega_c\left(\text{sign}(n)\sqrt{2|n|}\right) + \mu$ and another set of Landau levels that converge to $\epsilon_n = \hbar\omega_c\left(\text{sign}(n)\sqrt{2|n|}\right) - \mu$. These shifts persist for the former lower and upper excitation states even when μ is larger than several Landau level

Stellenbosch University http://scholar.sun.ac.za

energies.

These excitation states that were formerly upper and lower excitation states can no longer be classified by the behavior of $\frac{\partial \epsilon}{\partial q}$. This is because windows of q now exist for former upper excitations that allow propogation in a different direction and some former lower excitation states no longer have such windows. Propagation is still in opposite directions for the two valleys, however, and the allowed window for excitation energies remain $|\epsilon| < \Delta$. Furthermore, the zero'th Landau level still converges to Δ at large $|q|$ and a new former lower excitation state appears below Δ to also converge towards Δ at large $|q|$. Consequently, the only effect different in the $\mu \neq 0$ case than in the $\mu = 0$ case is the shift of the Landau levels. It is clear that the spectrum remains gapless if μ coincides with a Landau level energy.

5.3.3 Comparison with a real magnetic field — spectrum and kinematics

A system similar to ours has already been studied in [10]. The only difference in this paper is that the pseudo magnetic field is replaced by a real magnetic field. There are notable differences in the spectrum of the system if a pseudo magnetic field is applied as opposed to a real magnetic field. This can be understood already by only looking at the expected kinematics of propagation states along the NS interface. These states consist of particle and hole excitations that alternate due to Andreev reflection at the NS interface, as illustrated in Fig. (5.10) and Fig. (5.11).

Reflected hole excitations are in the valley opposite to that of the incoming particle, i.e.

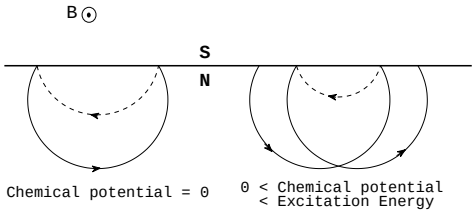

Figure 5.10: A schematic of the kinematics for propagating modes along the NS interface in the case of a real magnetic field

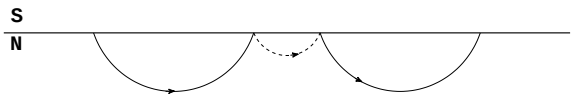

Figure 5.11: A schematic of the kinematics for propagating modes along the NS interface in the case of a pseudo magnetic field

an incident particle in valley $\vec{K}$ is reflected as a hole in valley $\vec{K}'$. The dynamics of a hole is determined by the time-reverse of the Hamiltonian that describes the particle that was removed to create the hole. Time-reversal switches the sign of the magnetic field. Thus a hole in valley $\vec{K}'$ experiences minus the magnetic field of a particle in valley $\vec{K}'$.

Stellenbosch University http://scholar.sun.ac.za

For a real magnetic field, particles in valley $\vec{K}$ and $\vec{K}'$ experience the same magnetic field. Thus for a real magnetic field, incident particles and their Andreev reflected holes experience opposite magnetic fields. These particles and holes trace cyclotron orbits in opposite directions. As illustrated in Fig. (5.10), perfect specular reflection at the interface then leads to closed orbits in which the excitations do not propagate along the interface. This explains the dispersionless interface states found for $\mu = 0$ in a real magnetic field.

For a pseudo magnetic field, however, particles in valley $\vec{K}$ and $\vec{K}'$ experience opposite magnetic fields. This implies that incident particles and Andreev reflected holes experience the same magnetic field. The particles and holes thus trace cyclotron orbits in the same direction. The specular reflection at the interface then leads to modes that may propagate even in the $\mu = 0$ case. Furthermore, since the magnetic field is of opposite sign for the different valleys in the case of a pseudo magnetic field, we would expect the direction of propagation to be opposite for the two valleys. In the case of a real magnetic field, where the sign is the same for both valleys, we would expect the direction of propagation to be the same for both valleys.

These results are clear when the spectrum for the NS-interface graphene system with real magnetic field, see Fig. (5.12), is compared with the results of the previous section. In the case of

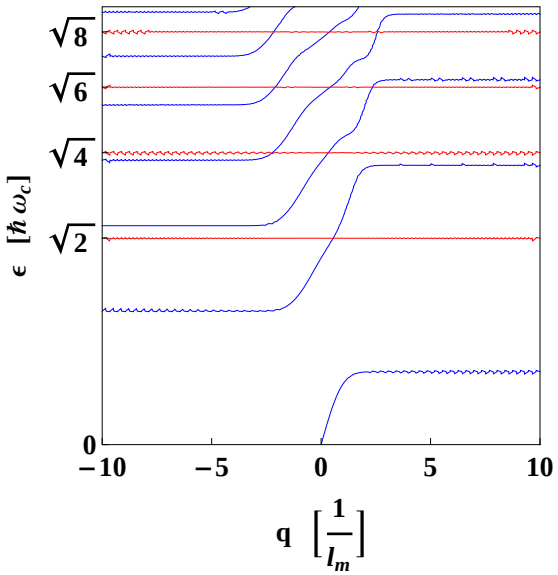

Figure 5.12: The spectrum for a real magnetic field NS interface system [10]. The red lines are for $\mu = 0$ and the blue lines for $\mu = 0.4\hbar\omega_c$

Stellenbosch University http://scholar.sun.ac.za

a real magnetic field being applied, the excitations in the two valleys have the same dispersion relation [10]. At a given energy excitations in different valleys therefore travel along the interface in the same direction and at the same velocity.

Furthermore, when $\mu = 0$, the Landau levels are dispersionless. For the pseudo magnetic field system, however, there are propagating modes at all energies that respect $|\epsilon| < \Delta$ in the $\mu = 0$ case. The spectrum is also gapless, whilst the real magnetic field system only becomes gapless (when the gap between the zero'th and first Landau level closes) at $|\mu| > \frac{\sqrt{2}}{2}\hbar\omega_c$.

The result of gap closing in the pseudo magnetic field system, when $\mu = 0$, is indeed a strange one since the two systems that were put together, that of a superconductor and a graphene sheet (which exhibits the QHE) have gaps in their spectra around the Fermi energy. In other words, this is an instance where there is a gapless edge spectrum at the interface between two gapped systems.

5.4 Armchair edge and Normal-Superconductor equivalence

During our calculations thusfar we have made use of the fact that simple transformations exist between all wave functions in the 8-component spinor of the Dirac equation. There exists a simple transformation between wave functions from different valleys and another simple transformation between wave functions from different sublattices in the same valley. The "transformation" between particle and hole excitations is usually a bit trickier as it cannot be written in the form of a linear operator acting in on a particle wave function to give a hole wave function for arbitarty μ or vector potential.

However, in the case where $\mu = 0$, such a transformation can indeed be found. This is because the relevent differential equation we wish to solve is

$$\hat{L}^\dagger \hat{L}\phi_2(E) = E^2 = (-E)^2 = \hat{L}^\dagger \hat{L}\phi_2(-E) \tag{5.28}$$

which implies that $\phi_2(E)$ and $\phi_2(-E)$ must be equal up to a multiplicative constant, due to the fact that they must both decay as $y \to -\infty$ and solve the same second order differential equation. This then implies that the spinors

$$\Psi_e = c_e \begin{pmatrix} \frac{1}{\epsilon}\hat{L}\phi_2(\epsilon) \\ \phi_2(\epsilon) \end{pmatrix} \qquad \Psi'_h = c'_h \begin{pmatrix} -\frac{1}{\epsilon}\hat{L}\phi_2(-\epsilon) \\ \phi_2(-\epsilon) \end{pmatrix} \to \Psi'_h = c'_h \begin{pmatrix} -\frac{1}{\epsilon}\hat{L}\phi_2(\epsilon) \\ \phi_2(\epsilon) \end{pmatrix} \tag{5.29}$$

Stellenbosch University http://scholar.sun.ac.za

are related by a simple linear transformation. The constant c'_h is redefined to contain the multiplicative constant.

It is the fact that we can, in the $\mu = 0$ case, relate excitations with different sublattice, valley and particle-hole indices by means of linear transformations that will help us to indicate an equivalence between systems with armchair edges and NS-interfaces. Indeed, Fig. (5.5) and Fig. (5.13) [10] tend to hint at such an equivalence, which will now be shown explicitly.

Any graphene sheet problem will boil down to solving for the two-component spinors Ψ_e,

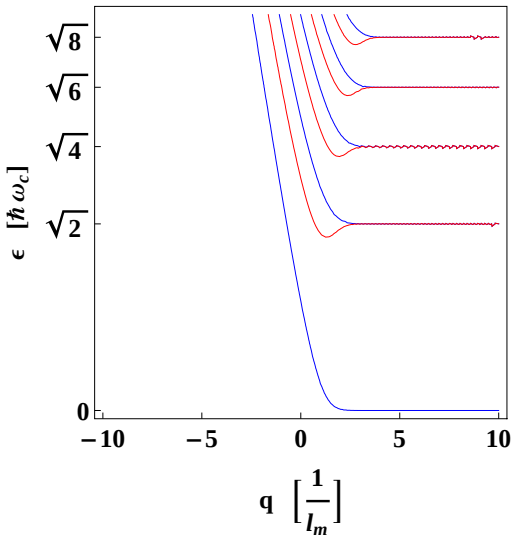

Figure 5.13: The spectrum of a real magnetic field applied to an half-infinite sample terminated by an armchair edge at $y = 0$ [10]

Ψ'_e, Ψ_h and Ψ'_h and then applying the boundary condition to ensure that the constants c_e, c'_e, c_h and c'_h are in an appropriate ratio. The problems we will be looking at will all be semi-infinite graphene sheets with a boundary orentiated along the angle α. For showing this equivalence we will be required to look at systems with real and pseudo magnetic fields and consider particle and hole excitations. This means that the spinors Ψ_e, Ψ'_e, Ψ_h and Ψ'_h can, up to a constant, be the following

$$\Psi_e^+ = \begin{pmatrix} \frac{1}{\epsilon}\hat{L}\phi_2(\epsilon) \\ \phi_2(\epsilon) \end{pmatrix} \tag{5.30}$$

$$\Psi_e^- = \begin{pmatrix} C\phi_2(\epsilon) \\ -\frac{1}{\epsilon}C\hat{L}\phi_2(\epsilon) \end{pmatrix} \tag{5.31}$$

Stellenbosch University http://scholar.sun.ac.za

$$\Psi_h^+ = \begin{pmatrix} -\frac{1}{\epsilon}\hat{L}\phi_2(\epsilon) \\ \phi_2(\epsilon) \end{pmatrix} \tag{5.32}$$

$$\Psi_h^- = \begin{pmatrix} C\phi_2(\epsilon) \\ \frac{1}{\epsilon}C\hat{L}\phi_2(\epsilon) \end{pmatrix} \tag{5.33}$$

where the superscript $\pm$ refers to the sign of the vector potential. The relevent constants are then determined by the boundary condition of the problem that we are investigating.

We shall be showing two equivalences. The first equivalence is between a semi-infinite graphene sheet with a real magnetic field, terminated by an armchair edge and a semi-infinite graphene sheet with a corresponding pseudo magnetic field and an NS interface. For the armchair edge, real magnetic field problem, the relevent 2×2 blocks are both particle excitations experiencing the same magnetic field. Thus, the boundary condition to impose is

$$\begin{aligned} c_e \Psi_e^+\big|_b &= c'_e \begin{pmatrix} 0 & -e^{-i(\theta+\alpha-\frac{\pi}{2})} \\ e^{-i(\theta-\alpha-\frac{\pi}{2})} & 0 \end{pmatrix} \Psi_e^+\Big|_b \\ \Rightarrow \Psi_e^+\big|_b &= c \begin{pmatrix} 0 & -e^{-i\alpha} \\ e^{i\alpha} & 0 \end{pmatrix} \Psi_e^+\Big|_b \end{aligned} \tag{5.34}$$

Then, for the NS-interface, pseudo magnetic field problem, the relevent 2×2 blocks are a particle and hole block experiencing the same magnetic field.

$$\begin{aligned} c_e \Psi_e^+\big|_b &= c'_h \begin{pmatrix} \cos(\beta) & \sin(\beta)e^{-i(\alpha-\frac{\pi}{2})} \\ \sin(\beta)e^{-i(-\alpha-\frac{\pi}{2})} & \cos(\beta) \end{pmatrix} \Psi_h^+\Big|_b \\ \Psi_e^+\big|_b &= c' \begin{pmatrix} 0 & e^{-i\alpha} \\ e^{-i\alpha} & 0 \end{pmatrix} \Psi_h^+\Big|_b \\ &= c' \begin{pmatrix} 0 & -e^{-i\alpha} \\ e^{-i\alpha} & 0 \end{pmatrix} \Psi_e^+\Big|_b \end{aligned} \tag{5.35}$$

after taking the $\beta \to \frac{\pi}{2}$ limit and using transformations in eqs. (5.30)-(5.33). Clearly these two problems lead to the same dispersion relation so that the spectrum will be identical. Note, however, that in the NS-interface, pseudo magnetic field problem the boundary condition needs to be applied to the other valley as well. There is not an equivalent problem for this in the armchair edge, real magnetic field problem. Thus the equivalence is between one of the two species of excitations in the pseudo magnetic field problem on the one hand and the full real

Stellenbosch University http://scholar.sun.ac.za

magnetic field system on the other.

An equivalence between another two problems can also be shown. These two problems are an NS interface with real magnetic field and an armchair edge with pseudo magnetic field system. First the NS interface system with real magnetic field system is investigated. This involves a particle excitation experiencing a certain magnetic field and a hole excitation experiencing minus the magnetic field coupled at an NS interface. Applying the boundary condition yields (in the $\beta \to \frac{\pi}{2}$ limit)

$$c_e \Psi_e^+\big|_b = c_h' \begin{pmatrix} 0 & e^{-i\alpha} \\ e^{i\alpha} & 0 \end{pmatrix} \Psi_h^-\Big|_b \quad \Rightarrow \quad \Psi_e^+\big|_b = c \begin{pmatrix} 0 & -e^{-i\alpha} \\ e^{i\alpha} & 0 \end{pmatrix} \Psi_e^-\Big|_b \tag{5.36}$$

again after consulting the equations (5.30)-(5.33). The boundary condition that must be solved for the other valley particle-hole pair is of exactly the same form and the spectrum is fully degenerate. Secondly, the armchair edge pseudo magnetic field system involves two particle excitations experiencing opposite magnetic field. The boundary condition in this case yields

$$c_e \Psi_e^+\big|_b = c_e' \begin{pmatrix} 0 & -e^{-i\alpha} \\ e^{i\alpha} & 0 \end{pmatrix} \Psi_e^-\Big|_b \quad \Rightarrow \quad \Psi_e^+\big|_b = c \begin{pmatrix} 0 & -e^{-i\alpha} \\ e^{i\alpha} & 0 \end{pmatrix} \Psi_e^-\Big|_b \tag{5.37}$$

which again indicates the equivalence of these two problems. This time the equivalence is to the full problem and not just half the problem.

This equivalence implies both that the spectrum of the two problems are identical and that the wave functions of the two problems are related to each other. Consequently, we may expect to find analogues in the distorted graphene with armchair edge system to quantum effects associated with superconductivity [26]. The investigation is not carried out further in this thesis, however.

5.5 A semi-infinite graphene sheet with armchair edge

The equivalence pointed out in the previous section implies that a graphene system terminated by an armchair edge along $y = 0$ with distortion $\vec{\alpha} = Bx\hat{y}$ produces dispersionless Landau levels. The question does arise whether or not this will also be the case if $\vec{\alpha} = -By\hat{x}$. Physically these two distortions lead to the same pseudo magnetic field. As was pointed out in Chapter 3, however, a transformation that changes the pseudo magnetic field is only strictly allowed

Stellenbosch University http://scholar.sun.ac.za

when the valleys remain uncoupled. If valleys are coupled, physical results may be altered. An armchair edge does, however, couple the valleys so it would appear as if changing the pseudo magnetic field may lead to different edge spectra.

This question will become relevent later when we will be investigation the conductance of a graphene system with an NS interface as well as two armchair edges. If the distortion of the lattice is chosen as perpendicular to the NS interface, it must be chosen as parallel to the armchair edges. It is therefore necessary to investigate the case where the distortion is not perpendicular to the armchair edge, but parallel.

Consequently, we now turn our attention to a system with a pseudo magnetic field terminated by an armchair edge. The system is rotated so that the edge now lies along the x-axis. This brings it even closer to the system we wish to investigate ultimately. We again have a semi-infinite graphene sheet, this time however defined in the region $x > 0$. This has an armchair edge at $x = 0$. The problem of the armchair edge terminated graphene sheet is sketched in Fig. (5.14). We choose the same constant pseudo magnetic field as before ($\vec{A} = By\hat{x}$) so that the Hamiltonian

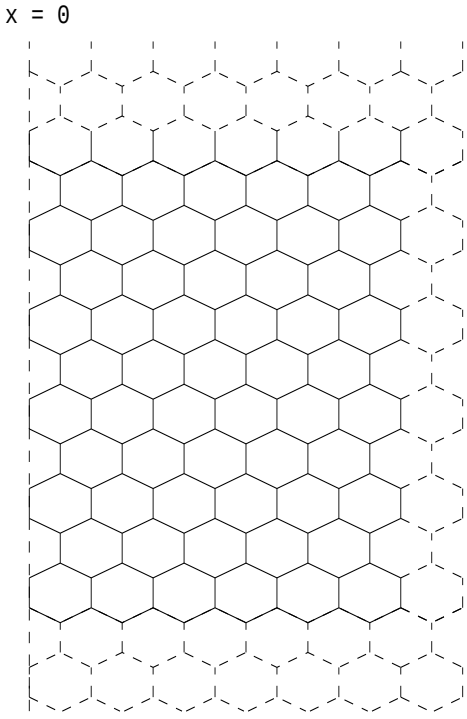

Figure 5.14: The semi-infinite graphene sheet terminated by an armchair edge

Stellenbosch University http://scholar.sun.ac.za

(this time only relevant for the particle excitations) reads

$$H\Phi = \begin{pmatrix} H_+ & 0 \\ 0 & H_- \end{pmatrix} \begin{pmatrix} \Psi_e \\ \Psi'_e \end{pmatrix} = \epsilon \begin{pmatrix} \Psi_e \\ \Psi'_e \end{pmatrix} \tag{5.38}$$

where $H_+ = \hat{l}^\dagger \hat{l}$ and $\hat{l} = \left(-i\frac{d}{dx} - y - \frac{d}{dy}\right)$. Translational invariance is broken in the direction parallel to the edge. The wave number parallel to the edge is therefore not a good quantum number. We restore translational invariance in the y-direction by performing different gauge transformations in the two valleys. The appropriate transformation is $\Psi_e = e^{-ixy}\Phi_e$

$$\begin{aligned} \begin{pmatrix} 0 & -i\frac{d}{dx} + y - \frac{d}{dy} \\ -i\frac{d}{dx} + y + \frac{d}{dy} & 0 \end{pmatrix} \Psi_e &= e^{-ixy} \begin{pmatrix} 0 & -i\frac{d}{dx} + ix - \frac{d}{dy} \\ -i\frac{d}{dx} - ix + \frac{d}{dy} & 0 \end{pmatrix} \Phi_e \\ &= e^{-ixy}\vec{\sigma}\cdot(\vec{p} - x\hat{y})\Phi_e \end{aligned} \tag{5.39}$$

while for the other valley transformation $\Psi'_e = e^{ixy}\Phi'_e$ will yield

$$\vec{\sigma}\cdot(\vec{p} - y\hat{x})e^{ixy}\Phi'_e = e^{ixy}\vec{\sigma}\cdot(\vec{p} + x\hat{y})\Phi'_e. \tag{5.40}$$

Now the particle has, after this transformation which is different for the two valleys, a Hamiltonian acting in on it which is translationally invariant parallel to the armchair edge. The solutions are derived in exactly the same way as they were above and then yield

$$\Psi_e = c_e e^{-ixy} e^{iq'y} e^{-\frac{1}{2}(x+q)^2} \begin{pmatrix} -i\epsilon H_{\frac{\epsilon^2}{2}-1}(x+q) \\ H_{\frac{\epsilon^2}{2}}(x+q) \end{pmatrix} \tag{5.41}$$

$$\Psi'_e = c'_e e^{ixy} e^{iq'y} e^{-\frac{1}{2}(x-q)^2} \begin{pmatrix} H_{\frac{\epsilon^2}{2}}(x-q) \\ -i\epsilon H_{\frac{\epsilon^2}{2}-1}(x-q) \end{pmatrix} \tag{5.42}$$

Under these system conditions the armchair edge boundary condition matrix is

$$M_I = \begin{pmatrix} 0 & 0 & 0 & -ie^{-i\theta} \\ 0 & 0 & ie^{-i\theta} & 0 \\ 0 & -ie^{i\theta} & 0 & 0 \\ ie^{i\theta} & 0 & 0 & 0 \end{pmatrix} \tag{5.43}$$

Stellenbosch University http://scholar.sun.ac.za

which then leads to

$$-ic_e\epsilon H_{\frac{\epsilon^2}{2}-1}(q) = -c'_e e^{-i\theta}\epsilon H_{\frac{\epsilon^2}{2}-1}(-q) \quad (5.44)$$

$$c_e H_{\frac{\epsilon^2}{2}}(q) = ic'_e e^{-i\theta} H_{\frac{\epsilon^2}{2}}(-q) \quad (5.45)$$

of which we can take the ratio to get

$$f_\epsilon(q) = -f_\epsilon(-q) \quad (5.46)$$

where f is defined in Eq. (5.27). Since $f_\epsilon(q)$ must be an uneven function this implies that either $H_{\frac{\epsilon^2}{2}}(q)$ or $H_{\frac{\epsilon^2}{2}-1}(q)$ must be odd (since the other one is then necessarily even). This implies that the excitation energy ϵ, in rescaled units, must be $\epsilon = \text{sign}(n)\sqrt{2|n|}$. The spectrum is then plotted in Fig. (5.15). As we would have expected from the equivalence of the previous section,

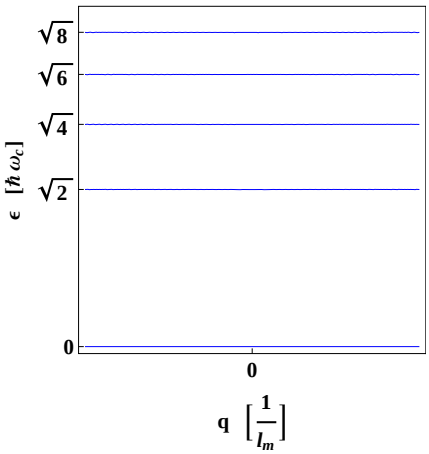

Figure 5.15: The spectrum for the semi-infinite graphene sheet terminated by an armchair edge

the states are dispersionless and excitation energies correspond to bulk Landau levels.

Stellenbosch University http://scholar.sun.ac.za

CHAPTER 6
Conductance in the real magnetic field problem

We will now begin utilising the numerical algorithm to calculate the conductance of graphene ribbons. In this chapter we will be considering specifically the case where a real, constant perpendicular magnetic field is applied to the sample. First we will look at the quantum hall effect to give an indication of the quality of results that are produced by the algorithm at our selected graphene sheet sizes and find a regime where our tight binding model coincides with the Dirac approximation.

Afterwards we will be looking at a graphene sheet with an applied constant magnetic field connected with an NS-interface. Such a system was studied analytically in [10]. This will serve as a test of the accuracy of the algorithm in systems with an NS-interface and allow us to verify the analytical results of [10] numerically. These results are that, firstly, excitations can propagate from an armchair edge to an NS interface without intervalley scattering. We will find in this chapter that the correspondence between the analytical and numerical results is good but not perfect. Intervalley scattering does take place, but not so much as to affect the nature of the results dramatically.

Secondly, it was argued in [10] that it is not necessary for the graphene ribbon to have perfect armchair edges, so long as there are two well-defined armchair edges a few magnetic lengths away from the interface. We confirm this by looking at ribbons where the width is not constant. These results will then be used as evidence that we have implemented the NS interface correctly in our numerical algorithm.

First, a short discussion of exactly how the algorithm must be employed in order for it to access the regime where the analytical results should hold.

6.1 Connecting with analytical results

The analytical results that we have derived in the previous chapters were all derived with the Dirac equation in specific energy regimes. These are that the energy levels that we probe must satisfy $|\epsilon| \ll t$ and $\epsilon < \Delta$. The magnetic fields must also satisfy $l_m \gg a$ and our system must be large enough to include several magnetic lengths. Magnetic fields are included as explained in chapter 2, by including a position dependent phase to the hopping terms. Also, our derivation

Stellenbosch University http://scholar.sun.ac.za

for the magnetic field, eq. (3.4), relied on the fact that we can throw away higher order terms, so that we should avoid magnetic fields that are too large i.e. magnetic lengths that are too small.

Secondly, the spectrum needs to be shifted in the leads by a large gate voltage [18]. This is to ensure, in the non-superconducting lead, that we avoid difficulties at the Dirac point in the device spectrum (see Fig. (6.1)) and to ensure, in the superconducting lead, that the Fermi wave vector in the superconductor is larger than the Fermi wave length in the device, i.e. $(\frac{\mu+V}{\hbar v} \gg \frac{\mu}{\hbar v})$. This ensures that the conditions for the M_{NS} boundary condition are satisfied. The other assumption of perfect leads, as relevent to the M_{NS} boundary condition, are already taken care of as assumptions of the Recursive Green's function approach.

Lastly, all potential steps must be turned on smoothly so as to avoid intervalley scattering, as done in [25]. Concretely, we define a length, D, over which potential steps (including the superconductor gap) is turned on continuously as

$$V_L(x,y) = \frac{1}{2}V\left(\tanh(1-\frac{2y}{D})+1\right) \tag{6.1}$$

$$V_R(x,y) = \frac{1}{2}V\left(\tanh(1+\frac{2(y-N)}{D})+1\right) \tag{6.2}$$

where indices L and R refer to the left or right lead and V is the value of of the potential step in the lead. Distances is measured in terms of column index, i.e. $\frac{\sqrt{3}a}{2}$. Both electrostatic potentials and superconductor gaps are turned on in the same way.

6.1.1 Quantum Hall effect

We first turn to the Quantum Hall effect in graphene. By considering the Quantum Hall effect it will allow us to benchmark good regimes for the magnetic field. In this example, there is no superconductor gap, and we are considering tranmission from the left to the right lead. The gate voltages on both sides compared to the hopping amplitude is selected as $V = \frac{t}{10}$, in arbitrary units. These are turned on over a length corresponding to $D = 30$ i.e. 30 rows of unit cells.

The device has an edge state spectrum similar to that shown in Fig. (2.8). Fig. (6.1) shows the accessible energy levels of the leads and device, along with an example of a chemical potential (the horizontal line). It is here that we can make use of the Landauer formula, eq. (4.4), which describes the conductance through a device to get an analytical answer for what we should expect. In order to calculate the transmission between the left and right lead we need to sum over

Stellenbosch University http://scholar.sun.ac.za

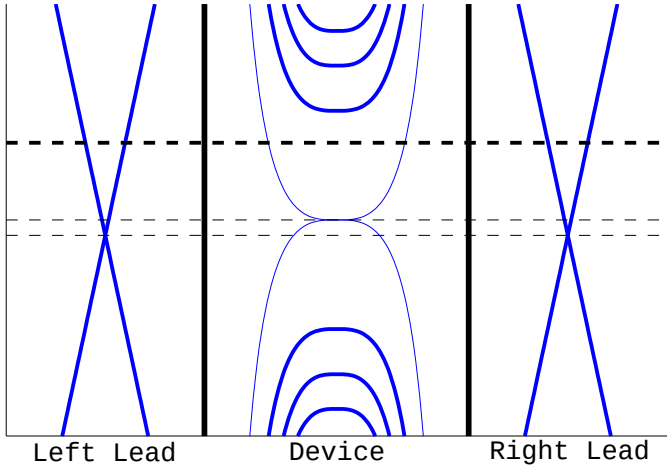

Figure 6.1: A plot of the spectra in the leads (left and right boxes) and the device (middle box) for a constant magnetic field applied in the device. Thick lines indicate degeneracy

all the channels $T_{LR} = \sum_n T_n(E)$. Transmission can only take place in a channel if the state is occupied ($\mu > E$) so that all channels with $\mu < E$ contributes nothing to transmission [20].

Since there is an absence of backscattering, transmission through an occupied channel should be one. Thus we should expect the transmission to be quantised as $2|n| + 1, n \in Z$ where $|n|$ is the index of the highest Landau level below the Fermi energy.

Calculating the transmission numerically then leads to Fig. (6.2). The results correspond well with what we anticipated. The zero'th Landau level contributes one to the transmission and so does crossing each subsequent channel. Crossing each subsequent level also adds two to transmission since it contains two channels. We can also see the fact that the armchair edge lifts the valley degeneracy of the spectrum. Between two consecutive plateaus ($2n + 1$ and $2n + 3$) there is a small region in which the transmission roughly equals $(2n + 2)$.

At higher excitations the plateaus are not quantised as well as they are for the low energy excitations. This can be attributed to mechanisms like backscattering to counter-propagating modes.

Stellenbosch University http://scholar.sun.ac.za

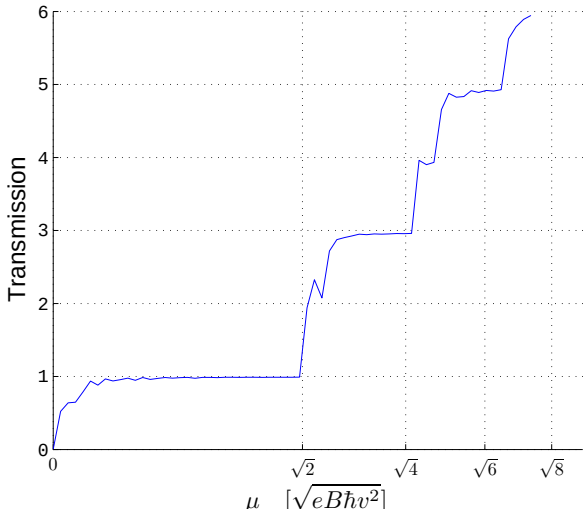

Figure 6.2: The Transmission plotted as a function of the chemical potential for the case of a constant magnetic field through the sample. The sample is 110 hexagons thick and 400 hexagons long and the magnetic length is 20 times the interatom spacing.

6.1.2 Conductance in an NS interface armchair edged system with real magnetic field

Other tests do exist for checking that the algorithm does indeed work for constructing the particle Hamiltonian (see for instance [25, 27]). Though these are useful to implement, they don't really give an idea in terms of variable regimes we may use for our calculations and are thus not explictly examined in this thesis. We now turn to the problem of an NS interface system terminated by two armchair edges and a real magnetic field perpendicular to the plane, as studied in [10].

In an NS-system (such as the one we wish to investigate) two additional energies are introduced into the system, namely that of the superconductor gap, Δ, and the superconductor gate voltage (which is set large in the boundary condition derivation [18]). Appropriate regimes for these parameters are that these must be large in comparison to the chemical potential, μ, but small in comparison to t.

It was found in [10] that at chemical potentials in an energy window between the zero'th and first Landau level only one propagating mode exists along the armchair edge and a set of two modes along the NS interface (valley-degenerate modes). It is then calculated that the

Stellenbosch University http://scholar.sun.ac.za

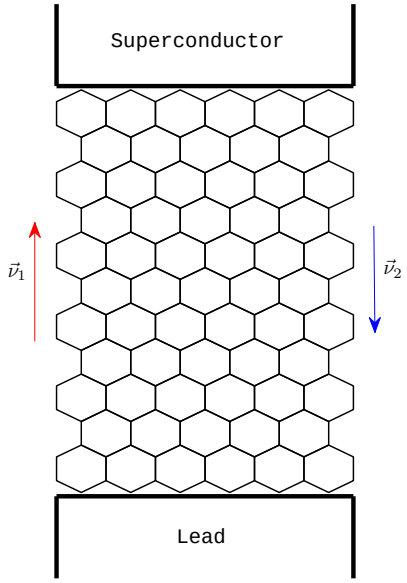

Figure 6.3: A schematic representation of the system that is going to be investigated. Conduction is expected to take place along the armchair edges and NS interface. The two armchair edges have valley polarisation $\vec{\nu}_1$ and $\vec{\nu}_2$ respectively.

transmission probability (which in this case is related to the conductance as $C_{NS} = \frac{4e^2}{h} T_{eh}$) of an electron entering the superconductor is given by

$$T_{eh} = \frac{1}{2}\left(1 - \vec{\nu}_1 \cdot \vec{\nu}_2\right) \tag{6.3}$$

where, $\vec{\nu_1}$ and $\vec{\nu_2}$ refers to the valley polarisation on the oppossite armchair edges, Fig. (6.3). In the case where the number of hexagons across the sample is a multiple of three, $\vec{\nu_1} = -\vec{\nu_2}$ so that $T_{eh} = 1$, while if it is not a multiple of three $\vec{\nu}_1 \cdot \vec{\nu}_2 = \frac{1}{2}$ so that $T_{eh} = \frac{1}{4}$.

Fig. (6.4) shows the conductance as a function of the width of the sample. Fig. (6.5) and Fig. (6.6) show the conductance as a function of chemical potential at 72 and 73 hexagons across the width respectively. The superconductor gap has been chosen as $\Delta = \frac{t}{2}$ and the step potential in the superconductor as $V = \frac{t}{10}$, compared to the hopping amplitude of $t = 10$ in arbitrary units. Chemical potential is measured in units of $\frac{t}{10}$.

Stellenbosch University http://scholar.sun.ac.za

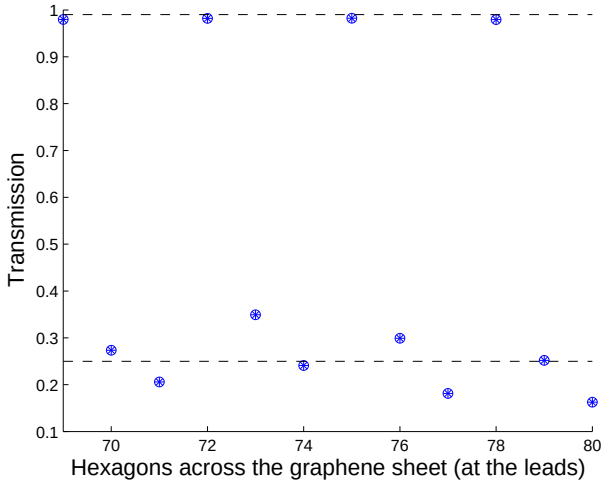

Figure 6.4: The transmission probability as a function of the width of the graphene sheet in the presence of a superconductor at $\mu = \frac{3t}{100}$ The sample is 150 hexagons long. The superconductor gap is chosen as half the hopping amplitude and the magnetic length $20a$.

In Fig. (6.4) the transmission probability is plotted, at a fixed chemical potential, as a function of number of hexagons across the width of the sample. The expected modulo 3 behavior is reproduced at chemical potentials small enough to only allow one propagating mode along the armchair edge. If the number of hexagons across the width of the sample is a multiple of 3, the transmission probability is very nearly equal to one while it is approximately a quarter otherwise.

Fig. (6.5) shows how the transmission probability varies as a function of chemical potential for 72 hexagons across the width. It is clear that as $\mu \to 0$, the transmission probability is not equal to one. We need a sufficiently large chemical potential for the transmission probability to approach unity.

The transmission probability as a function of chemical potential for 73 hexagons across the width is drawn in Fig. (6.6). Here we note a damped oscillatory behavior of transmission probability as the chemical potential is increased. This converges gradually towards the value of $\frac{1}{4}$, the expected analytical value.

The above discussion confirms the first result of [10] numerically. The assumption made that intervalley scattering is not present is good, though not perfect. This can be seen especially in graphs where the number of hexagons across the lead is not a multiple of three. Here the

Stellenbosch University http://scholar.sun.ac.za

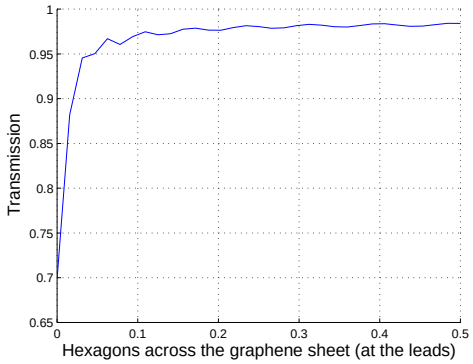

Figure 6.5: An example of transmission probability as a function of chemical potential for 72 hexagons across the lead in graphene with perfect armchair edges. Since the number of hexagons is a factor of three, the transmission probability is close to 1 when the chemical potential is large enough.

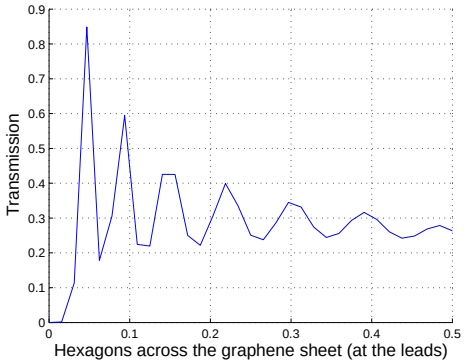

Figure 6.6: An example of transmission probability as a function of chemical potential for 73 hexagons across the lead in graphene with perfect armchair edges. Since the number of hexagons is not a factor of three, the transmission probability is close to 0.25 when the chemical potential is large enough.

analytical value of $\frac{1}{4}$ for the transmission probability is only reached as a limit, though it does come very close already at small chemical potentials.

6.2 Conductance in non-perfect armchair edge system

We now turn our attention a second statement of [10], namely that the armchair edge does not have to be perfect. Specifically the statement is made that the width of the armchair edge in the region of the NS interface does not need to be constant. The NS interface is the important region here since there are no counterpropagating modes along the interface. We will be investigating the validity of the modulo 3 behavior when the width of the graphene ribbon is no longer constant.

Fig. (6.8), Fig. (6.10) and Fig. (6.12) show different edge configurations which tend further and further away from the perfect armchair edge. Figs. (6.7), (6.9) and (6.11) show the corresponding transmission probability as a function of the width of the graphene sheet at the NS interface.

Even though some edge configurations are very far away from a perfect armchair edge, we still uncover the modulo three behavior of the transmission probability. If the width (at the interface) is a multiple of three the transmission probability is approximately one while it is a quarter otherwise.

Stellenbosch University http://scholar.sun.ac.za

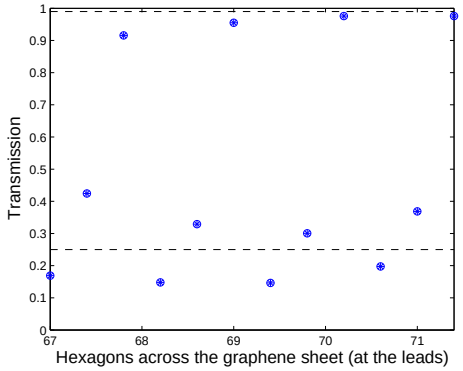

Figure 6.7: The transmission probability as a function of the width of the graphene sheet in the presence of a superconductor at $\mu = \frac{3t}{100}$. The corresponding edge defect graph is Fig. (6.8)

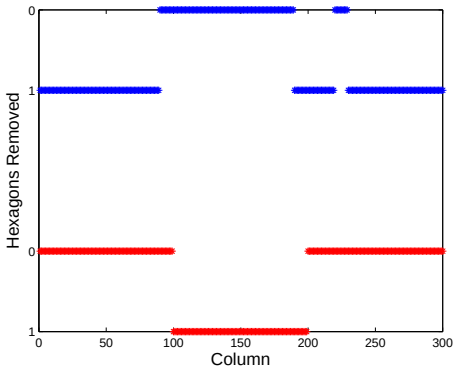

Figure 6.8: The corresponding edge random walk. The blue indicates the number of hexagons taken away at the top and the red the hexagons taken away at the bottom. This gives an indication of the shape of the graphene sheet.

Fig. (6.13) and Fig. (6.14) show the transmission probability as a function of chemical potential for the 72 and 73 hexagons across the interface respectively, for the edge configuration in Fig. (6.12). The transmission probability is supressed for a larger chemical potential window as $\mu \to 0$ for both cases. For the 72 hexagon lead the transmission probability soon plateaus at one. For the 73 hexagon lead the transmission probability has been affected quite significantly. The transmission probability no longer seems to plateau exactly at $\frac{1}{4}$ and the regular oscillatory behavior is no longer present. The transmission probability does however remain in the region of $\frac{1}{4}$, despite the edge being significantly different to a perfect armchair edge.

The results imply that the modulo three behavior of a graphene sheet with armchair edge and an NS interface, under influence of a perpendicular magnetic field, remains even if the edge is disordered. This is the case as long as the width remains constant for several magnetic lengths in the normal region next to the NS interface.

Stellenbosch University http://scholar.sun.ac.za

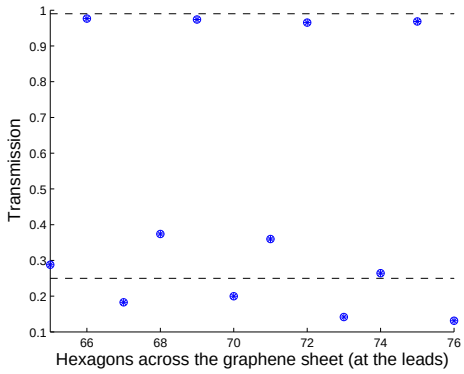

Figure 6.9: The transmission probability as a function of the width of the graphene sheet in the presence of a superconductor at $\mu = \frac{3t}{100}$. The corresponding edge defect graph is Fig. (6.10)

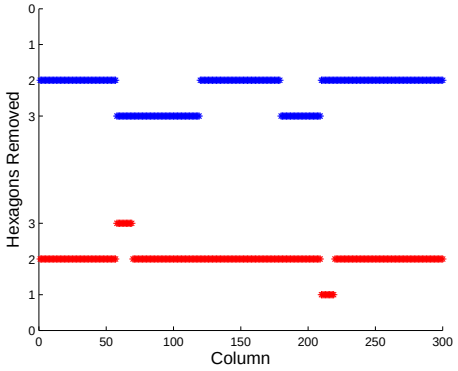

Figure 6.10: The corresponding edge random walk. The blue indicates the number of hexagons taken away at the top and the red the hexagons taken away at the bottom. This gives an indication of the shape of the graphene sheet.

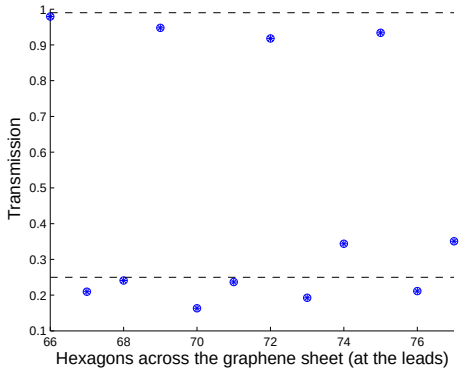

Figure 6.11: The transmission probability as a function of the width of the graphene sheet in the presence of a superconductor at $\mu = \frac{3t}{100}$. The corresponding edge defect graph is Fig. (6.12)

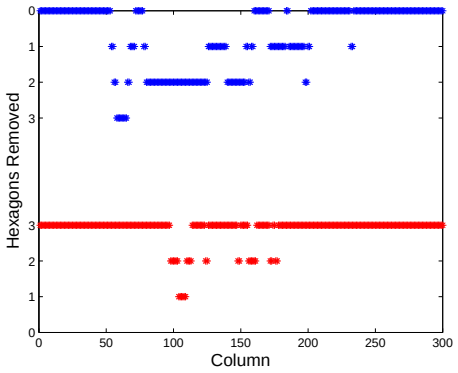

Figure 6.12: The corresponding edge random walk. The blue indicates the number of hexagons taken away at the top and the red the hexagons taken away at the bottom. This gives an indication of the shape of the graphene sheet.

Stellenbosch University http://scholar.sun.ac.za

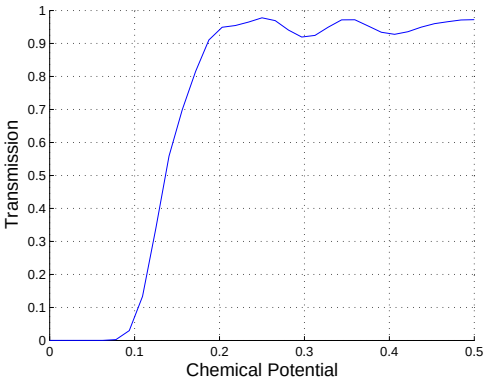

Figure 6.13: An example of transmission probability as a function of chemical potential for 72 hexagons across the lead. Significant alterations are present (see Fig. (6.12)), but the main characteristics remain.

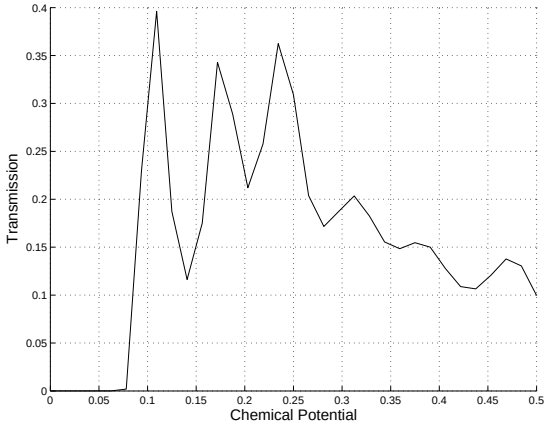

Figure 6.14: An example of transmission probability as a function of chemical potential for 73 hexagons across the lead. Significant alterations are present (see Fig. (6.12)), but the main characteristics remain.

Stellenbosch University http://scholar.sun.ac.za

CHAPTER 7
The finite distorted graphene with an NS interface problem

Consider the system where we have a graphene ribbon terminated by two armchair edges and an NS interface. This graphene ribbon is distorted slightly so as to give rise to a constant pseudo magnetic field, with the vector potential perpendicular to the NS interface. Our results from Chapter 5 showed that, far away from the NS interface where the effect of the armchair edge dominates, we would expect no propagating modes. Inside the bulk of the system we only expect propagation to take place in a small window around the bulk Landau levels.

Along the NS interface, however, our results indicated that we can always expect propagating modes. These propagating modes travel in opposite directions along the interface for the different valleys. States along the interface can, in other words, not leave the region around the interface if their energies do not correspond to Landau levels. Thus states propagating in different directions along the interface must hybridise and form bound states.

Such bound states would be very interesting to find in graphene and as a consequence, our attention will now turn to such a finite distorted graphene system with an NS interface. We do not necessarily have to calculate the spectrum explicitly as other quantities can reveal their existence. One example is the conductance of a sample of graphene. If the energy of an incoming particle is close to that of one of these bound states, it can tunnel through to the NS interface where Andreev reflection takes place, after which an outgoing hole can tunnel back. This can be observed as resonance peaks in the transmission as a function of chemical potential.

The results of Chapter 5 were uncovered in the context of an ideal system, however. This is because the Dirac equation is only valid in the corners of the Brillouin zone. Away from these corners it is possible that we might find that the armchair edges are not fully dispersionless. Furthermore, it is not physically possible for us to deform a graphene sheet so that a constant pseudo magnetic field forms along the entire length of the semi-infinite ribbon. This is simply because the deformations of the bonds between adjacent atoms will become unphysical.

To address these issues it will be necessary to first verify that the armchair edge is still dispersionless in a finite ribbon. Secondly it will be necessary to specify a finite region, of length L_A, over which deformation of the ribbon takes place. Outside of this region, including the

Stellenbosch University http://scholar.sun.ac.za

leads, the graphene ribbon retains its normal shape. The region of length L_A will be required to contain the NS interface. These calculations will have to be performed numerically.

The algorithm that we have constructed can handle a superconducting lead and the extention from a real magnetic field to a pseudo magnetic field is a very simple procedure within the algorithm. The results of the previous chapter have, among others, indicated that the machinery we have developed can successfully deal with NS-interface systems from first principles.

7.1 The non-propagation of armchair edge states in finite graphene

We first turn our attention to the transmission of an armchair ribbon with pseudo magnetic field. Two normal leads are attached to a graphene ribbon of length L_A, terminated by two armchair edges. The distortion is chosen such as to give rise to a constant pseudo magnetic field. Fig. (7.1) shows the transmission as a function of chemical potential. The relevent Green's function is G_{1N} as we are looking at conductance from the left lead to the right lead. The parameter choices here are again $V = \frac{t}{10}$.

In Fig. (7.1) we see that transmission takes place in a small energy window around the bulk

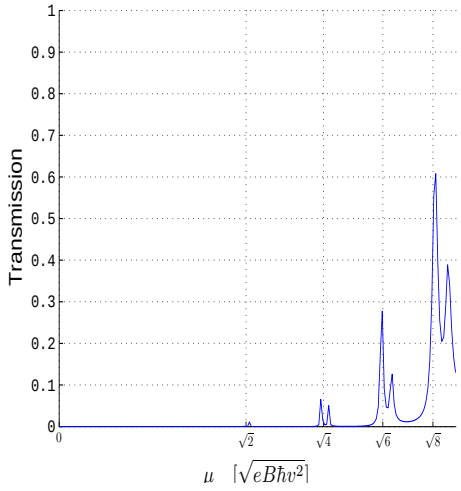

Figure 7.1: Transmission through a distorted graphene sheet with two armchair edges with $M = 100$ and $L_A = 100$. The pseudo-magnetic field is constant. Away from bulk energies, the transmission is greatly suppressed.

Landau levels. Away from these energies, the transmission goes down to zero as no propagating modes are available.

Stellenbosch University http://scholar.sun.ac.za

This phenomenon should be visualised as follow. Again, similar to the real magnetic field case, an infinite graphene sheet will have dispersionless Landau levels at the bulk Landau energies of graphene. When an armchair ribbon is considered these levels disperse slightly (and split slightly for the different valleys). There are propagating edge states. However, their energies do not completely fill the gaps between bulk Landau levels, as happens in a real magnetic field. Consequently, a small propagation window opens up around Landau levels, but closes again before the next Landau level is reached.

7.2 Bound states near the NS interface

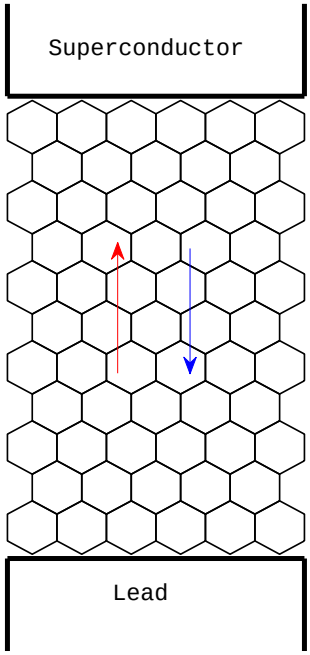

Figure 7.2: A schematic representation of the system that is going to be investigated. Conduction is expected to take through the bulk (via tunneling), since no propagation is allowed along the armchair edges.

What we have confirmed in the previous section is that the armchair edge is a good insulator. As stated before it is very important that the armchair edge does not allow propagation of states, otherwise the NS interface states will leak away along the armchair edges and the bound states will not be able to form. This means that we can begin simulations to uncover the resonances associated with the NS interface. The system setup is drawn in Fig. (7.2). Before the numerical

Stellenbosch University http://scholar.sun.ac.za

analysis resumes, however, it is sensible to discuss some of the properties that we expect these states to exhibit.

7.2.1 Size of the system and width of the peaks

In order for the transmission to exhibit clear signs of the resonances associated with the NS interface, it is necessary for tunnelling to take place. Thus, L_A must be short enough so that all tunneling amplitudes are not entirely suppressed. L_A must also be large enough so that the excitations cannot tunnel through the pseudo magnetic field region easily. This will allow for clear resonance peaks to be seen once the chemical potential is close to that of a bound state energy.

As a consequence of the above, we should expect the width of the peaks to be sensitive to L_A. For larger L_A, the tunneling amplitudes will be suppressed more so that only energies closer to the energy of the bound states will allow transmission. Thus, with increasing L_A we expect the width of the peaks, γ, to become smaller.

7.2.2 The number of peaks

In order to get a rough estimate of how many peaks we expect in the energy regime between the zero'th and first Landau level, we can do the following: We take the spectrum far away from the armchair edges and a magnetic length away from the NS interface to be that of the NS interface problem calculated in Chapter 5. We then quantise the wave numbers as $q_n = \frac{\pi n}{W}, \quad n \in \mathbb{Z}$, where W is the width of the ribbon, and plot these along with the dispersion relation, see Fig. (7.3).

Up to slight deviations we should expect approximately one bound state, i.e. one resonance peak per section. The expected chemical potentials for the resonances are contained in the sections. In the regions where the dispersion is nearly linear this implies that the spacing between resonances scales as $\frac{1}{W}$.

7.3 A numerical confirmation of resonances associated with the NS interface

In order to carry out the investigation we introduce the distance over which distortion takes place as L_A. The distortion is done in such a way such that at the center of the region ($\frac{L_A}{2}$) the distortion is zero. Here we must always be careful to not select distortions that are too large, since our analytical derivations were really only valid for small distortions. The parameters we have selected are again $V = \frac{t}{10}$ and the distortion as $\lambda_1 = \lambda_2 = \frac{1}{50}(y - \frac{L_A}{2})$, which gives a

Stellenbosch University http://scholar.sun.ac.za

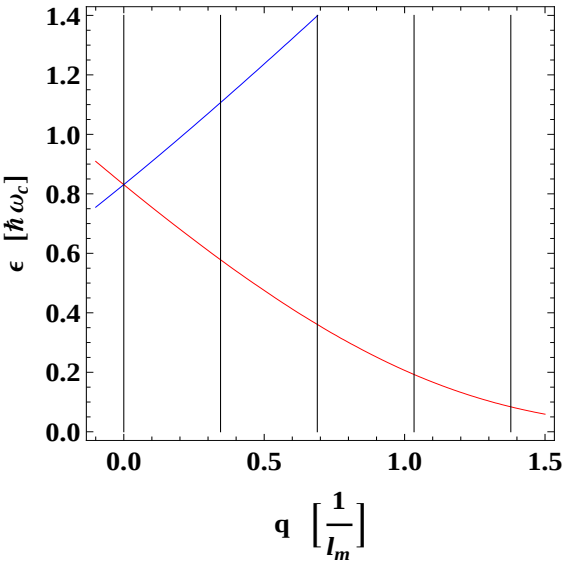

Figure 7.3: The NS interface spectrum (for both valleys) drawn with the expected window of solution q's. The bound state energies occur approximately as one per section.

magnetic length of $(5)(3)^{\frac{1}{4}}a$.

We will go through the predictions stated in the previous section systematically.

7.3.1 System size

The first discussion related to the fact that the system size needs to be sufficient in order for the bound states to exist. Figs. (7.4) - (7.7) shows how the bound states start appearing from a plain background.

The figures indicate that the resonances become visible for $L_A \geq 45$. The resonance width is very sensitive to the value of L_A, as anticipated. A large quantitative difference can be seen between Fig. (7.5) and Fig. (7.7), even though only 2 additional columns are added to the system.

7.3.2 Dependence on the length, L_A

In Figs. (7.8) - (7.11) we investigate the dependence on L_A of the width of the resonance peaks more carefully. The figures show that the peaks become thinner rapidly. In order to investigate the width of the peak more carefully we need to choose a specific function with a well-defined width that we can use as a benchmark. The function we choose here is a Lorentzian. The

Stellenbosch University http://scholar.sun.ac.za

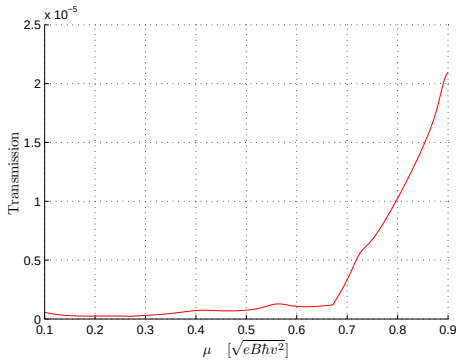

Figure 7.4: The transmission as a function of chemical potential between the 0th and 1st Landau level for a distorted graphene sheet with an NS interface. Here $L_A = 44$ and $M = 100$.

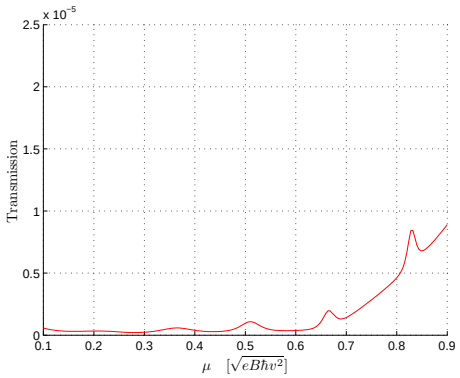

Figure 7.5: The transmission as a function of chemical potential between the 0th and 1st Landau level for a distorted graphene sheet with an NS interface. Here $L_A = 45$ and $M = 100$.

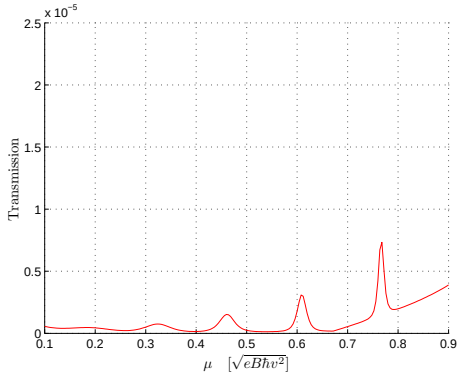

Figure 7.6: The transmission as a function of chemical potential between the 0th and 1st Landau level for a distorted graphene sheet with an NS interface. Here $L_A = 46$ and $M = 100$.

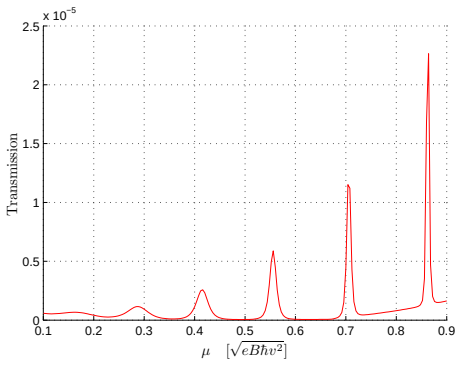

Figure 7.7: The transmission as a function of chemical potential between the 0th and 1st Landau level for a distorted graphene sheet with an NS interface. Here $L_A = 47$ and $M = 100$.

Lorentzian is defined as

$$L = I\frac{\gamma^2}{(\epsilon_n - \epsilon)^2 + \gamma^2} \tag{7.1}$$

where I is the height of the peak, ϵ_n will be the center point of the peak and γ is the width of the peak. We examine the peaks situated between $\mu = 0.5\hbar\omega_c$ and $\mu = 0.6\hbar\omega_c$ of Figs. (7.8)-(7.11) more closely. A Lorentzian is fitted with height, I, chosen as the maximal value of the peak and the center point, ϵ_0 chosen as the corresponding value for μ. A least squares fit is then made to find the parameter γ, the width of the peak.

Stellenbosch University http://scholar.sun.ac.za

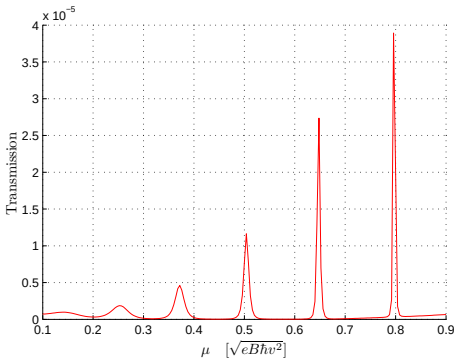

Figure 7.8: The transmission as a function of chemical potential between the 0th and 1st Landau level for a distorted graphene sheet with an NS interface. Here $L_A = 48$ and $M = 100$.

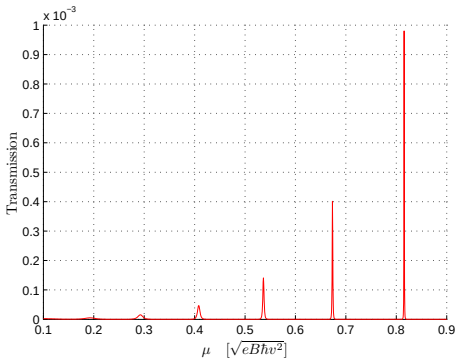

Figure 7.9: The transmission as a function of chemical potential between the 0th and 1st Landau level for a distorted graphene sheet with an NS interface. Here $L_A = 50$ and $M = 100$.

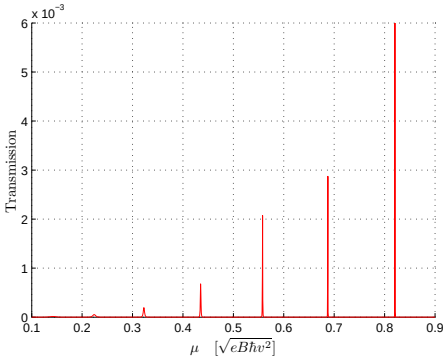

Figure 7.10: The transmission as a function of chemical potential between the 0th and 1st Landau level for a distorted graphene sheet with an NS interface. Here $L_A = 52$ and $M = 100$.

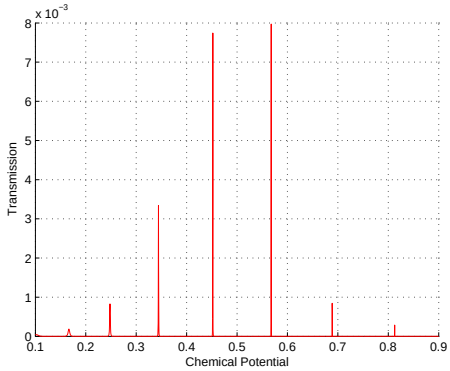

Figure 7.11: The transmission as a function of chemical potential between the 0th and 1st Landau level for a distorted graphene sheet with an NS interface. Here $L_A = 54$ and $M = 100$.

In the region of the peaks, the Lorentzian is a very reasonable fit. Away from the peaks the fit becomes less accurate. It is clear for Figs. (7.12)-(7.15) that the width of the resonance peaks decrease significantly as the length of the system is adjusted. Note also the order of magnitude increase of the height of the peak as L_A is increased. The peak becomes much thinner, but also much higher. We do not yet have an explanation for this height increase.

7.3.3 Dependence on the width of the system

The last prediction that we need to check is whether the number of peaks increase as the width of the system, M, is increased. We would further, from the spectrum near the NS inter-

Stellenbosch University http://scholar.sun.ac.za

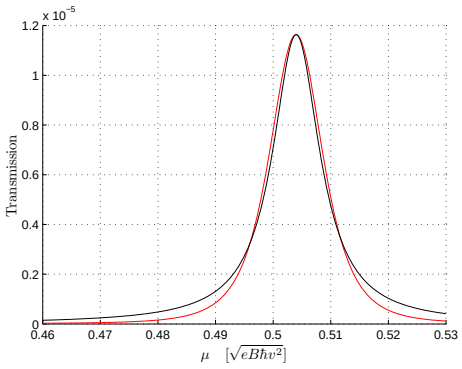

Figure 7.12: A zoomed in image of one of the peaks for $L_A = 48$ and $M = 100$. Red curves are data and black curves are the best Lorentzian fit. The value for the width of the peak is determined as $\gamma = 0.00499$

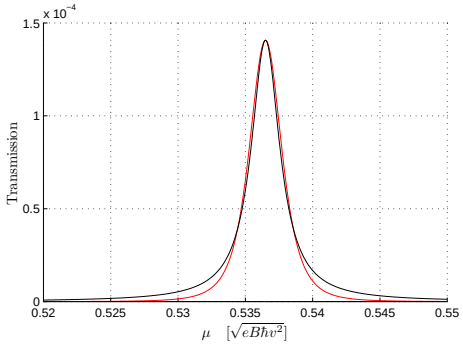

Figure 7.13: A zoomed in image of one of the peaks for $L_A = 50$ and $M = 100$. Red curves are data and black curves are the best Lorentzian fit. The value for the width of the peak is determined as $\gamma = 0.0012876$

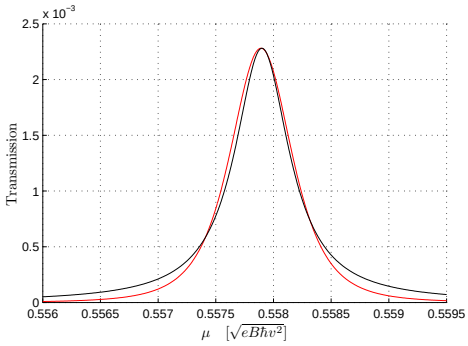

Figure 7.14: A zoomed in image of one of the peaks for $L_A = 52$ and $M = 100$. Red curves are data and black curves are the best Lorentzian fit. The value for the width of the peak is determined as $\gamma = 0.000287536$

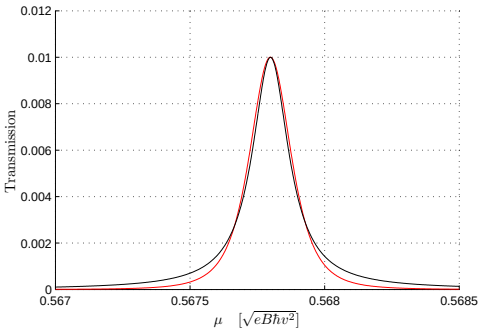

Figure 7.15: A zoomed in image of one of the peaks for $L_A = 54$ and $M = 100$. Red curves are data and black curves are the best Lorentzian fit. The value for the width of the peak is determined as $\gamma = 0.0000082177$

face, expect the peaks at lower μ to be more densely spaced than for higher values of μ. Figs. (7.16)-(7.19) show the behavior of the resonance peaks as the width of the system, M is increased.

The number of peaks certainly increase as M is increased and the spacing of the peaks closer to $\mu = 0$ is also more dense than for higher values of μ. The increase is also approximately what we would expect from our estimate that the spacing of the peaks should scale as $\frac{1}{M}$. For $M = 40$ we see 2 peaks, for $M = 80$ we see 4 peaks and for $M = 160$ we see 8 peaks. Note, however, that the shape of the individual peaks are fairly insensitive to the value of M.

Stellenbosch University http://scholar.sun.ac.za

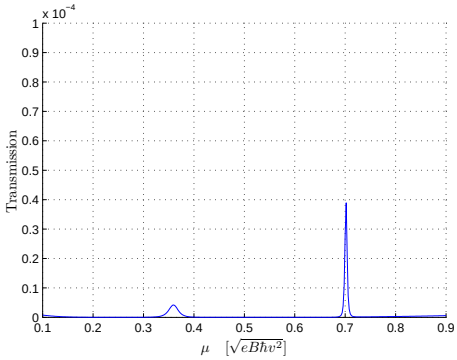

Figure 7.16: The transmission as a function of chemical potential between the 0th and 1st Landau level for a distorted graphene sheet with an NS interface. Here $L_A = 48$ and $M = 40$.

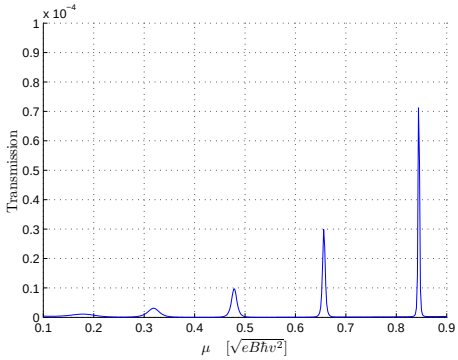

Figure 7.17: The transmission as a function of chemical potential between the 0th and 1st Landau level for a distorted graphene sheet with an NS interface. Here $L_A = 48$ and $M = 80$.

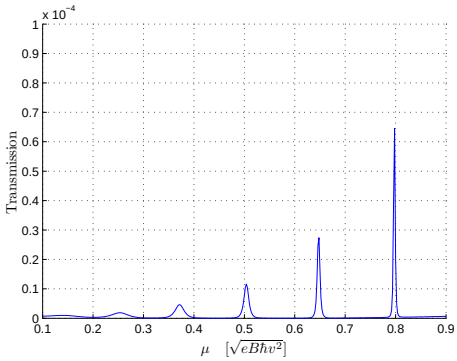

Figure 7.18: The transmission as a function of chemical potential between the 0th and 1st Landau level for a distorted graphene sheet with an NS interface. Here $L_A = 48$ and $M = 120$.

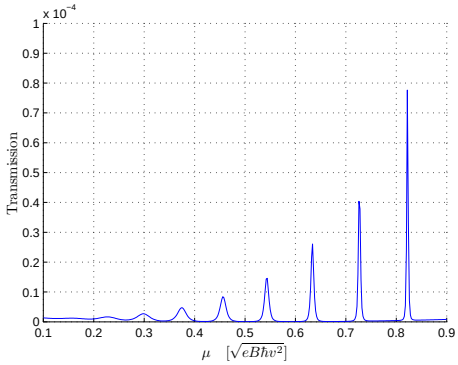

Figure 7.19: The transmission as a function of chemical potential between the 0th and 1st Landau level for a distorted graphene sheet with an NS interface. Here $L_A = 48$ and $M = 160$.

7.4 Summary

In this chapter we investigated an armchair ribbon that is deformed in order to give rise to a constant pseudo magnetic field. The study was conducted by numerical means, using the graphene tight binding Hamiltonian as a starting point. In other words, the Dirac approximation was not made. The transmission through such a system was shown to be non-zero only in small regions around the bulk Landau level, implying that the armchair edge in such a system serves as an insulator. This holds even outside the Dirac limit.

When this system is attached to a superconductor, resonances are seen in the sub-gap transmis-

Stellenbosch University http://scholar.sun.ac.za

sion. This is due to the fact that the NS interface allows states to propagate in both directions while the armchair edge serves as an insulator. Thus, bound states form near the NS interface and resonances are seen when excitations have energies close to the energies of the bound states.

These resonances depend on the width of the system as well as the length over which the ribbon is distorted in the normal region adjacent to the NS interface. The width of the system affects the spacing of the resonance peaks and, consequently, the number of peaks. The wider the system, the more peaks are expected. This can be expected since an increasing width allows more possible wave number quantisations along the interface.

The length over which the ribbon is distorted has the effect of making the resonance peaks both thinner and higher. This can be explained since the transmission of these excitations requires the excitations to tunnel through the length of the distortion. An explanation for the change in the height of these resonances could not be found at this point, and warrants further investigation. The system is very sensitive to this parameter and large quantitative differences can be observed for very small changes in this length.

These states indicate two interesting things, namely that the localisation of excitations in graphene can be caused without the use of a large external potential or one that varies very quickly. Secondly, these effects would not have been possible without the different dynamics present in the two graphene valleys (this is due to the distortion of the lattice). In other words, the different dynamics in the two valleys lead to observable effects in this setup.

The effect does remain small, however, and the resonances are usually thin and not of a high intensity. Furthermore, the formation of a constant pseudo magnetic field is likely to be difficult. However, the hope is that these results will be applicable as long as the magnetic field remains constant over a few magnetic lengths. This is something that can be investigated further in future.

In the case of a zig-zag edge terminating the system as opposed to an NS interface, quasi-bound states are also expected to feature. This system, despite being a much simpler experimental setup than an NS interface system, would only have one lead. Thus, there will not be any resonances in transport. The investigation is not carried out in this thesis.

Stellenbosch University http://scholar.sun.ac.za

CHAPTER 8
Conclusion

The results of this thesis can be split up into three categories: (1) Analytical studies of semi-infinite distorted graphene sheets. (2) Numerical analysis of results pertaining to the transmission through an armchair ribbon subject to a real magnetic field and an NS interface. (3) Numerical analysis of a distorted armchair ribbon with an NS interface. These will now be discussed pointwise.

Firstly, distortions of a graphene sheet which give rise to a constant pseudo magnetic field were considered [13]. A pseudo magnetic field is a magnetic field that affects the two valleys of graphene in opposite ways. Thus, the dynamics of the two valleys are different. Coupling the system then to a superconductor was motivated by the fact that rich dynamics can potentially be obtained when these valleys are coupled. Two specific ways to couple the valleys were looked at, namely the inclusion of an NS interface and the termination of the system by means of an armchair edge. A similar calculation was carried out in [10], though with a real magnetic field being applied to that system as opposed to a pseudo magnetic field.

Adding an NS interface to the distorted graphene system produced some interesting results. The spectrum of this system was found to be gapless in the case where the chemical potential, μ, equals zero. Furthermore, excitations associated with different valleys were shown to propagate in opposite directions along the NS interface. These phenomenon were explained in the light of specular Andreev reflection [18]. In a pseudo magnetic field, particles and holes from different valleys see the same magnetic field. This results in the fact that the cyclotron orbits along the interface are the same for particles and their Andreev reflected holes. Thus, propagation even takes place when $\mu = 0$. Furthermore, since the magnetic field is opposite for the two different particle excitations, the orbitals associated with different different valleys are of opposite direction. Consequently the different valley excitations travel in opposite directions along the NS interface.

This behaviour differs quite significantly from some aspects of the system's real magnetic field counterpart as studied in [10]. In the case of the real magnetic field system gap closing only occurs if the chemical potential exceeds half the energy of the first Landau level. Propagation along the interface is in the same direction for both valleys and no propagation is present if $\mu = 0$.

Stellenbosch University http://scholar.sun.ac.za

Systems with a real magnetic field and pseudo magnetic field are not entirely unrelated, however. An equivalence was shown between systems of a real magnetic field with an NS interface (armchair edge) and a pseudo magnetic field with an armchair edge (NS interface). The equivalence makes statements involving both the spectrum and wave functions of the two systems. The spectra of two equivalent systems are identical. Furthermore, given a wave function in the one system, the wave function in the equivalent system can be constructed. The suspicion exists that analogues of quantum mechanical effects of superconductors can thus be found in systems with armchair edges, similar to [26]. Such an investigation is not carried out in this thesis, however.

The spectrum of the distorted semi-infinite graphene sheet terminated by an armchair edge system was investigated next. The spectrum (in the case where the distortion is perpendicular to the edge) follows immediately from the equivalence and reference to [10]. However, it was investigated whether the spectrum is dependent on whether the applied distortion is perpendicular to the edge or not i.e. if the same result would hold it the distortion was applied parallel to the edge. This is not straightforward since physical results may change if the pseudo vector potential is changed in a system where different valleys are coupled, even if they result in the same pseudo magnetic field. The spectrum for the distorted graphene sheet with armchair edge system was shown not to change, however. The dispersionless Landau levels were still shown to exist.

Secondly, our investigation continued to armchair ribbons. The Recursive Green's Function method of [20] was employed and extended to be able to handle ribbons with an NS interface. After this machinery was developed, results of [10] were studied numerically. In [10], the transport of an armchair ribbon with a real magnetic field and NS interface was investigated analytically. Our investigation looked at two aspects of this paper, namely the assumption of the absence of intervalley scattering and the statement that only the width of the ribbon near the interface is important in [10]. The numerical investigation also served as a test of whether the NS interface was implemented correctly in the algorithm.

The assumption of the absence of intervalley scattering was shown to not be perfect. Some intervalley scattering does take place. This is especially noticable in cases where the width of the sample is not a multiple of three. However, the intervalley scattering was shown to not affect the results greatly and the results agreed well with the analytical results at small (though not

Stellenbosch University http://scholar.sun.ac.za

too small) chemical potentials. The transmission as a function of chemical potential converges to a value of one if the width of the ribbon is a multiple of three and converges to a quarter otherwise. The statement that only the width of the system near the interface is important was investigated and shown to be a very reasonable. The qualitative results remained unchanged, though they did differ quantitatively.

In our last investigation, we looked at a distorted armchair ribbon connected to an NS interface. This study was motivated by results found when the semi-infinite distorted graphene sheet was investigated. The armchair edge serves as an insulator (confirmed numerically). The NS interface allows propagation in both directions. Also, only small windows around the bulk Landau levels allow for propagation through the bulk. These factors were suspected to give rise to bound states, since a particle at the NS interface won't be able to leave if its energy did not coincide with that of a bulk Landau level. Bound states would form near the NS interface as a hybridisation of the counterpropagating modes along the NS interface.

These bound states were shown to result in resonances associated with the NS interface. The energy window was chosen to be between the zero'th and first Landau level. The spacing of the resonances were shown to change with the width of the system. The number of resonances corresponded well with what was expected from analytical estimates. If the width of the system is doubled, one would expect the number of peaks to also double, which was indicated. The height and width of the peaks were shown to be very sensitive to the length over which the ribbon is distorted. If this length increased, the width of the resonance peaks decreased and the height increased rapidly. A reason for why the height increased could not be found at this time.

Further investigation is still possible. Specifically it can be investigated whether the resonance peaks strictly require the distortion to lead to a constant pseudo magnetic field. Also, the behavior of peaks between higher Landau levels can be investigated. The zig-zag edged system is also worth investigating, though no resonances in transport can be expected.

Stellenbosch University http://scholar.sun.ac.za

BIBLIOGRAPHY

[1] Wallace P.R 1947 *Phys. Rev.* **71** 622

[2] Mouras S 1987 *Revue de Chimie Minérale* **24** 572-582

[3] Peierls R.E 1935 *Ann. I.H Poincare* **5** 177

[4] Landau L.D 1937 *Phys. Z. Sowjetunion* **11** 26

[5] McClure J.W 1957 *Phys. Rev.* **107** 612

[6] Slonczewski J.C, Weiss P.R 1958 *Phys. Rev* **109** 272

[7] Novoselov K.S, Geim A.K, Morozov S.V, Jian D., Zhang Y, Dubonos S.V, Gregorieva I.V, Firsov A.A 2004 *Science* **306** 666

[8] Novoselov K.S, Geim A.K, Morozov S.V, Jian D., Zhang Y, Dubonos S.V, Gregorieva I.V, Firsov A.A 2005 *Nature* **438** 197-200

[9] Beenakker C.W.J 2008 *Rev. Mod. Phys* **80** 1337

[10] Akhmerov A.R, Beenakker C.W.J 2007 *Phys. Rev. Lett.* **98** 157003

[11] Rycerz A, Tworzydło J, Beenakker C.W.J 2007 *Nature Physics* **3**, 172-175

[12] Akhmerov A.R, Bardarson J.H, Rycerz A, Beenakker C.W.J, 2008 *Phys. Rev. B* **77** 205416

[13] Castro Neto A.H, Guinea F, Peres N.M.R, Novoselov K.S, Geim A.K 2009 *Rev. Mod. Phys.* **81** 109

[14] Ashcroft N.W., Mermin N.D 1976 *Solid State Physics* (Holt, Rinehart, and Winston, New York)

[15] McCann E, Fal'ko V.I 2004 *J. Phys. Condens. Matter* **16** 2371

[16] Brey L, Fertig H.A 2006 *Phys. Rev. B.* **73** 195408

[17] De Gennes P.G 1995 *Superconductivity of Metals and Alloys* (Perseus Books Group)

[18] Beenakker C.W.J 2006 Phys. Rev. Lett. **97** 067007

[19] Titov M, Beenakker C.W.J 2006 *Phys. Rev. B* **74** 041401

Stellenbosch University http://scholar.sun.ac.za

[20] Deitl P 2009 *Numerical Studies of Electronic Transport Through Graphene Nanoribbons with Disorder* (Universität Karlsruhe, Master's dissertation)

[21] Datta S 1995 *Electronic Transport in Mesoscopic Systems* (Cambridge University Press)

[22] Ferry D.K, Goodnick S.M 1997 *Transport in nanostructures* (Cambridge University Press)

[23] Abramowitz M, Stegun I.A 1972 *Handbook of Mathematical Functions With Formulas, Graphs, and Mathematical Table* (U.S. Department of Commerce)

[24] Sivan U, Imry Y 1986 *Phys Rev B* **33** 551-558

[25] Tworzydło J, Snyman I, Akhmerov A.R, Beenakker C.W.J 2007 *Phys. Rev. B* **76** 035411

[26] Beenakker C.W.J, Akhmerov A.R, Recher P, Tworzydlo J 2008 *Phys. Rev. B* **77** 075409

[27] Tworzydło J, Trauzettel B, Titov M, Rycerz A, Beenakker C.W.J 2006 *Phys. Rev. Lett.* **96** 246802